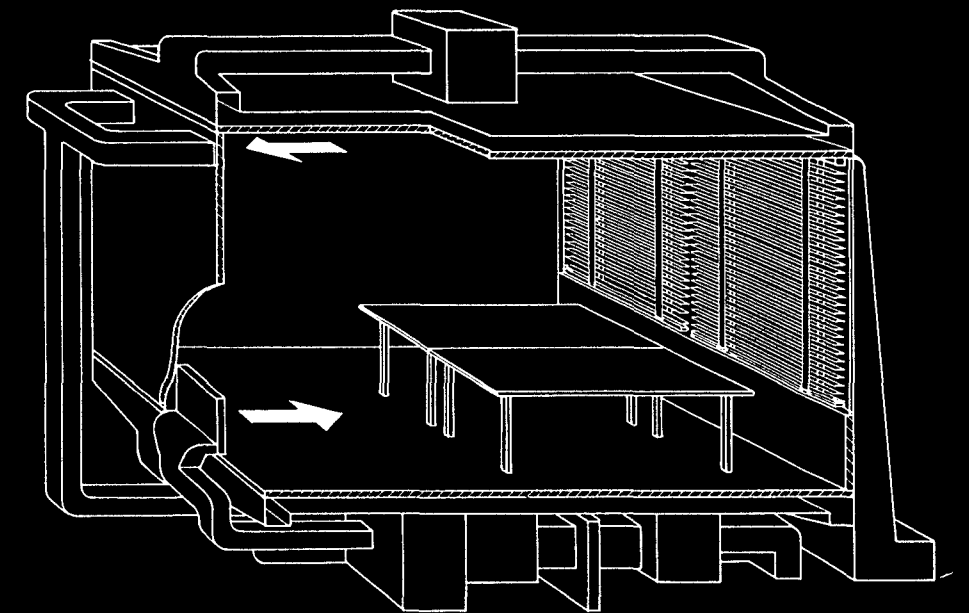


INDOOR AIRFLOW, AIR QUALITY AND
ENERGY CONSUMPTION OF BUILDINGS



Chen Qingyan

TR diss
1687

001902
217 89 08
7a des 1607

INDOOR AIRFLOW, AIR QUALITY AND
ENERGY CONSUMPTION OF BUILDINGS

ISBN 90-9002435-2

INDOOR AIRFLOW, AIR QUALITY AND ENERGY CONSUMPTION OF BUILDINGS

Proefschrift

ter verkrijging van de graad van doctor
aan de Technische Universiteit Delft,
op gezag van de Rector Magnificus,
Prof. drs. P.A. Schenck
in het openbaar te verdedigen
ten overstaan van
een commissie aangewezen door
het College van Dekanen
op dinsdag 29 november 1988 te 16.00 uur

door



CHEN QINGYAN

geboren te Fujian, China
Werktuigkundig Ingenieur



krips repro meppel

TR diss
1687

Dit proefschrift is goedgekeurd door de promotoren
Prof. ir. R.W.J. Kouffeld
Prof. dr. ir. F.T.M. Nieuwstadt

Dr. ir. J. van der Kooi
heeft als begeleider in hoge mate bijgedragen
aan het totstandkomen van het proefschrift.
Het College van Dekanen heeft hem als zodanig aangewezen.

To Rong and Shang

献给蓉和熵

The results presented in this thesis are related to the following publications. They are reprinted by the permission of the publishers of articles five to seven.

1. Kooi, J. van der and Chen, Qingyan 1986. "Numerical simulation of air movement and temperature field in a room with cold and hot window surface", EUROMECH-207 Colloquium on Natural Convection, Dept. of Applied Physics, Delft University of Technology, Delft.
2. Chen, Qingyan and Kooi, J. van der 1987. "Experiments and 2D approximated computations of 3D air movement, heat and concentration transfer in a room", Proceedings of the International Conference on Air Distribution in Ventilated Spaces, Vol.4a, ROOMVENT-87, SWEDVENT, Stockholm.
3. Chen, Qingyan and Kooi, J. van der 1987. "Measurements and computations on air movement and temperature distribution in a climate room", Proceedings of XVIIth International Congress of Refrigeration, Vol.E, Vienna.
4. Kooi, J. van der and Chen, Qingyan 1987. "Improvement of cooling load programs by combination with an air flow program." Proceedings of the XVIIth International Congress of Refrigeration. Vol.E. Vienna.
5. Chen, Qingyan and Kooi, J. van der 1988. "ACCURACY - a computer program for combined problems of energy analysis, indoor airflow and air quality", ASHRAE Transactions, Vol.94, Part 2.
6. Chen, Qingyan; Kooi, J. van der and Meyers, A. 1988. "Measurements and computations of ventilation efficiency and temperature efficiency in a ventilated room", Energy and Buildings, Vol.12, No.2.
7. Chen, Qingyan and Kooi, J. van der 1988. "Indoor airflow, air quality and energy consumption of buildings: new starting points, new opportunities", to appear in Journal of Refrigeration (in Chinese).
8. Chen, Qingyan and Kooi, J. van der 1988. "Buoyancy-affected flow and its influence in cooling load determination of a ventilated room: comparison between computations and experiments", to be published.
9. Chen, Qingyan; Hoornstra, T.G. and Kooi, J. van der 1988. "Energy analysis of buildings with different air supply and exhaust systems", to be published.
10. Kooi, J. van der and Chen, Qingyan 1988. "Flow and thermal performance in a room with air displacement terminals", to be published.
11. Chen, Qingyan and Kooi, J. van der 1988. "Comfort and energy consumption analysis in buildings with radiant panels", to be published.

CONTENTS

CHAPTER 1. INTRODUCTION	1
1.1 Statement of the Problem	1
1.2 Methodology of the Research	2
1.3 State of the Art	3
1.3.1 Numerical calculation of indoor airflow	3
1.3.2 Numerical calculation of transient heat transfer in a room	4
1.4 Aim of the Present Work	4
CHAPTER 2. INDOOR AIR MOVEMENT MODELLING	6
2.1 Review of Turbulence Models	6
2.1.1 Nature and origin of turbulence	6
2.1.2 Predicting methods of turbulence	7
2.1.2.1 Turbulent transport models	7
2.1.2.2 Large-eddy simulation	7
2.1.3 Turbulent transport models	8
2.1.3.1 Models using Boussinesq suggestion	8
2.1.3.2 Reynolds stress models	10
2.1.4 Closure	10
2.2 Differential Equations of Turbulent Flow	11
2.2.1 The continuity equation	12
2.2.2 The momentum equation	13
2.2.2.1 Reynolds equation	13
2.2.2.2 Reynolds stress	13
2.2.2.3 Effective viscosity of turbulence	14
2.2.3 The equation of kinetic energy of turbulence	14
2.2.4 The equation of dissipation rate of turbulence energy	16
2.2.5 The energy equation	18
2.2.6 The concentration equation	18
2.2.7 Closure	19
2.3 Derivation of Finite-Domain Equations	19
2.3.1 The discrete equations for general variables	20
2.3.2 The finite-domain equation for pressure correction	24
2.4 Boundary Conditions	26
2.4.1 "No-flux" boundary	26
2.4.2 Conventional boundary	26
2.4.2.1 The Couette-flow	26
2.4.2.2 The Couette-flow equations	27
2.4.2.3 The wall functions	28
2.4.3 Improvement of the wall functions	30
2.5 A Brief Description of the Airflow Programs PHOENICS and	

CHAMPION SGE	34
2.5.1 PHOENICS	34
2.5.2 CHAMPION SGE	34
2.5.3 The calculation procedure of CHAMPION SGE	35
2.6 Conclusions	37
CHAPTER 3. EXPERIMENTAL SETUP	38
3.1 Field Measurements of Air Velocity, Temperature and Contaminant Concentration Distributions	38
3.1.1 Mixed convection situations	40
3.1.1.1 Cooling cases	40
3.1.1.2 Heating cases	40
3.1.2 Natural convection situations	41
3.2 Measurements of Convective Heat Exchanges on Enclosure Surfaces	41
3.3 Measurements of Air-Conditioning Loads	42
CHAPTER 4. COMPUTATIONS AND VALIDATIONS OF INDOOR AIRFLOW, HEAT TRANSFER AND AIR QUALITY	43
4.1 Two-Dimensional Calculations and Validations	43
4.1.1 Method with thermal sources/sinks for heat transfer in the third dimension	43
4.1.2 Concentrated method	45
4.1.3 Adjusted inlet temperature method	47
4.1.4 Remarks and conclusions of the two-dimensional computations	50
4.2 Three-Dimensional Simulations and Validations	50
4.2.1 Different ventilating systems for cooling	51
4.2.2 Different ventilation rates	58
4.2.3 Different heat gains from the venetian blinds	59
4.2.4 Different heating systems	64
4.2.5 Remarks and conclusions of the three-dimensional computations	65
CHAPTER 5. AIR-CONDITIONING LOAD MODELLING	67
5.1 Review of Air-Conditioning Load Predictions	67
5.1.1 Heating load	67
5.1.2 Cooling load	67
5.1.3 Air-conditioning load components	70
5.1.3.1 Solar radiation through fenestration area	70
5.1.3.2 Infiltration	71
5.1.3.3 Lights, appliances and occupants	71
5.2 Description of the Computer Program ACCURACY	72
5.2.1 Solar radiation	72
5.2.1.1 ASHRAE method	72
5.2.1.2 Dutch weather data	75
5.2.1.3 Short reference year weather data	75
5.2.2 Transient heat conduction through walls	75
5.2.2.1 Basic equations of heat conduction	76

5.2.2.2	S-transfer function for a multilayer wall	77
5.2.2.3	Z-transfer function for a multilayer wall	79
5.2.3	Heat transfer on surfaces of enclosure	82
5.2.3.1	Convective heat exchange coefficients	82
5.2.3.2	Radiative heat exchange coefficients	83
5.2.3.3	Absorptivity, transmissivity and reflectivity of a window	85
5.2.3.4	Shadow factor	87
5.2.3.5	Thermal balance on the outside surface of a wall	88
5.2.3.6	Thermal balance on the inside surface of a wall	89
5.2.3.7	Thermal balance on the outside layer of a window	90
5.2.3.8	Thermal balance on the inside layer of a window	91
5.2.4	The influence of indoor air temperature distributions	92
5.2.5	Room energy balance equations	94
5.2.5.1	Heat gain components	94
5.2.5.2	Heat balance of a room	95
5.2.5.3	Determination of the heat extraction of a room	97
5.2.5.4	The solving procedure of ACCURACY	99
5.2.5.5	The heat extraction of a room and a cavity	100
5.2.5.6	Other remarks	101
5.2.6	The program structure of ACCURACY	101
5.3	Conclusions	102
CHAPTER 6.	COMPUTATIONS AND VALIDATIONS OF AIR-CONDITIONING LOAD AND ROOM AIR TEMPERATURE	103
6.1	Cooling Situation	103
6.1.1	Cooling load predictions	103
6.1.2	The calculations of room air temperature and contamination distributions	107
6.2	Heating Situation	108
6.3	Further Remarks	110
6.4	Conclusions	111
CHAPTER 7.	PREDICTIONS OF BUILDING ENERGY CONSUMPTION	112
7.1	Theories of Building Energy Analysis	112
7.1.1	Methodology of building energy analysis	112
7.1.2	The fundamentals of the energy analysis program ENERK	113
7.2	Annual Energy Consumption of the Climate Room	115
7.2.1	Variable air volume system	115
7.2.1.1	With the same supply air temperature	116
7.2.1.2	With different supply air temperatures	120
7.2.2	Constant air volume system	121
7.3	Conclusions	125

SUMMARY	126
Summary	126
Samenvatting (summary in Dutch)	128
Zhai Yao (summary in Chinese)	130
REFERENCES	132
NOMENCLATURE	140
CURRICULUM VITAE	145
ACKNOWLEDGEMENTS	146

CHAPTER 1

INTRODUCTION

To be comfortable, people require that environmental parameters (e.g. temperature, humidity, air velocity) are maintained within a fairly limited range. Equally, modern technology frequently requires a defined indoor atmosphere. The factors which can influence the environment in a given space, typically a room, can be divided into two groups. The first one includes climatic parameters (e.g. solar radiation and outdoor air temperature). Heat, moisture and pollutants generated by people and production processes comprise the second group. As all of these will influence the indoor environment, it is necessary to study their inter-relationships in order to develop more effective and economical air-conditioning methods and systems.

1.1 Statement of the Problem

Since the energy crisis of 1970's, the insulation of buildings has been improved in order to reduce heat loss in winter, heat gain in summer and infiltration of outdoor air. As a consequence, the heat extracted from, or supplied to a room for maintaining a comfortable air temperature is smaller. Because the heat extracted or heat supplied is related to the air supply and the temperature difference between the air inlet and the outlet of a room, the amount of air supplied or the air temperature difference can be reduced. From the view point of energy saving, it is more economical to decrease the air supply and this becomes the trend in design after 1970's.

Such a reduction of air supply causes an increase of the concentration of indoor pollutants and sometimes generates a non-uniform distribution of air temperature. Due to the decrease of the air supply, density differences, as a result of temperature differences, become one of the dominant factors to influence the indoor airflow. In many cases, this results in a vertical temperature stratification and the temperature in the upper part of the room will then be higher than that in the lower part. If the air exhaust outlets of the room are near the ceiling, the temperature of extracted air is higher than that in the well-mixed situation which occurs with a large air supply. This means that the temperature difference between the inlet and outlet air is larger for cooling situations. To extract the same amount of heat from the room, the amount of air supply can thus be smaller. This, in fact, is an additional reason why the air supply can be reduced. The indoor air temperature distribution and the inlet and outlet locations in a room have a large influence on energy consumption, because the air supply is directly related to the energy consumption.

In order to estimate the influence of the inlet and outlet locations and the amount of air supplied on human comfort and on energy consumption, the air velocity, the temperature and the contaminant distributions in the room must be predicted, together with the transient heat transfer through the

walls. Other important factors for these predictions are, for instance, room geometry, the properties of wall materials and outdoor climate parameters. With this data, the designer of an air-conditioning system is able to choose the optimum design from among a number of alternative possibilities.

During recent years, the predictions of indoor airflow distributions have made a considerable progress, but most of the research interest was aimed at studying the influence of indoor airflow on comfort. However, few results, especially for a room with small air supply, are appropriate for applications. Predictions of building energy consumption are based on the assumption of a uniform indoor air temperature distribution, and the influence of the air supply and air exhaust system can therefore not be calculated.

In order to solve this problem, the nature of the indoor airflow and the transient heat transfer in the walls must be predicted simultaneously, especially under small air supply conditions. This is because the airflow and transient heat transfer in a room are interrelated. Until now, this type of study has not been attempted.

1.2 Methodology of the Research

Predictions of airflow and transient heat transfer in a room can be obtained by three main approaches: experimental investigation, theoretical analysis and numerical calculation.

Experimental Investigation: The most realistic information concerning indoor airflow and transient heat transfer in a room is, in principle, given by direct measurement. An experimental investigation of indoor airflow often requires a full-scale climate room in order to reveal air velocity, temperature and pollutant concentration distributions under given conditions. Such full-scale tests are, in most cases, expensive. It also must be remembered that some of the measurements present serious difficulties in many situations. These include the measurements of the flow directions under low velocities and turbulent intensities. Moreover, the measuring instruments are not free from errors.

Theoretical Analysis: Nearly all airflows encountered in a room are turbulent and, in addition, the transient heat transfer in the room must be determined with random boundary conditions, for instance, climatic variations of outdoor air temperature. However, the theories concerning turbulent flows and transient heat transfer could not, until now, be used for a direct solution of such applications.

Numerical Calculation: Due to the limitations of the approaches described above and to the development of digital computer systems, numerical calculations of airflow and heat transfer in a room have been used extensively in recent years. Encouraging results have been achieved by using numerical solutions for a number of problems concerning the airflow and transient heat transfer in a room. For example, success has been achieved in calculating indoor air velocity, temperature and pollutant concentration distributions, and in computing the hourly heat supply or heat extraction of a room. This approach involves the numerical solution of a set of partial differential equations for the turbulent flow and heat transfer. Approximation is often required in these equations in order to make them solvable. For example, the details of turbulent flow are difficult to calculate and engineers are mainly interested in the mean values. Therefore, one turns to so-called turbulence models by which it is possible to compute

the mean values. One of these models is the $k-\epsilon$ turbulence model. With the $k-\epsilon$ turbulence model, all fluctuating variables can be connected to mean values. Due to the development in computer speed and capacity, such a numerical approach is becoming cheaper and cheaper.

We have used this numerical approach for the problem stated in the preceding section. However, validation of the computed results by comparison with experimental data is often necessary, because the approximations used in the numerical approach may not be valid for the current investigations.

1.3 State of the Art

1.3.1 Numerical calculation of indoor airflow

The study of airflows in rooms using numerical calculation techniques has continued for nearly twenty years and has achieved some successes. The range of airflow simulations, which originally comprised laminar, one- and two-dimensional, steady and isothermal situations, has been enlarged to include turbulent, three-dimensional, transient and buoyancy-affected flows. Nielson (1974) was one of the earliest researchers to use numerical predictions of indoor airflow. His work mainly involved two-dimensional, steady and isothermal flows. Although his two-dimensional results are not very useful for engineering applications, the methods he used showed a very strong potential for solving practical airflow problems in a room. Later, he and his co-workers extended the numerical calculations for the indoor airflow problems in non-isothermal situations (Nielson et al 1979) and pollutant concentrations (Nielson 1981). Since the end of the 1970's, three-dimensional computations of turbulent airflow in a room became more and more popular because some powerful computers became available. Many researchers validated their computational results with experiments, including Nielson (1979), Sakamoto and Matsuo (1980), and Gosman et al (1980). Later, publications concerning indoor airflow dealt with more specific practical problems. Examples are the assessment of the safety and quality of flow in industrial buildings (Broyd et al 1983), the evaluation of ventilation systems in a room (Ishizu and Kaneki 1984), the exploration of the possibilities of applying the computational results to engineering design (Markatos 1983), and the study of the flow characters of air supply terminals, for instance, a radial air distributor (Reinartz and Renz 1984) and an air conditioner unit (Yamazaki et al 1987). The results indicate that numerical calculation with the $k-\epsilon$ turbulence model can be used to study indoor airflows problems. However, discrepancies between the calculated data and the measurements were always found. This is probably because some of the approximations used in the turbulence model may not be very appropriate for airflows in a room.

In addition, almost all of the computations are carried out with the assumption that boundary conditions such as wall surface temperatures and the convective heat of solar radiation through windows, which in fact cannot always be prescribed, are known.

From this previous work, we may therefore conclude that numerical calculation techniques can be used to predict the air velocity, temperature and concentration distributions in a room, but validation of the computed results by corresponding measurements is always required. Furthermore, the boundary conditions used in the airflow calculations must be provided more precisely.

1.3.2 Numerical calculation of transient heat transfer in a room

The methods for computing the complex heat transfer in walls have evolved from one-dimensional with periodic boundary conditions to one- or two-dimensional with random boundary conditions (e.g. climatic variations). The hourly heat exchange among walls and the annual energy consumption of a building can be accurately determined. Because of the introduction of computers in this field in late 1960's, the transient heat transfer in a room with random boundary conditions can be calculated by the finite difference method or by the finite element method.

Stephenson and Mitalas (1967, 1971) presented the response factors and the z-transfer factors methods for calculating transient heat conduction. These methods are generally accepted as the cornerstone of building thermal analysis. These methods have made it possible to numerically invert the difficult Laplace transform functions for multilayer heat conduction problems. Thermal response factors and z-transfer factors are the results of an exact solution of the heat conduction equations, unlike the approximate solutions such as the finite difference method or the finite element method. The response factors and z-transfer factors, once computed for a given multilayer wall, can be used over and over again to evaluate the heat flux and surface temperature of that wall.

The response factors method and z-transfer factors method have since been successfully combined with the calculation of heat transfer among the walls of a room and of the heat and mass transfer of air-conditioning systems. This allows an hour-by-hour computation of heat supply and heat extraction of a room (Kimura 1977). As a result, one may obtain an estimation of the annual energy consumption of a building based on the hourly approach (ASHRAE 1981). However, most air-conditioning load programs which are used to calculate the heat supply or heat extraction of a room assume uniform indoor air temperatures. Hence, they are inappropriate to be applied for studying the influence of air supply and air exhaust systems on building energy consumption and on human comfort.

The preceding results show that the response factors and z-transfer factors methods are adequate for calculating transient heat transfer in a room with random boundary conditions. Hour-by-hour heat supply or heat extraction of the room and annual energy consumption can also be computed. However, modification of the existing approach is necessary in order to consider the influence of indoor air temperature distributions.

1.4 Aim of the Present Work

The present state of the art allows us to combine an airflow program and an air-conditioning load program for solving the problem mentioned in section 1.1. The inputs required by an airflow program are enclosure surface temperatures, inlet and outlet locations, inlet mass flow rate, and inlet air temperature. These can be obtained from the outputs of an air-conditioning load program. On the other hand, the outputs of the airflow program, such as room air velocity, temperature and contamination distributions and convective heat exchange coefficients, are a part of the inputs for the air-conditioning load program. Both programs can, therefore, be coupled, in order to obtain more accurate results and to reveal the overall physics phenomena. This implies that the combination of an airflow program with an air-conditioning load program can be used to estimate more accurately boundary conditions for airflow simulations and to study the influence of the indoor airflow and

temperature distribution on room energy consumption and comfort. However, this is still an unexplored territory, because research activities on both fields were quite isolated. Hence, our work will concern the combined problem.

Our aim is to study airflow, contaminant concentration distributions and air temperature fields in an air-conditioned room with different kinds of air supply and air exhaust systems and to predict the heat extracted from and supplied to the room, and consequently the energy consumption of these systems. This will allow the development of reliable methods for estimating the influence of indoor airflow on the comfort and energy consumption of buildings, for controlling the pollutant dispersion, and for increasing the efficiency of energy utilization. The research is principally carried out by numerical techniques. In particular a two-dimensional airflow program and a three-dimensional airflow program are used, and an air-conditioning load program is constructed.

The second aim of this research is to compare the computational results with experiments. Therefore, corresponding measurements are performed.

In other words, this thesis is, in principle, an approach to the combination of fluid dynamics and transient heat transfer of buildings. It presents the scientific basis of the approach and some details of the numerical techniques employed therein. It demonstrates a number of computational results on the problem together with the validations by measurements.

In this thesis, chapter 2, after a review on turbulence modelling, presents the detailed description of the $k-\epsilon$ model and the discrete equations of the model, which were used in the airflow programs. The experimental setup and the measuring techniques are concerned in chapter 3. The computations and validations of airflow, air temperature and contaminant concentration distributions of the room with different kind of air supply and air exhaust systems are the main subject of chapter 4. Chapter 5 reviews the air-conditioning load modelling (predictions of heat extracted from or supplied to rooms) and describes the air-conditioning load program constructed for the research. In this program, the influence of air temperature distributions in the room with different kinds of air supply and air exhaust systems on heat supply and heat extraction can be studied. In chapter 6, the computational heat supply or heat extraction of the room is compared with the experimental data. Finally, the energy consumption of the room with different kinds of air supply and air exhaust systems is discussed in chapter 7.

CHAPTER 2

INDOOR AIR MOVEMENT MODELLING

2.1 Review of Turbulence Models

2.1.1 Nature and origin of turbulence

Laminar flows (Pan 1980) can be described exactly in terms of the partial differential equations for the conservation of the controlling physical quantities (e.g. mass, momentum, energy, concentration species, etc.). Although approximations are made, such as neglecting the temperature dependence of fluid properties, it is from the point of view of mathematical simplicity rather than from necessity.

Turbulence is defined in terms of irregularity, diffusivity, large Reynolds numbers, three-dimensional vorticity fluctuations, dissipation and continuum (Tennekes and Lumley 1972). Turbulent flows cannot even in principle be described exactly, as almost all the physical properties (such as velocity components, enthalpy, pressure, density, species concentrations, reaction rates) fluctuate and interact with each other. Among the fluctuating quantities, the corrections create new unknowns for which the conservation laws in terms of known quantities are not well established. An iterative process for constructing the conservation laws for the unknown corrections leads to higher order unknown corrections. Thus the complete set, which can provide a detailed description of the turbulent motion, ends up in an infinite set of partial differential equations, which is mathematically intractable.

Turbulence is considered to be generated mainly from the shear of the mean flow (i.e. primary streamline) and also from the buoyancy (i.e. external body) force. If turbulence arrives in an environment where there is no shear and buoyancy, the turbulent motion decays to become laminar again. Kumar (1983) considered the origin of turbulence as being visualized as an instability of laminar flow at high Reynolds numbers ($=\rho VL/\mu$), where non-linear inertial effects (ρV^2) are dominant over viscous effects ($\mu V/L$). The non-linear inertial effects accelerates the instability to make the flow turbulent.

Tennekes and Lumley (1977) based their view on some developed statistical concepts and pointed out that turbulence is viewed as a fluid flow consisting of a highly disordered array of eddies of widely different sizes. The eddies are stretched in a preferred direction by the mean flow and in a random direction by each other. This mechanism ultimately leads to the breaking down of large eddies into smaller ones. This process is called the "energy cascade" which suggests that only eddies of comparable size can exchange energy with one another (Tennekes and Lumley 1977). The large eddies obtain the kinetic energy from mean motion. This energy is then transferred to eddies of smaller size and continued to smaller and smaller scales until the eddies lose energy by the direct action of viscous stresses. At this final

stage, the energy is converted into internal thermal energy (Frost and Bitte 1977).

The larger the Reynolds number, the wider the spectrum of frequencies. This means that the difference between the low frequency large-eddies and high frequency small-eddies is significant under high Reynolds numbers. Kovaszny (1970) proposed that the turbulent motion can be described by a three-level procedure, namely, a mean motion, a large-eddy motion and a small-eddy motion. Because the larger-eddies are mainly responsible for the transport of momentum and heat which implies the direct interaction with the mean flow, they need to be properly simulated in a turbulence model.

The large-eddies are normally bigger than the (numerical) grid size accessible to present-day computers and can therefore be simulated. They appear to have a tendency to adjust themselves as if they were independent of the details of dissipation mechanism. The small-eddies are then thought of as an essentially isotropic turbulence carried along by the mean motion and by large-eddies.

2.1.2 Prediction methods of turbulence

Prediction of turbulence in fluid flows by theoretical calculation has been attempted by two parallel methods classified as follows.

2.1.2.1 Turbulent transport models

Turbulent transport models are the basis of the engineers' approach, where attempts are concentrated in looking for simplified models of turbulent flows. They are based on good physical insight, which can be applicable to complicated flows encountered in reality. Since attempts were made to model directly the terms governing the transport of momentum, heat and concentration, etc., the models are referred to as turbulent transport closure models. These models treat dynamical quantities as some sort of statistically averaged turbulent fields and simulate only the gross features of the turbulent flows.

2.1.2.2 Large-eddy simulation

Deardorff (1970) departed from the hypothesis that the turbulent motion could be separated into large-eddies and small-eddies such that the separation between the two does not have a significant effect on the evolution of large-eddies. He developed a method named as "large-eddy simulations" for meteorological applications. In large-eddy simulations, although the Reynolds number does not come explicitly into picture, it can, however, be related implicitly to the separation of the two scales. The attempt is made to resolve the large-eddy motion by numerically solving a "filtered" set of equations governing this three-dimensional time-dependent motion. The large-eddies corresponding to the three-dimensional time-dependent equation are chosen such that they can be simulated on existing computers. Turbulent transport approximations are then made for small-eddies and the small-eddy motions can be modelled independently from the flow geometry. The success of the method stems from the fact that the main contribution to turbulent transport comes from the large-eddy motion. Thus the large-eddy simulation is clearly superior to turbulent transport closure wherein the transport terms (e.g. Reynolds stresses, turbulent heat fluxes, etc.) are treated with full empiricism. Although the large-eddy simulation can be involved in the solution of many turbulence problems, Lafeber's (1987) results indicated that the large-eddy simulation still requires too much computational time to be

useful for engineering applications. However, it can be quite valuable as an aid to develop transport closure models.

Although two numerical approaches for turbulence modelling have been pointed out, the turbulent transport field models seems to be suitable for the air movement predictions in a room. This is due to the fact that turbulent transport models are capable of describing quite generally the complex fluid flows and heat transfer encountered in an air conditioned room (gross features are sufficient). The large-eddy calculations have shown much promise in other fields such as in meteorology (Nieuwstadt 1986), but the technique is much too costly at present to be considered as an engineering tool. In the following section, a few main turbulent transport models will be generally discussed.

2.1.3 Turbulent transport models

The Navier-Stokes equation of isothermal turbulent flow is:

$$\frac{\partial \bar{v}_i}{\partial t} + \frac{\partial \bar{v}_i \bar{v}_j}{\partial x_j} = - \frac{1}{\rho} \frac{\partial \bar{p}}{\partial x_i} + \frac{\partial}{\partial x_j} \left[\frac{\mu}{\rho} \left(\frac{\partial \bar{v}_i}{\partial x_j} + \frac{\partial \bar{v}_j}{\partial x_i} \right) - \overline{v'_i v'_j} \right] \quad (2.1)$$

where t stands for time, \bar{p} for mean pressure, ρ for density and μ for viscosity of the fluid. In the equation, \bar{v}_i and \bar{v}_j are the mean velocity components in x_i and x_j directions and v'_i and v'_j are their fluctuating components.

The term $-\rho \overline{v'_i v'_j}$ is called Reynolds stress or apparent turbulent shearing stress and is a second-order tensor. It is this term that makes the solution of the Navier-Stokes equation very complicated. Therefore, the starting point of all transport models is how to determine the Reynolds stress. Turbulent transport models are divided into two types according to whether or not the Boussinesq suggestion is used for the Reynolds stress.

Boussinesq (1877) suggested that the apparent turbulent shearing stress might be related to the rate of mean stream through an apparent scalar turbulent or "eddy" viscosity. For the general Reynolds stress tensor in incompressible flow, the Boussinesq suggestion gives:

$$-\rho \overline{v'_i v'_j} = \mu_t \left(\frac{\partial \bar{v}_i}{\partial x_j} + \frac{\partial \bar{v}_j}{\partial x_i} \right) - \frac{2}{3} \delta_{ij} \rho k \quad (2.2)$$

where μ_t is the turbulent viscosity and is determined from turbulence models and k is the kinetic energy of turbulence, $k = \overline{v'_i v'_i} / 2$.

Most models currently employed in engineering calculations use this suggestion. Experimental evidence indicates that the turbulent viscosity hypothesis is a good approximation in many flow circumstances.

The following section gives the principal authors of some of the turbulence models together with their dates of publication.

2.1.3.1 Models using Boussinesq suggestion

Prandtl's mixing-length model (1926) was proposed for two-dimensional boundary layers:

$$\mu_t = \rho l^2 \left| \frac{\partial V}{\partial y} \right|$$

where l is a "mixing length". It can be thought of as a transverse distance over which small eddies maintain their original momentum. The mixing length is somewhat on the order of a mean free path for the collision or mixing of globes of fluid. The product $l \left| \frac{\partial V}{\partial y} \right|$ can be interpreted as the characteristic velocity of turbulence.

The Prandtl mixing length model, after further modification and development by McDonald and Fish (1973), Cebeci and Smith (1974), Bushnell et al. (1975), Adams and Hodge (1977), and Pletcher (1978), has accumulated an impressive record of good performance for relatively simple viscous flows. But, they need to be modified in order to accurately predict flows with "complicated" features.

Kolmogorov (1942) may be regarded as the father of turbulence modelling (Spalding 1981). He proposed that turbulent-flow phenomena should be completed by way of the solution of two equations. The first of these is the energy of the turbulent motion and the second is its "frequency". The second equation normally is regarded as an auxiliary one.

Prandtl's (1945) proposal was similar, with respect to the energy equation. But the distribution of the length scale l was to be prescribed beforehand and not computed from a second differential equation. The length scale was needed by Prandtl, because he used the same effective-viscosity concept as Kolmogorov.

Bradshaw and his co-workers (1967) made an independent proposal for a one-equation model. This was similar to that of Prandtl (1945) in requiring specification of the length-scale distribution. However, it is different in supposing the transfer rates of both momentum and energy to be proportional to the energy itself. The Bradshaw's method has enjoyed good success in the prediction of the wall boundary layers. Even so, the predictions have not been notably superior to other models mentioned above.

In the one equation models (such as Kolmogorov (1942), Prandtl (1945) and Bradshaw (1967)), a length parameter still appears which is generally evaluated by an algebraic expression dependent only on local parameters. Researchers in turbulent flow have long felt that the length scale in the turbulence models should also depend upon the upstream "history" of the flow and not just local flow conditions. An obvious way to provide more complex dependence of l on the flow is to derive a transport equation for the variation of l .

Harlow and Nakayama (1968) and Spalding (1969) made independent proposals for two-equations models. The energy equation was used in both cases, but the former authors proposed that the quantity $\frac{\overline{v'v'}}{l}^{3/2}$ (= dissipation rate of turbulent energy ϵ) should be the dependent variable of the second equation, while the latter proposed the use of $\overline{v'v'}/l^2$. The Harlow-Nakayama's model, after modification by Launder and Spalding (1974), is called the "k- ϵ " model. Numerous other two-equation models have been suggested, the most frequently used ones being the Ng-Spalding (1972) model and the Wilcox-Traci model (1976). Rubesin (1976) summarized the main differences between the models while Chambers and Wilcox (1976) explored the similarities and differences in more detail. Rubesin (1976) showed that it is very difficult to identify the best model from his comparisons.

Most applications of the k- ϵ model have made use of wall functions to treat the near wall region. Due to the uncertainty in inner region modelling

of complex flows (low Reynolds number $k^{1/2}l/\nu$), this fact appears to limit the range of applicability of the $k-\epsilon$ model (and nearly all other models) at the present time. Anderson et al. (1984) pointed out that there were two major restrictions. First, two-equation models of the type discussed here are merely turbulent viscosity models which assume that the Boussinesq suggestion holds. If this assumption fails, then also the two-equation model fails. But, numerous applications with the Boussinesq suggestion models present realistic results for engineering purposes (including air movement in a room). The second shortcoming of the two-equation models is the need to make assumptions in evaluating the various terms in the model transport equations, especially in evaluating the third-order turbulent correlations.

2.1.3.2 Reynolds stress models

When turbulent transport models do not assume that the turbulent shearing stress is proportional to the rate of mean strain (the Boussinesq suggestion fails), that is,

$$-\overline{\rho V'_i V'_j} \neq \mu_t \left(\frac{\partial \bar{V}_i}{\partial x_j} + \frac{\partial \bar{V}_j}{\partial x_i} \right) - \frac{2}{3} \delta_{ij} \rho k$$

those models are regarded as Reynolds stress models. In complex flow situations such as in re-circulating flows, the mean turbulent energy models (which are based on Boussinesq suggestion) are sometimes considered inadequate to represent the local state of turbulence. This deficiency has to be overcome in mean Reynolds stress models which explicitly employ transport equations for the individual Reynolds stresses $-\overline{\rho V'_i V'_j}$. An exact mean Reynolds equation, first is derived by Chou (1945) and then by Rotta (1951).

For near-equilibrium anisotropic flow situations, it is undesirable to solve the partial differential equation form of the mean Reynolds stress model. Rodi (1976) proposed that the transport of $\overline{V'_i V'_j}$ is proportional to the transport of k , with the proportionality factor as the ratio $\overline{V'_i V'_j}/k$. This is the so-called algebraic Reynolds stress model. Other most widely known Reynolds stress models at the present time are probably those of Hanjalić and Launder (1972), Daly and Harlow (1970), and Donaldson (1972). The status and prospects of Reynolds stress closure have been described by Launder (1979) and Kumar (1983).

Although Reynolds stress models are not restricted by the Boussinesq suggestion, they still must utilize approximations and assumptions in modelling. These models have been used to date largely as tools in turbulence research rather than to solve engineering problems, because they are rather complicated.

2.1.4 Closure

The mathematical modelling of the airflow in an air conditioned room is now within the capabilities of modern mathematical and numerical methods. Although many simulation methods have been pointed out in this review, the two-equation $k-\epsilon$ turbulent transport model is chosen as the most suitable one. Launder and Spalding (1974) have compared the $k-\epsilon$ model with the $k-W$ ($W = \epsilon^2 / (C_D k)^2$) model and the $k-kl$ ($l = C_D k^{3/2} / \epsilon$) model, where C_D is a constant. They have found that when the constants of the turbulence models are used to

calculate the turbulent Prandtl number, σ_t , the resulting value is -0.8 for the k-k1 model, 2.9 for the k-W model and 1.3 for the k- ϵ model. Only the latter value is of a magnitude which fits the experimental data of the various entities at locations far from walls. Therefore, the k- ϵ model is used for the present study and its governing equations will be presented in detail in the following section. Many contributions by using the k- ϵ model in this field have been published, such as Hjertager and Magnussen (1977), Nielson et al. (1979), Yamazaki et al. (1987) and those in the ROOMVENT-87 (1987) international conference. A more extensive literature review is presented by Chen and Van der Kooi (1988b).

2.2 Differential Equations of Turbulent Flow

The governing differential equations of viscous flow, which are normally used for a room, consist of the continuity equation, the momentum equation, the energy equation and the concentration equation. Often the Boussinesq approximation is used for airflow calculation in a room. This approximation takes air density as constant and considers buoyancy influence on air movement in the momentum equation. The air in a room is treated as ideal gas and therefore, these differential equations can be written as (Pan 1980):

(1) Continuity equation:

$$\text{div } (\vec{V}) = 0 \quad (2.3)$$

(2) Momentum equation:

$$\frac{\partial v_i}{\partial t} + \frac{\partial v_i v_j}{\partial x_j} = - \frac{1}{\rho} \frac{\partial p}{\partial x_i} + \frac{\partial}{\partial x_j} \left[\frac{\mu}{\rho} \left(\frac{\partial v_i}{\partial x_j} + \frac{\partial v_j}{\partial x_i} \right) \right] + \rho \frac{\beta}{C_p} (H_0 - H) g_i \quad (2.4)$$

where the final term on the right side is buoyancy.

(3) Energy equation (which can be called as enthalpy equation in this case):

$$\frac{\partial \rho H}{\partial t} + \frac{\partial}{\partial x_j} (\rho v_j H) = \frac{\partial}{\partial x_j} \left(\frac{\lambda}{C_p} \frac{\partial H}{\partial x_j} \right) + S_H \quad (2.5)$$

where λ is the heat conductivity of air and S_H is a source term which may be caused by viscosity and chemical reaction, etc..

(4) Concentration equation:

$$\frac{\partial \rho C}{\partial t} + \frac{\partial}{\partial x_j} (\rho v_j C) = \frac{\partial}{\partial x_j} (\rho D \frac{\partial C}{\partial x_j}) + S_C \quad (2.6)$$

where D is the diffusion coefficient of concentration and S_C is a source term which may be generated from chemical reaction, etc..

As has been discussed in the previous section, the most evident difference between laminar flow and turbulent flow is that the turbulent one has a more complicated structure. There are some methods which are in principle capable of predicting the details of any turbulent flow by starting

from the highly reliable Navier-Stokes equations (Spalding 1981). However, the practical possibility of doing this is very small, because of the great disparity of scale between the size of most practical flow domains and the size of the eddies which exist within them. Schumann (1973) sought to compute simple turbulence phenomena in this way, but the cost is great and the success so far small (Spalding 1981). Phenomena of engineering or environmental practice could not possibly be computed in this way with current computers. In other words, the main problem is that time and space scales of turbulent motion are small. Hence, the number of grid points and the small time steps required make the practical computation by this method unrealistic with present computers.

The main thrust of present day research in computational fluid mechanics and heat transfer in turbulent flows is through the averaged Navier-Stokes equations. The Reynolds equations are derived in such a way: (1) by decomposing the dependent variables in the conservation into mean and fluctuating components and (2) by averaging the entire equation. Averaging the equations of motion gives rise to new terms which can be interpreted as "apparent" stress gradients and heat-flux quantities associated with the turbulent motion. These new quantities must be related to the mean flow variables through turbulence models. This process introduces further assumptions and approximations. In this section, the governing equations of turbulent mean flow will be introduced with the k-ε turbulence model.

In order to obtain the mean conservation equations for turbulent flow, the instantaneous quantities in the equations are replaced by the sum of their mean and fluctuating parts. Let superscripts " $\bar{\quad}$ " and " \prime " stand for the mean and fluctuating components respectively. Then the following equations are yielded:

$$V_i = \bar{V}_i + V'_i; \quad p = \bar{p} + p'; \quad \rho = \bar{\rho} + \rho'; \quad H = \bar{H} + H'; \quad C = \bar{C} + C' \quad (2.7)$$

Averaging Equation (2.7) results in:

$$\bar{V}'_i = 0; \quad \bar{p}' = 0; \quad \bar{\rho}' = 0; \quad \bar{H}' = 0; \quad \bar{C}' = 0 \quad (2.8)$$

2.2.1 The continuity equation

Substitution of Equation (2.7) into Equation (2.3) leads to:

$$\text{div} (\bar{V} + V') = 0 \quad (2.9)$$

Averaging of Equation (2.9) changes the continuity equation into:

$$\text{div} (\bar{V}) = 0 \quad \text{and} \quad \text{div} (V') = 0 \quad (2.10)$$

The mean velocity component and the fluctuating component both satisfy the incompressible continuity equation (2.3).

2.2.2 The momentum equation

2.2.2.1 Reynolds equation

Substituting Equation (2.7) to Equation (2.4) and averaging for both sides of Equation (2.4), all linear fluctuating components in the equation are equal to zero except the second term on the left side of the equation, i.e.

$$\frac{\partial}{\partial x_j} [(\bar{v}_i + v'_i)(\bar{v}_j + v'_j)] = \frac{\partial}{\partial x_j} (\bar{v}_i \bar{v}_j) + \frac{\partial}{\partial x_j} (\overline{v'_i v'_j}) \quad (2.11)$$

Obviously, the second term on the right side of Equation (2.11) is a second order tensor, and it is this term that makes modelling of turbulent flow very complicated. Now the momentum equation (2.4) changes to:

$$\frac{\partial \bar{v}_i}{\partial t} + \frac{\partial \bar{v}_i \bar{v}_j}{\partial x_j} = -\frac{1}{\rho} \frac{\partial \bar{p}}{\partial x_i} + \frac{\partial}{\partial x_j} \left[\frac{\mu}{\rho} \left(\frac{\partial \bar{v}_i}{\partial x_j} + \frac{\partial \bar{v}_j}{\partial x_i} \right) - \overline{v'_i v'_j} \right] + \frac{\beta}{C_p} (\bar{H}_0 - \bar{H}) g_i \quad (2.12)$$

This equation is known as Reynolds equation. In fact the term $-\overline{v'_i v'_j}$ in Equation (2.12) may be considered as the effect of turbulence on the averaged flow and may be interpreted as additional shear stress in Equation (2.4). It is sometimes written as the Reynolds stress, τ_t , viz.

$$\tau_t = -\rho \overline{(v'_i v'_j)} \quad (2.13)$$

2.2.2.2 Reynolds stress

In order to calculate the Reynolds stress τ_t , the Boussinesq suggestion (2.2) is used, i.e.

$$\tau_t = \mu_t \left(\frac{\partial \bar{v}_i}{\partial x_j} + \frac{\partial \bar{v}_j}{\partial x_i} \right) - \frac{2}{3} \delta_{ij} \rho k \quad (2.14)$$

According to the definition of the Kronecker delta, δ_{ij} , the substitution of Equations (2.13) and (2.14) into Equation (2.12) leads to:

$$\frac{\partial \bar{v}_i}{\partial t} + \frac{\partial \bar{v}_i \bar{v}_j}{\partial x_j} = -\frac{\partial}{\partial x} \left(\frac{\bar{p}}{\rho} + \frac{2}{3} k \right) + \frac{\partial}{\partial x_j} \left[\frac{\mu_{eff}}{\rho} \left(\frac{\partial \bar{v}_i}{\partial x_j} + \frac{\partial \bar{v}_j}{\partial x_i} \right) \right] + \frac{\beta}{C_p} (\bar{H}_0 - \bar{H}) g_i \quad (2.15)$$

where the effective turbulent viscosity, μ_{eff} , is:

$$\mu_{eff} = \mu + \mu_t \quad (2.16)$$

Comparing Equation (2.15) with Equation (2.4), the differences are that:

- the pressure has been augmented with an additional term $2/3k$, which may be considered as a dynamic pressure and will be ignored later on, because it is small;
- the molecular viscosity has changed into the effective viscosity of turbulence; and

- the variables in Equation (2.4) have been converted into averaged ones.

If the second term on the right side of Equation (2.15) is considered as the diffusion caused by turbulence, and $\bar{p} + 2/3 k\rho$ is set as a new \bar{p} for the first term on the right side of the equation, it follows:

$$\frac{\partial(\rho\bar{V}_i)}{\partial t} + \text{div}(\rho\bar{V}_i\bar{V}_i - \mu_{\text{eff}}\text{grad}\bar{V}_i) = -\frac{\partial\bar{p}}{\partial x_i} + \rho\frac{\beta}{C_p}(\bar{H}_0 - \bar{H})g_i \quad (2.17)$$

2.2.2.3 Effective viscosity of turbulence

The effective viscosity of turbulence can be expressed as the product of turbulent velocity $k^{1/2}$ and the length representing the macroscale of turbulence l , according to the Prandtl-Kolmogorov assumption. That is:

$$\mu_{\text{eff}} = C_\nu \rho k^{1/2} l + \mu \quad (2.18)$$

where C_ν is a constant. The k and l may be expressed as functions of the positions in the flow field. Although k and l are unknown, there are many methods used for calculating the k and l . When the l is assumed, the turbulence model is known as one-equation model, because k has to be calculated from an additional equation. If the l is calculated from other dependent variables, such as dissipation rate of kinetic energy (ϵ), then the model is a two-equation one. Launder and Spalding (1974) used the following equation to connect the l and the ϵ :

$$l = C_1 k^{3/2} / \epsilon \quad (2.19)$$

where C_1 is a constant and the ϵ is defined as:

$$\epsilon = \frac{\mu}{\rho} \overline{\frac{\partial V'_i}{\partial x_j} \frac{\partial V'_i}{\partial x_j}} \quad (2.20)$$

Combination of Equations (2.18) and (2.19) leads to:

$$\mu_t = C_\mu \rho k^2 / \epsilon \quad (2.21)$$

where $C_\mu = C_\nu C_1 = 0.09$ (Launder and Spalding 1974). Now we focus on the problem of how to calculate k and ϵ .

2.2.3 The equation of kinetic energy of turbulence

As it has been described above, it is necessary to derive the equation of kinetic energy of turbulence, in order to calculate the turbulent viscosity μ_t . First we derive an equation for V' by substituting Equation (2.7) into Equation (2.4), separating the mean variables and fluctuating ones, and subtracting the resulting equation from Equation (2.12). The final form then leads to:

$$\frac{\partial \bar{v}'_i}{\partial t} + \frac{\partial}{\partial x_j} (\bar{v}'_i v'_j + v'_i \bar{v}'_j + v'_i v'_j - \overline{v'_i v'_j}) = - \frac{1}{\rho} \frac{\partial \bar{p}'}{\partial x_i} + \frac{\partial}{\partial x_j} \left[\frac{\mu}{\rho} \left(\frac{\partial v'_i}{\partial x_j} + \frac{\partial v'_j}{\partial x_i} \right) \right] - \frac{\beta}{C_p} H' g_i \quad (2.22)$$

The equation governing the mean turbulent kinetic energy k is obtained by multiplying both sides of Equation (2.22) with $\overline{v'_i v'_i}$ and averaging the resulting equation:

$$\begin{aligned} \frac{\partial k}{\partial t} + \frac{\partial}{\partial x_j} (\bar{v}'_j k) &= - \frac{\partial}{\partial x_j} \overline{[v'_j (\frac{p'}{\rho} + \frac{v'_i v'_i}{2})]} - \overline{v'_i v'_j} \frac{\partial \bar{v}'_i}{\partial x_j} + \frac{\mu}{\rho} \frac{\partial}{\partial x_j} \frac{\partial}{\partial x_j} k \\ \text{Convection} & \quad \text{Diffusion} \quad \text{Shear generation} \quad \text{Molecular transport} \\ & - \frac{\mu}{\rho} \frac{\partial \bar{v}'_i}{\partial x_j} \frac{\partial \bar{v}'_i}{\partial x_j} - \frac{\beta}{C_p} \overline{v'_i H' g_i} \\ & \quad \text{Dissipation} \quad \text{Buoyancy production} \end{aligned} \quad (2.23)$$

It is obvious that not all the fluctuating variables in Equation (2.23) can be calculated, therefore, the following approximations are required to close these fluctuating variables. Because the first term on the right side of the equation may be explained as the diffusion of the total turbulence

energy depending on turbulent velocity v'_j , provided that $-\frac{\partial}{\partial x_j} \overline{[v'_j (\frac{p'}{\rho} + \frac{v'_i v'_i}{2})]}$ is proportional to the slope of turbulence energy k . Hence:

$$-\frac{\partial}{\partial x_j} \overline{[v'_j (\frac{p'}{\rho} + \frac{v'_i v'_i}{2})]} = \frac{1}{\rho} \frac{\partial}{\partial x_j} (\Gamma_{k,t} \frac{\partial k}{\partial x_j}) \quad (2.24)$$

where $\Gamma_{k,t}$ is a diffusion coefficient. This is calculated from:

$$\Gamma_{k,t} = \frac{\mu_t}{\sigma_{k,t}} \quad (2.25)$$

where $\sigma_{k,t}$ is the Schmidt number for turbulence energy k .

The second term on the right side of Equation (2.23) can be connected to the average variables by Equations (2.13) and (2.14), because it is equivalent to Reynolds stress, i.e.:

$$-\overline{v'_i v'_j} \frac{\partial \bar{v}'_i}{\partial x_j} = \left[\frac{\mu_t}{\rho} \left(\frac{\partial \bar{v}'_i}{\partial x_j} + \frac{\partial \bar{v}'_j}{\partial x_i} \right) - \frac{2}{3} k \delta_{ij} \right] \frac{\partial \bar{v}'_i}{\partial x_j} = \left[\frac{\mu_t}{\rho} \left(\frac{\partial \bar{v}'_i}{\partial x_j} + \frac{\partial \bar{v}'_j}{\partial x_i} \right) \right] \frac{\partial \bar{v}'_i}{\partial x_j} \quad (2.26)$$

The fourth term on the right side of Equation (2.23) is the dissipation rate of turbulence energy (Equation (2.20)).

Following a similar manner as used in Equation (2.24), the last term in Equation (2.23) can be expressed as:

$$-\frac{\beta}{C_p} \overline{v'_i H'} g_i = \frac{1}{\rho} \frac{\beta}{C_p} \Gamma_{H,t} \frac{\partial \bar{H}}{\partial x_i} g_i \quad (2.27)$$

where $\Gamma_{H,t}$ is the turbulent diffusion coefficient of enthalpy.

Substituting Equations (2.24) to (2.27) into Equation (2.23), and introducing the effective diffusion coefficient, $\Gamma_{k,eff}$,

$$\Gamma_{k,eff} = \frac{\mu_t}{\sigma_{k,t}} + \mu = \frac{\mu_{eff}}{\sigma_k} \quad (2.28)$$

the k equation changes into:

$$\frac{\partial \rho k}{\partial t} + \text{div} (\rho \vec{V} k - \Gamma_{k,eff} \text{grad } k) = S_k \quad (2.29)$$

where S_k is the source for kinetic energy of turbulence. This is:

$$S_k = \mu_t \left(\frac{\partial \bar{v}_i}{\partial x_j} + \frac{\partial \bar{v}_j}{\partial x_i} \right) \frac{\partial \bar{v}_i}{\partial x_j} - \rho \epsilon + \frac{\beta}{C_p} \Gamma_{H,t} \frac{\partial \bar{H}}{\partial x_i} g_i \quad (2.30)$$

2.2.4 The equation of dissipation rate of turbulence energy

The dissipation rate of turbulence energy (ϵ) needs to be calculated, in order to determine μ_t in Equation (2.21). The governing equation for ϵ is derived by differentiating Equation (2.22) for x_k , multiplying both sides of

the equation by $2 \frac{\mu}{\rho} \frac{\partial v'_i}{\partial x_k}$, averaging of the equation, and using the continuity equation and definition for ϵ . The equation of dissipation of turbulence energy is then obtained as:

$$\begin{aligned} \frac{\partial \epsilon}{\partial t} + \frac{\partial}{\partial x_j} (\bar{v}_j \epsilon) &+ \frac{\partial}{\partial x_j} \left(\bar{v}_j \frac{\mu}{\rho} \frac{\partial v'_i \partial v'_i}{\partial x_k \partial x_k} \right) + 2 \frac{\mu}{\rho} \frac{\partial \bar{v}_i}{\partial x_j} \left(\frac{\partial v'_i \partial v'_j}{\partial x_k \partial x_k} + \frac{\partial v'_k \partial v'_k}{\partial x_j \partial x_i} \right) \\ &\text{Convection} \quad \text{Turbulent transport} \quad \text{Shear production} \\ + 2 \frac{\mu}{\rho} \frac{\partial^2 \bar{v}_i}{\partial x_k \partial x_j} \bar{v}_j \frac{\partial v'_i}{\partial x_k} &+ 2 \frac{\mu}{\rho} \frac{\partial v'_i}{\partial x_k} \frac{\partial v'_j}{\partial x_k} \frac{\partial v'_i}{\partial x_j} + 2 \frac{\mu^2}{\rho} \frac{\partial^2 v'_i}{\partial x_j \partial x_k} \frac{\partial^2 v'_j}{\partial x_j \partial x_k} \\ &\text{Gradient production} \quad \text{Turbulent Production} \quad \text{Dissipation} \end{aligned}$$

$$= - 2\frac{\mu}{\rho} \frac{\partial}{\partial x_i} \left[\frac{\partial V'_i}{\partial x_k} \frac{\partial}{\partial x_k} \left(\frac{p'}{\rho} \right) \right] + \frac{\mu}{\rho} \frac{\partial}{\partial x_j} \frac{\partial}{\partial x_j} \epsilon - 2\frac{\mu}{\rho} \frac{\beta}{C_p} \frac{\partial V'_i}{\partial x_k} \frac{\partial H'}{\partial x_k} \quad (2.31)$$

Diffusion Viscous transport Buoyancy production

Similar to the manner used in the k-equation, the fluctuating variables have to be connected with averaged variables. The third term on the left side of Equation (2.31) may be considered as turbulent diffusion caused by turbulent velocity V'_j . If $\Gamma_{\epsilon, t}$ stands for the turbulent dissipation coefficient for ϵ , the term can be approximated as:

$$\frac{\partial}{\partial x_j} \left(V'_j \frac{\mu}{\rho} \frac{\partial V'_i}{\partial x_k} \frac{\partial V'_i}{\partial x_k} \right) = - \frac{1}{\rho} \frac{\partial}{\partial x_j} (\Gamma_{\epsilon, t} \frac{\partial \epsilon}{\partial x_j}) \quad (2.32)$$

According to the analysis by Tennekes and Lumley (1972), terms four and five on the left side of Equation (2.31) are much smaller than term six at sufficiently high Reynolds numbers and therefore, they are negligible.

The sixth term then is approximated as:

$$2\frac{\mu}{\rho} \frac{\partial V'_i}{\partial x_k} \frac{\partial V'_j}{\partial x_k} \frac{\partial V'_i}{\partial x_j} = - C_{1k} \frac{\epsilon}{\rho} \frac{\mu}{\rho} \left(\frac{\partial \bar{V}_i}{\partial x_j} + \frac{\partial \bar{V}_j}{\partial x_i} \right) \frac{\partial \bar{V}_i}{\partial x_j} + C_{3p} \frac{\beta}{C_p} \frac{\epsilon}{\rho} \frac{1}{\Gamma_{H, t}} \frac{\partial \bar{H}}{\partial x_i} \quad (2.33)$$

where C_1 is a constant ($C_1=1.44$) (Launder and Spalding 1974) and C_3 is another constant ($C_3=1.44$) (Gunton et al 1983).

The seventh term on the left side of Equation (2.31) is approximated as:

$$2\frac{\mu^2}{\rho} \frac{\partial^2 V'_i}{\partial x_j \partial x_k} \frac{\partial^2 V'_i}{\partial x_j \partial x_k} = C_{2k} \epsilon^2 \quad (2.34)$$

where C_2 is a constant ($C_2=1.92$).

The first term and the last term on the right side of the equation are small and can be neglected.

The second term on the right side of Equation (2.31) is the transport term, which is caused by molecular diffusion, and needs not to be changed because of no fluctuating component.

Substitution of Equations (2.32) to (2.34) into Equation (2.31), the equation then changes into:

$$\frac{\partial \rho \epsilon}{\partial t} + \text{div} (\rho \bar{V} \epsilon - \Gamma_{\epsilon, \text{eff}} \text{grad} \epsilon) = S_{\epsilon} \quad (2.36)$$

where $\Gamma_{\epsilon, \text{eff}}$ is the effective dissipation coefficient for ϵ

$$\Gamma_{\epsilon, \text{eff}} = \Gamma_{\epsilon, t} + \mu = \frac{\mu_{\text{eff}}}{\sigma_{\epsilon}} \quad (2.37)$$

and

$$S_\epsilon = C_1 \mu_{tk} \frac{\epsilon}{\partial x_j} \left(\frac{\partial \bar{v}_i}{\partial x_j} + \frac{\partial \bar{v}_j}{\partial x_i} \right) \frac{\partial \bar{v}_i}{\partial x_j} - C_2 \rho \frac{\epsilon^2}{k} + C_3 \frac{\beta}{C_p} \xi_{ik} \frac{\epsilon}{\Gamma_{H,t} \partial x_i} \frac{\partial \bar{H}}{\partial x_j} \quad (2.38)$$

is the source for the dissipation of turbulence energy. Equations (2.29) and (2.36) are the so-called transport equations of the k- ϵ model which is used in fully developed turbulent flows. It was presented first by Harlow and Nakayama (1968) and revised by Launder and Spalding (1974).

2.2.5 The energy equation

Substituting Equation (2.7) into Equation (2.5), separating the mean variables and the fluctuating variables, and averaging for every term in the equation, the energy equation changes into:

$$\frac{\partial \rho \bar{H}}{\partial t} + \frac{\partial}{\partial x_j} (\rho \bar{v}_j \bar{H}) = \frac{\partial}{\partial x_j} \left(\frac{\lambda}{C_p} \frac{\partial \bar{H}}{\partial x_j} \right) - \rho \frac{\partial}{\partial x_j} (\overline{v_j' H'}) + S_H \quad (2.39)$$

The term related to fluctuating variables is $-\rho \frac{\partial}{\partial x_j} (\overline{v_j' H'})$ and may be considered as the additional enthalpy diffusion caused by turbulence. It can be approximated as:

$$-\rho \frac{\partial}{\partial x_j} (\overline{v_j' H'}) = \frac{\partial}{\partial x_j} (\Gamma_{H,t} \frac{\partial \bar{H}}{\partial x_j}) \quad (2.40)$$

If the effective turbulent diffusion coefficient for H, $\Gamma_{H,eff}$, is introduced:

$$\Gamma_{H,eff} = \Gamma_{H,t} + \frac{\lambda}{C_p} = \frac{\mu_{eff}}{\sigma_H} \quad (2.41)$$

then the energy equation can be expressed as:

$$\frac{\partial \rho \bar{H}}{\partial t} + \text{div} (\rho \bar{\mathbf{v}} \bar{H} - \Gamma_{H,eff} \text{grad} \bar{H}) = S_H \quad (2.42)$$

2.2.6 The concentration equation

The same method applied in Equation (2.5) can be used for the concentration equation (2.6) to yield:

$$\frac{\partial \rho \bar{C}}{\partial t} + \frac{\partial}{\partial x_j} (\rho \bar{v}_j \bar{C}) = \frac{\partial}{\partial x_j} (\rho D \frac{\partial \bar{C}}{\partial x_j}) - \rho \frac{\partial}{\partial x_j} (\overline{v_j' C'}) + S_C \quad (2.43)$$

The turbulent diffusion coefficient for concentration, $\Gamma_{C,t}$, is introduced for the second term on the right side of Equation (2.43) to yield:

$$-\frac{\partial}{\partial x_j}(\overline{\rho V_j' C'}) = \frac{\partial}{\partial x_j}(\Gamma_{C,t} \frac{\partial \bar{C}}{\partial x_j}) \quad (2.44)$$

where $\Gamma_{C,t}$ is calculated from:

$$\Gamma_{C,t} = \frac{\mu_t}{\sigma_C} \quad (2.45)$$

The σ_C in Equation (2.45) is the turbulent Schmidt number of concentration. If the effective diffusion coefficient $\Gamma_{C,eff}$ is employed, i.e.

$$\Gamma_{C,eff} = \rho D + \Gamma_{C,t} = \frac{\mu_{eff}}{\sigma_C} \quad (2.46)$$

and Equations (2.44), (2.45) and (2.46) are substituted into Equation (2.43), the concentration equation in turbulent flow is:

$$\frac{\partial \bar{C}}{\partial t} + \text{div}(\rho \vec{V} \bar{C} - \Gamma_{C,eff} \text{grad } \bar{C}) = S_C \quad (2.47)$$

2.2.7 Closure

If the superscript '-' over the variables in the governing equations is omitted, all these equations can be expressed in a single form:

$$\frac{\partial(\rho\phi)}{\partial t} + \text{div}(\rho \vec{V} \phi - \Gamma_{\phi,eff} \text{grad } \phi) = S_\phi \quad (2.48)$$

where ϕ , $\Gamma_{\phi,eff}$ and S_ϕ are given in Table 2.1.

2.3 Derivation of Finite-Domain Equations

Numerical simulations in a computer imply that the time and space dimensions have to be broken into finite intervals. Then the variables are correspondingly computed at only a finite number of locations in a four-dimensional space, the so-called grid points. This means that the continuous information contained in the exact solution of the differential equations is replaced with discrete values. The algebraic equations involving the unknown variable values at chosen grid points, which now are named the discrete equations, are derived from the differential equations.

From section 2.2, we obtained the transport equation for any one of the variables: 1, V_i , k , ϵ , H , and C as:

$$\frac{\partial(\rho\phi)}{\partial t} + \text{div}(\rho \vec{V} \phi - \Gamma_{\phi,eff} \text{grad } \phi) = S_\phi \quad (2.48)$$

TABLE 2.1

Values of ϕ , $\Gamma_{\phi,eff}$ and S_{ϕ} terms

ϕ	$\Gamma_{\phi,eff}$	S_{ϕ}
1	0	0 (continuity)
V_i	μ_{eff}	$-\partial p / \partial x_i - \rho \frac{\beta}{C_P} g_i \theta$
k	μ_{eff} / σ_k	$G - \rho \epsilon + G_B$
ϵ	$\mu_{eff} / \sigma_{\epsilon}$	$[\epsilon (C_1 G - C_2 \rho \epsilon) / k] + C_3 \frac{\epsilon}{k} G_B$
H	μ_{eff} / σ_H	S_H
C	μ_{eff} / σ_C	S_C
$G = \mu_t (\partial V_i / \partial x_j + \partial V_j / \partial x_i) \partial V_i / \partial x_j$ $G_B = \frac{\beta}{C_P} g_i \sigma_{H,t} \frac{\partial \theta}{\partial x_i}$ $\theta = H - H_0$ $C_1 = 1.44, C_2 = 1.92, C_3 = 1.44, C_D = 0.09, \sigma_k = 1.0, \sigma_{\epsilon} = 1.3, \sigma_H = 0.9, \sigma_C = 1.0$		

When $\phi=1$, Equation (2.48) is the continuity equation. It is often associated with the pressure variable in anticipation of the so-called pressure-correction equation. This equation is deduced from the finite-difference form of the continuity equation and will be discussed in section 2.3.2.

For simplicity, the problem is dealt with only in cartesian coordinates. The discrete method is the "finite-domain" manner (FDM) because the method is convenient in a regular geometry condition.

Figure 2.1 shows how the point is arranged in a control volume. For the grid point P, points E and W are its X-direction neighbours. The control volume around P is shown by thick lines. The location of the control-volume faces in relation to the grid point is midway between the neighbouring grid points. The "staggered grid" is introduced in the program. Figure 2.1 shows the point at which velocity components u, v, and w, pressure p and other main cell variable ϕ (k, ϵ , H, and C) are stored. The dashed-lines enclose the triads of points denoted by a single letter P. The cross-stream velocity u, v, and w are stored at just the points at which they are needed for the calculation of the convective contribution to the balances of ϕ . And the pressures are stored so as to make it easy to calculate the pressure gradient which affects u, v, and w.

2.3.1 The discrete equations for general variables

Integration of the general conservation equation (2.48) over the control cell P gives:

$$\iiint_V \frac{\partial(\rho\phi)}{\partial t} dV + \iiint_V \text{div} (\rho \vec{V} \phi - \Gamma_{\phi,eff} \text{grad } \phi) dV = \iiint_V S_{\phi} dV \quad (2.49)$$

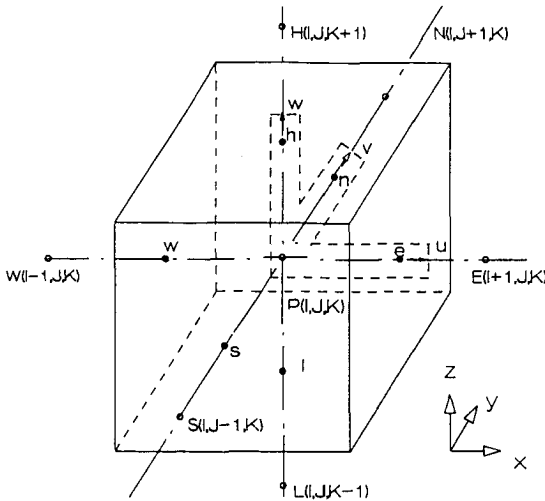


Figure 2.1 Grid information.

where V denotes the cell volume and A its surface area. Due to the "staggered grid", the control volume for velocities (u , v , and w) is different to that for main cell variables (k , ϵ , H , and C). The discrete equations for the main cell variables will be described first as follows.

In the transient term, ϕ is presumed uniform through-out the control cell, thus:

$$\iiint_V \frac{\partial(\rho\phi)}{\partial t} dV = V \frac{\partial(\rho\phi)}{\partial t} = \frac{V_P}{\delta t} (\rho\phi_P - \rho\phi_{P-}) \quad (2.50)$$

where V_P is the cell volume of P and ϕ_P is the ϕ in point $P(I,J,K)$ as shown in Figure 2.1. The "-" subscript refers to values prevailing at the start of the time interval δt . The transient terms will be treated as additional convection terms, because they may be considered as the mass flows through the two temporal faces of the control cell P (Rosten and Spalding 1981). This is why the space is defined as a four-dimensional one.

In the surface, integral variables are presumed constant over each cell face, thus:

$$\iiint_V \text{div} (\rho\vec{V}\phi - \Gamma_{\phi, \text{eff}} \text{grad } \phi) dV = \sum_{e,s,n,h,l} (\rho\vec{V}\phi - \Gamma_{\phi, \text{eff}} \text{grad } \phi) \cdot \vec{A} \quad (2.51)$$

The upwind scheme is introduced in the computer programs PHOENICS and CHAMPION SGE, in order to obtain correct and convergent solutions. This means that for the convection term, the value of ϕ at the grid point is on the upwind side of the face. If $\max(A,B)$ is defined to denote the greater of A and B , then the upwind scheme implies:

- when $i = e, n, h$

$$C_i \phi_i = \phi_P \max(\rho V_i A_i, 0) - \phi_I \max(-\rho V_i A_i, 0) \quad (2.52)$$

- when $i = s, w, l$

$$C_i \phi_i = \phi_P \max(-\rho V_i A_i, 0) - \phi_I \max(\rho V_i A_i, 0) \quad (2.53)$$

where C_i is the convective flux given in Table 2.3, and ϕ_I is the ϕ in point E, S, N, W, H, or L as shown in Figure 2.1.

Combining Equations (2.50) to (2.53), the expression for transient and convective terms becomes:

$$[\sum_i \max(0, \pm C_i)] \phi_P - [\sum_i \max(0, \pm C_i)] \phi_I \quad (2.54)$$

The Σ means over the cell face e, w, n, s, h, l, and t- and subscript I stands for the corresponding neighbour nodes E, W, N, S, H, L, and t-.

The diffusive flux contribution to the finite-domain equation given in Equation (2.51) may be written as:

$$\sum_i (-\Gamma_{\phi, \text{eff}} \text{grad } \phi) \cdot \vec{A} = - \sum_i D_i (\phi_I - \phi_P) \quad (2.55)$$

TABLE 2.2
Formulae for coefficients in Equation (2.59)

Coeff.	Formulae for the coefficients	
	Main cell variable	Velocity variable
a_E	$\max(D_e, D_e - C_e)$	$\max[0.5(D_e + D_{eF}), 0.5(D_e + D_{eF}) - 0.5(C_e + C_{eF})]$
a_W	$\max(D_w, D_w + C_w)$	$\max[0.5(D_w + D_{wF}), 0.5(D_w + D_{wF}) + 0.5(C_w + C_{wF})]$
a_N	$\max(D_n, D_n - C_n)$	$\max[0.5(D_n + D_{nF}), 0.5(D_n + D_{nF}) - 0.5(C_n + C_{nF})]$
a_S	$\max(D_s, D_s + C_s)$	$\max[0.5(D_s + D_{sF}), 0.5(D_s + D_{sF}) + 0.5(C_s + C_{sF})]$
a_H	$\max(D_h, D_h - C_h)$	$\max[0.5(D_h + D_{hF}), 0.5(D_h + D_{hF}) - 0.5(C_h + C_{hF})]$
a_L	$\max(D_l, D_l + C_l)$	$\max[0.5(D_l + D_{lF}), 0.5(D_l + D_{lF}) + 0.5(C_l + C_{lF})]$
a_T	C_t	C_t

TABLE 2.3
Formulae for the C's and D's in Table 2.2

Cell face	Convective fluxes	Diffusive coefficients
e	$\rho u_e A_e$	$[2 / (1/\Gamma_P + 1/\Gamma_E)] [A_e / (X_e - X_P)]$
w	$\rho u_w A_w$	$[2 / (1/\Gamma_P + 1/\Gamma_W)] [A_w / (X_P - X_w)]$
n	$\rho v_n A_n$	$[2 / (1/\Gamma_P + 1/\Gamma_N)] [A_n / (Y_n - Y_P)]$
s	$\rho v_s A_s$	$[2 / (1/\Gamma_P + 1/\Gamma_S)] [A_s / (Y_P - Y_s)]$
h	$\rho w_h A_h$	$[2 / (1/\Gamma_P + 1/\Gamma_H)] [A_h / (Z_h - Z_P)]$
l	$\rho w_l A_l$	$[2 / (1/\Gamma_P + 1/\Gamma_L)] [A_l / (Z_P - Z_l)]$
t	$\rho V_P / \delta_t$	-

where D_i is indicated in Table 2.3.

In the source term, ϕ is presumed uniform through-out the control cell, thus:

$$\iiint_V S_\phi dV = V_P S_\phi \quad (2.56)$$

where $V_P S_\phi$ may be expressed in the linearized form $S_O + S_P \phi_P$, viz.

$$V_P S_\phi = S_O + S_P \phi_P \quad (2.57)$$

Therefore, the finite-domain equation of the general conservation equation over the control cell P is:

$$[\sum_i \max(0, \pm C_i)] \phi_P - [\sum_i \max(0, \pm C_i)] \phi_I - \sum_i D_i (\phi_I - \phi_P) = S_O + S_P \phi_P \quad (2.58)$$

After re-arranging Equation (2.58), the general finite-domain equation for the value of ϕ at P becomes:

$$\phi_P = \frac{a_E \phi_E + a_W \phi_W + a_N \phi_N + a_S \phi_S + a_H \phi_H + a_L \phi_L + a_T \phi_T + S_O}{a_P} \quad (2.59)$$

where

$$a_P = a_E + a_W + a_N + a_S + a_H + a_T - S_P \quad (2.60)$$

and $a_E, a_W, a_N, a_S, a_H, a_L$, and a_T are the coefficients of the finite-domain equation for main cell variable ϕ and are given in Table 2.2 (Rosten and Spalding 1981). The subscripts refer to edges of main control cells.

The derivation of the discrete equations for velocities is similar to that for main cell variables. The final form is the same as Equation (2.59), but the coefficients are different and are presented in Table 2.2. (The subscript F denotes next cell face in the direction of the velocity component considered.) The source S_O for velocities is:

$$S_O = [-(p_* - p_P)A_*] + S_B V_P \quad (2.61)$$

where p stands for pressure and

$$[-(p_* - p_P)A_*] \begin{cases} = (p_P - p_E)A_e & \text{when } \phi = u \\ = (p_P - p_N)A_n & \text{when } \phi = v \\ = (p_P - p_H)A_h & \text{when } \phi = w \end{cases} \quad (2.62)$$

S_B is the source term caused by buoyancy.

2.3.2 The finite-domain equation for pressure correction

Thus far, finite-domain equations have been provided for calculating the three components of momentum and other main cell variables such as k , ϵ , H , and C . However, this does not ensure that the continuity equation is satisfied. The pressure-correction equation fills this gap. The momentum equations can be solved only when the pressure fields are given or somehow estimated. Unless the correct pressure field is employed, the resulting velocity field will not satisfy the continuity equation. Such an imperfect velocity field based on a guessed pressure field p^* will be denoted by u^* , v^* , and w^* . This "starred" velocity field will result from the solution of Equations (2.59) and (2.61) by replacing the variables with the "starred" ones. That is:

$$\phi_P^* = \frac{a_E \phi_E^* + a_W \phi_W^* + a_N \phi_N^* + a_S \phi_S^* + a_H \phi_H^* + a_L \phi_L^* + a_T \phi_T^* + [-(p_*^* - p_P^*) A_*] + S_B V_P}{a_P} \quad (2.63)$$

Now the aim is to find a way of improving the guessed pressure p^* in such a way that the resulting "starred" velocity field will progressively reach closer to satisfy the continuity equation. Let us propose that the correct pressure p is obtained from:

$$p = p^* + p' \quad (2.64)$$

where p' is called the pressure correction. The corresponding velocity corrections u' , v' , and w' can be introduced in a similar manner, viz.

$$u = u^* + u'; \quad v = v^* + v'; \quad w = w^* + w' \quad (2.65)$$

If Equation (2.59) is subtracted from Equation (2.63) and the terms, $a_I(\phi_I - \phi_I^*)$ ($I = E, W, \dots, P$), are dropped, the equation changes into:

$$\phi_P' = -d_* (p_*' - p_P') \quad (2.66)$$

where

$$d_* = \frac{A_*}{a_P} \quad (2.67)$$

According to Equation (2.62), Equation (2.66) can also be written as:

$$u' = d_e (p_P' - p_E'); \quad v' = d_n (p_P' - p_N'); \quad w' = d_h (p_P' - p_H') \quad (2.68)$$

The reason for dropping the terms, $a_I(\phi_I - \phi_I^*)$, is that otherwise they would have to be expressed in terms of the pressure corrections and the velocity corrections at the neighbours of the ϕ_P . These neighbours would, in

turn, bring up their neighbours and so on. Ultimately, the velocity-correction formula would involve the pressure correction at all grid points in the calculating domain. The resulting pressure-correction equation would then become unmanageable. The omission of the terms enables us to cast the p' equation in the same form as the general equation, and to adopt a sequential, one-variable-at-a-time, solution procedure. The omission of any term would, of course, be unacceptable, if it meant that the ultimate solution would not be the true solution of the discrete forms of the momentum and continuity equations. It so happens that the convergent solution given by the algorithm built in the program does not contain any error, which is resulted from the omission of the terms, $a_I(\phi_I - \phi_I^*)$ (Patankar 1980). This has been also checked in all the computations where the residual of continuity must be less than a specified small value.

The pressure correction equation is derived from the integration form of continuity Equation (2.10). The practice adopted for the fluxes across faces of the velocity cells is to average the fluxes through the nearby faces of main cells. This ensures that the fluxes used in the momentum balances satisfy local continuity, whenever the fluxes for the main cells satisfy continuity. Thus:

$$C_e - C_w + C_n - C_s + C_h - C_l + C_t - C_{t-} = 0 \quad (2.69)$$

The velocities calculated, which are based on the guessed pressure p^* , will not in general satisfy local continuity, so there is a finite continuity error. That is:

$$R^* = C_e^* - C_w^* + C_n^* - C_s^* + C_h^* - C_l^* + C_t^* - C_{t-}^* \quad (2.70)$$

where R^* is defined as the continuity error in the control cell P.

If now all the velocity components in Equation (2.69) are substituted by the expression given in the velocity-correction formulas, Equations (2.65) and (2.68), after re-arrangement by Equation (2.70), give the following finite-domain equation for pressure correction p' :

$$p'_P = \frac{a_E p'_E + a_W p'_W + a_N p'_N + a_S p'_S + a_H p'_H + a_L p'_L - R^*}{a_P} \quad (2.71)$$

where

$$a_P = a_E + a_W + a_N + a_S + a_H + a_L \quad (2.72)$$

The a 's are:

$$\begin{aligned} a_E &= \rho d_e A_e; & a_W &= \rho d_w A_w; & a_N &= \rho d_n A_n; \\ a_S &= \rho d_s A_s; & a_H &= \rho d_h A_h; & a_L &= \rho d_l A_l. \end{aligned} \quad (2.73)$$

Now all the equations needed have been formulated for obtaining the velocity components, all the main cell variables, and the pressure. They are

Equations (2.59) and (2.71). Equation (2.71) can also be regarded as a universal form as Equation (2.59), because it can be solved in the same procedure of Equation (2.59). A more detailed description on the mathematical derivation is presented by Chen (1987a).

2.4 Boundary Conditions

In order to complete the mathematical solution of the problem, it is necessary to provide boundary conditions. These, of course, depend on the problem but some general comments will now be discussed.

There are three types of boundary which are of practical importance:

(1) Free boundary: The boundary surface may be adjacent to an inviscid stream. An example is the outer edge of a turbulent jet.

(2) "No-flux" boundary: The boundary surface may coincide with a line of symmetry.

(3) Conventional boundary: The boundary surface coincides with a wall and this will arise from flow over solid bodies.

The first kind of the boundary condition is not met in our study and will therefore not be discussed.

2.4.1 "No-flux" boundary

If the y coordinate is supposed to be vertical to the surface, the "no-flux" boundary conditions can be described as:

$$\frac{\partial v_i}{\partial y} = 0, \quad \frac{\partial k}{\partial y} = 0, \quad \frac{\partial \epsilon}{\partial y} = 0, \quad \frac{\partial H}{\partial y} = 0, \quad \frac{\partial C}{\partial y} = 0 \quad (2.74)$$

In real flow problems, such boundaries do occur. For example, symmetry planes are of this kind. Often the zero flux boundary conditions present a large part of the boundary of the domain.

2.4.2 Conventional boundary

2.4.2.1 The Couette-flow

Near a wall, the velocity along the wall (assumed in x -direction) is small and therefore, the x -wise convection is locally negligible with respect to normal transport. Thus, near the wall, there exists a "Couette flow", i.e. a one-dimensional flow in which the conditions are determined primarily by the fluxes of mass, momentum and energy across the layer (Patankar and Spalding 1970). For this region, the mathematical problem is essentially that of solving ordinary rather than partial differential equations. Besides, the more attractive consequence is that such Couette-flow solutions can be obtained once for all and can be used as boundary conditions of particular solutions of the partial differential equations. It would be most convenient if the results of these Couette-flow analyses were expressed in the form of algebraic relationships. Indeed, it has been proved possible to derive some relations of this kind and the most commonly used relations are so-called wall-functions (Piece et al. 1982).

2.4.2.2 The Couette-flow equations

Patankar and Spalding (1970) presented the momentum and energy equations of boundary layer near a wall as:

$$\rho u \frac{\partial u}{\partial x} + \rho v \frac{\partial u}{\partial y} = \frac{\partial \tau}{\partial y} - \frac{dp}{dx} \quad (2.75)$$

$$\rho u \frac{\partial H}{\partial x} + \rho v \frac{\partial H}{\partial y} = - \frac{\partial}{\partial y}(q - u\tau) \quad (2.76)$$

where $q = \frac{\lambda}{C_p} \frac{\partial H}{\partial y}$ is the heat conduction on the surface, $\frac{\partial u\tau}{\partial y} = S_H$ is the work by shear stress. These two equations are derived from Equations (2.12) and (2.39).

If the variations of u and H with x can be neglected (Couette flow), Equations (2.75) and (2.76) can now be integrated immediately to yield:

$$\tau = \tau_s + m_s u + y \frac{dp}{dx} \quad (2.77)$$

$$-q = -q_s + m_s (H - H_s) - u\tau \quad (2.78)$$

where m_s is introduced for the product $\rho_s v_s$. It represents the mass flux across the layer, and must have a value independent of y , if matter is to be conserved. The subscript s denotes conditions in the fluid which is immediately adjacent to the wall (s stands for surface).

In order to simplify these equations prior to algebraic manipulation, the following set of dimensionless variables are used where the subscript c denotes the boundary of the Couette flow which is remote from the wall:

$$\begin{aligned} \tau^+ &= \tau/\tau_s; & y^+ &= y\sqrt{\tau_s \rho/\mu_c}; & u^+ &= u/\sqrt{\tau_s/\rho}; \\ p^+ &= \mu_c (dp/dx)/\sqrt{\tau_s^3 \rho}; & m^+ &= m_s/\sqrt{\tau_s \rho}; & q^+ &= q/q_s; \\ T^+ &= (H-H_s)\sqrt{\tau_s \rho}/(-q_s); & \mu^+ &= \mu_{eff}/\mu_c; & W &= \sqrt{\tau_s^3/\rho}/(-q_s) \end{aligned} \quad (2.79)$$

Then Equation (2.77) becomes:

$$\tau^+ = 1 + p^+ y^+ + m^+ u^+ \quad (2.80)$$

and Equation (2.78) takes the form:

$$q^+ = 1 + m^+ T^+ - W u^+ \tau^+ \quad (2.81)$$

In addition to these equations, the transport laws, Newton's for momentum and Fourier's for heat, are applied to Equations (2.80) and (2.81) to yield:

$$\frac{du^+}{dy^+} = \frac{1 + m^+ u^+ + p^+ y^+}{\mu^+} \quad (2.82)$$

$$\frac{dT^+}{dy^+} = \frac{1 + m^+ T^+}{\mu^+ / \sigma_{eff}} + \left(\frac{1 - \sigma_{eff}}{2} \right) W \frac{d(u^+)^2}{dy^+} \quad (2.83)$$

2.4.2.3 The wall functions

If the mixing-length hypothesis of Prandtl (1926) can be taken to describe the momentum transport in the fully turbulent part of a Couette-flow region, and if the magnitude of the mixing-length there can be taken as equal to κy ($\kappa = 0.435$ is von Karman constant), Patankar and Spalding (1970) reduced for this region:

$$\mu^+ = \kappa^2 (y^+)^2 \frac{du^+}{dy^+} \quad (2.84)$$

Substitute Equation (2.84) in Equation (2.82) in the following simple case:

$$m^+ = p^+ = 0; \quad u^+ = \frac{\ln(Ey^+)}{\kappa} \quad (2.85)$$

Here E is an integration constant and should be determined by experiment. For a smooth wall, however, E can be calculated with the supposition of the mixing-length hypothesis and the utilization of Van Driest's hypothesis (1956):

$$\mu_{eff} = \mu + \rho \kappa^2 y^2 [1 - \exp\{-y\sqrt{\tau\rho}/(\mu A^+)\}]^2 [\partial u / \partial y] \quad (2.86)$$

where A^+ is a constant ($A^+ = 26.0$ for a smooth wall). As the result, E is 9.0 for a smooth wall.

Often the equation (2.85) is written as:

$$u^+ = \frac{1}{\kappa} \ln(y^+) + C \quad (2.87)$$

where $C = \frac{1}{\kappa} \ln(E)$.

A special case where Equation (2.83) allows an analytical solution is that in which the mixing-length hypothesis prevails in the outer part of the Couette flow. Furthermore, there is no pressure gradient and there is negligible kinetic heating. Then Equations (2.83) and (2.82) can be combined, with the result:

$$\frac{dT^+}{du^+} = \sigma_{eff} \frac{1 + m^+ T^+}{1 + m^+ u^+} \quad (2.88)$$

Now, in the fully turbulent part of the layer, σ_{eff} takes on the constant value σ_t . Provided that the outer boundary lies in the fully turbulent region, we may integrate (2.88) to yield:

$$\ln(1 + m^+ T^+) = \sigma_t \{ \ln(1 + m^+ u^+) + m^+ P \}$$

where P is independent of u^+ , but may be expected to depend on both σ_t and m^+ . When the mass transfer rate is zero, this equation reduces to:

$$T^+ = \sigma_t (u^+ + P) \quad (2.89)$$

P can be regarded as an integration constant. For the part of the Couette flow where both laminar and turbulent transport are significant, according to Van Driest's hypothesis (1956), Patankar and Spalding (1970) showed that P can be determined from:

$$P = \frac{\pi}{4 \sin(\pi/4)} \left(\frac{A^+}{\kappa} \right)^{1/2} (\sigma/\sigma_t - 1) (\sigma_t/\sigma)^{1/4}$$

Equations (2.85) and (2.89) are the wall functions used by the author in the computer program PHOENICS for outside viscous layer. When uniform shear stress prevails in the boundary layer, the wall functions reproduce identically the full implications of the "logarithmic velocity profile". If the first grid point is located in the viscous sub-layer, linear velocity and temperature distributions are assumed.

Equation (2.87) is used as the "boundary condition" for velocities with the following expression for shear stress:

$$\tau_s/\rho = C_\mu^{1/2} k_p \quad (2.90)$$

The quantity k_p , the value of k for the grid point p (Figure 2.2), should be calculated from the regular balance equation of the finite-difference grid. Because of the steep velocity gradients in boundary layers, source terms of k for near wall are best expressed through τ_s (Pun and Spalding 1976),

$$S_k = \tau_s \frac{\partial u}{\partial y} - C_D \frac{\rho^2 k^2}{\tau_s} \frac{\partial u}{\partial y} \quad (2.91)$$

The boundary condition of energy-dissipation rate are calculated from (Pun and Spalding 1976):

$$\epsilon_p = C_\mu^{3/4} k_p^{3/2} / (\kappa y_p) \quad (2.92)$$

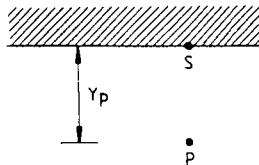


Figure 2.2 The near wall nodes.

For the concentration of contaminant, a wall function is not available in the program PHOENICS and CHAMPION SGE.

The wall functions for velocity and enthalpy used in the computer program CHAMPION SGE are similar to those for PHOENICS. They were presented by Van de Leur (1983).

2.4.3 Improvement of the wall functions

The logarithmic wall function derived in the former section is valid for turbulent boundary layers outside the viscous sub-layer which is identical to a y^+ value between 30 to 130. Moreover, it is applicable in fully developed boundary layers with a high Reynolds number as shown in Figure 2.3. For a zero-pressure-gradient turbulent boundary layer and a plane wall jet boundary layer, the figure indicates that the logarithmic equation (2.87) presents rather good results for both in the range $30 < y^+ < 130$. However, Hammond (1982a) showed that the logarithmic form presents a too high u^+ value for a plane wall jet when y^+ is greater than about 130. In contrast, Anderson et al (1984), Hancock and Bradshaw (1983) and Castro (1984) indicated that for a zero-pressure-gradient turbulent boundary layer, the logarithmic form gives a too small u^+ value in the outer region. The boundary velocity profile of airflow in a room may be located somewhere between that of the flow boundary of a wall plane jet and that of a zero-pressure-gradient turbulent boundary in the outer region. Nevertheless, there is no sufficient evidence to prove that the logarithmic equation can be applied for this region. Therefore, in numerical simulations of airflows in a room, the distance of the first grid node near a wall should be chosen to ensure its corresponding y^+ values to be less than 130.

But this choice may result in y^+ values which are in a range between 11.5 and 30 in some of the grid nodes. In computer programs PHOENICS and CHAMPION SGE, the linear velocity profile is applied for $y^+ < 11.5$ and the logarithmic velocity profile is used for $y^+ \geq 11.5$. Figure 2.3 shows that both the logarithmic velocity profile and linear velocity profile give a too high u^+

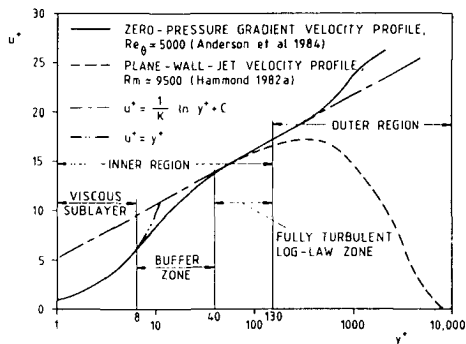


Figure 2.3 Velocity profiles in the turbulent boundary layer over a smooth flat plate.

value in the range $11.5 \leq y^+ \leq 30$. Therefore, it is necessary to develop another velocity profile for this range.

On the other hand, the overall turbulent Reynolds number ($Re_\tau = k^2/\epsilon\nu$) is considerably small in the present study. The logarithmic equation may not present good results under low Reynolds numbers. Many contributions have been published for the inner and outer regions of turbulent boundaries under low overall Reynolds numbers. Simpson (1970) presented an approach to the low Reynolds number effect by varying the von Karman constant κ and the Van Driest's constant A^+ for $R_\theta < 6000$ in the logarithmic velocity profile equation, where $R_\theta = u_\infty \theta/\nu$ is the Reynolds number based on momentum-deficit thickness θ . This implies a breakdown of the logarithmic profile at low Reynolds numbers. κ and A^+ are known to be functions of R_θ . Huffman and Bradshaw (1972) attempted to resolve the controversy by analyzing the existing data in duct flow. They felt if κ and C in Equation (2.87) are found to be constant in the turbulent duct flow, it would demonstrate the constancy of κ and C in the turbulent boundary layer flow since low Reynolds number turbulence is expected to be greater in duct flow than in boundary flow. They showed κ and C to be constant throughout the range of Reynolds numbers. Granville (1976) examined low Reynolds number data by means of an elaborate technique of curve-fitting and extrapolation. He estimated a minimum value of $R_\theta = 740$ for the existence of a turbulent boundary layer. Purtell (1978) performed low-velocity experiments which resulted in low Reynolds number boundary layer flows. He found that the logarithmic profile applies to all Reynolds number flows. It will produce similarity of the data at all Reynolds numbers in both the inner and outer layers. White (1981) presented experimental wind-tunnel data that show the universal logarithmic velocity profile for zero-pressure-gradient turbulent layer flow is valid for values of R_θ as low as 600. However, for values of R_θ between 425 and 600, the κ and C vary and are shown to be functions of R_θ and a shape factor H . Hammond (1982a) integrated Gebeci and Smith's (1974) velocity profile for jet flow and pointed out that for the inner layer κ should remain constant while Van Driest's constant, A^+ , is related to local Reynolds number $R_m (=u_m y_m/\nu)$ in power-law form when $2000 < R_m < 35000$. Here y_m is the cross-stream distance from the wall to the point where the jet velocity is maximum. The correspondence of the log-law "constant" E is also related to the local Reynolds number R_m in power-law form. However, he also indicated that the relations can only be used in the region $70 < y^+ < 170$.

It is observed from the foregoing studies that there is limited agreement about the nature of the turbulent boundary layer at low Reynolds numbers. In particular, the question about the universality of κ and C is not settled. Therefore, the logarithmic equation is used for the present study in the range $40 < y^+ < 130$ but with some modifications in the buffer zone of the boundary layer. The modifications are performed by introducing a logarithmic equation for the buffer zone ($8 \leq y^+ \leq 40$). That is, a new log-law velocity profile as shown in Figure 2.4 is presented by an equation of the form:

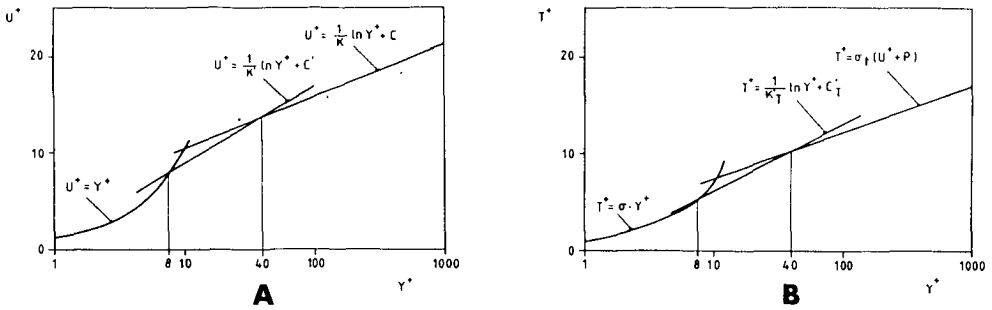


Figure 2.4 The near wall velocity and temperature profiles. (A) Velocity; (B) temperature.

$$u^+ = \frac{1}{\kappa'} \ln(y^+) + C' \quad (\text{when } 8 \leq y^+ \leq 40) \quad (2.93)$$

The κ' and C' in this equation can be determined by applying the following boundary conditions:

$$y^+ = 8, u^+ = y^+ = 8 \quad (\text{linear form}) \quad (2.94)$$

and

$$y^+ = 40, u^+ = \frac{1}{\kappa'} \ln(y^+) + C' = \frac{1}{0.435} \ln(40) + 5.05 = 13.53 \quad (\text{log-law form}) \quad (2.95)$$

Then, we obtain:

$$\kappa' = 0.291 \quad (2.96)$$

and

$$C' = 0.853 \quad (2.97)$$

The new log-law velocity profile gives better agreement with most of the measured results (Castro 1984) under low Reynolds numbers which are based on momentum-deficit thickness θ .

In the computer program PHOENICS, the original wall function for the wall heat transfer rate is evaluated from the Chilton-Colburn form of the Reynolds analogy (Gunton et al 1983). In this method, the Stanton number ($St = \alpha / (\rho V \cdot C_p)$, where α is the convective heat exchange coefficient and V is the velocity parallel to the wall), is related to the friction coefficient (C_f) as follows:

$$St = 0.5 C_f \sigma^{-2/3} \quad (2.98)$$

and C_f is related to the wall surface shear stress (τ_s) and V as follows:

$$C_f = \frac{\tau_s}{1/2 \rho V^2} \quad (2.99)$$

The heat-transfer rate at the wall q is then deduced from:

$$q = St \cdot \rho \cdot V \cdot C_p (T_p - T_s) \quad (2.100)$$

This equation and the log-law form equation (Equation 2.89) give more or less the same results. Compared to measurements in a room, the convective heat exchange coefficients calculated from the two equations are always too small (computations: 1.0-3.0 W/m²K and measurements: 2.0-5.0 W/m²K). Probably, this is because the overall turbulent Reynolds numbers in the room are lower than those under which the two equations were developed. Therefore, it is necessary to present an improved wall function for enthalpy.

If the similar method is employed for the temperature profile as for the velocity profile, the improved temperature profile equation can be written as:

$$T^+ = \frac{1}{\kappa'_T} \ln(y^+) + C'_T \quad (\text{when } 8 \leq y^+ \leq 40) \quad (2.101)$$

The boundary conditions are:

$$y^+ = 8, T^+ = \sigma \cdot y^+ = 5.68 \quad (2.102)$$

and

$$y^+ = 40, T^+ = \sigma_t (u^+ + P) = 10.44 \quad (2.103)$$

Hence, we have:

$$\kappa'_T = 0.338 \quad (2.104)$$

and

$$C'_T = -0.478 \quad (2.105)$$

Equations (2.93) and (2.101) have been used to simulate airflow in boundary layers in a room for the region $8 \leq y^+ \leq 40$. In this region, the convective heat exchange coefficients calculated from Equation (2.101) show better agreement with measurements (1.5 - 4.0 W/m²K).

It should be pointed out that in the region $y^+ < 8$, the linear temperature profile gives a too low value of convective heat exchange coefficient. Hence, it is necessary to explore another wall function for this region. Alamdari and Hammond (1983) and Bauman et al. (1984) presented some experimental formulas which can be employed for such kind of boundary conditions. Even so, these formulas are not suitable for mixed convections. Modifications of the formulas are necessary.

2.5 A brief Description of the Airflow Programs PHOENICS and CHAMPION SGE

In sections 2.3 and 2.4, we have formulated all the finite-domain equations needed to obtain the velocity components, enthalpy, concentration, kinetic energy, dissipation rate of turbulence energy and pressure and the corresponding equations for boundary conditions. The computer programs used and the solving algorithm will be discussed in this section.

2.5.1 PHOENICS

The computer code PHOENICS (Gunton et al. 1983) is the acronym for Parabolic, Hyperbolic or Elliptic Numerical Integration Code Series. This series of codes is capable of solving fluid-flow and heat- and mass-transfer problems in circumstances ranging in complexity from one-dimensional single-phase and steady, to three-dimensional multi-phase and transient. PHOENICS is used here to solve the three-dimensional conservation equations, in finite-domain form, of air mass, momentum, energy, concentration, kinetic energy and dissipation rate of kinetic energy, etc. which have been described in the former sections. The program is only available in binary code.

2.5.2 CHAMPION SGE

The computer program CHAMPION SGE (CHAMPION stands for Concentration, Heat And Momentum Program Instruction Outfit, the final N being added for euphony, and SGE for Satellite, Ground-station and Earth structure) is of the similar capacity as PHOENICS but it is a two-dimensional program (Chen 1987a). It has been developed by the author from CHAMPION 2/E/FIX (Pun and Spalding 1976) in following ways:

- Develop the code for concentration computations.
- Introduce a universal formula for all kinds of boundary condition descriptions which are often encountered in reality. That is:

$$S_{\phi, \text{Boundary}} = [C_{\phi} + C_{\text{mass}} (V_{\text{mass}} - p)] [V_{\phi} - \phi] \quad (2.106)$$

- Provide some new devices for getting convergent computational results and obtaining the results in a time as short as possible (such as false time step).
- Equip the program with certain limiting-value facilities: specific values can be prescribed to upper and lower limits of u , v , k , ϵ , H , C , etc., so that the relevant values cannot overstep the bounds of physical realism because the values of dependent variables may wander during their approach to a convergent solution. The final solution will not be affected, but the danger of divergence resulting from a poor initial guess will be greatly reduced.
- Construct a graphics computer code GROCS (which stands for Graphical Representation Of CHAMPION SGE) which provides display facilities for the numerical predictions obtained from the CHAMPION SGE code.
- Reorganize the original code CHAMPION 2/E/FIX into a user-friendly data input, general purpose code, which can easily be adapted for the solution of particular problems, in such a way that users can communicate with the code in very limited subroutines.
- Derive a very detailed description of the governing equations, boundary conditions, solving procedure and code structure (Chen 1987a). A general

instruction manual and a complete listing are also available (Chen 1987b, 1987c). The code can be installed in a micro-computer.

The CHAMPION SGE code is constructed from a central "Earth" code, which is the main solver and a "Satellite", which provides data input, defining specific problem. For special purposes, there are possibilities to provide additional coding which interacts with "Earth" during operations. This function is performed by the so-called "Ground-station" subroutine. The structure of CHAMPION SGE is shown in Figure 2.5 and is of very similar form as that of PHOENICS.

2.5.3 The calculation procedure of CHAMPION SGE

The detailed solving procedure of PHOENICS is unknown, because it is only available in binary code. However, CHAMPION SGE is very similar to PHOENICS and the complete listing is available. Therefore the calculating procedure of CHAMPION SGE will be described in this section.

From Tables 2.2 and 2.3, we can see that the coefficients in Equation (2.59) are functions of the ϕ 's and they are strongly-coupled. In order to obtain convergent and right results, an iterative, guess and correct procedure must be employed for the non-linear finite-domain equations.

The solution option of the finite-domain equations is the Jacobi point-by-point procedure. This means that ϕ_p (such as u , v , k , ϵ , H , and C etc.) is updated, for all nodes of the grid, from its neighbours, because all ϕ 's on the right-hand-side of Equation (2.59) have the values which they possessed before the updating "sweep" through the grid was commenced. That is, line values in x-direction are treated as known (temporarily), reducing the

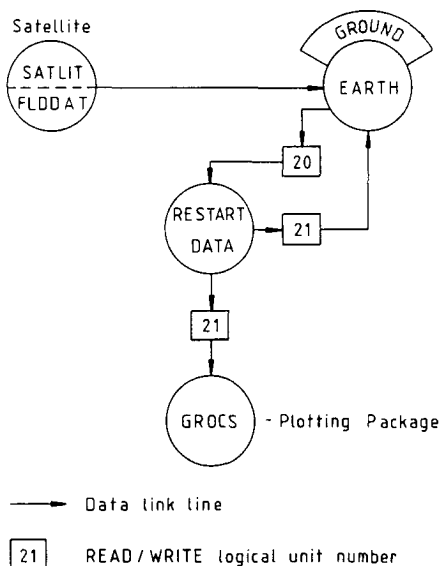


Figure 2.5 The structure for CHAMPION SGE.

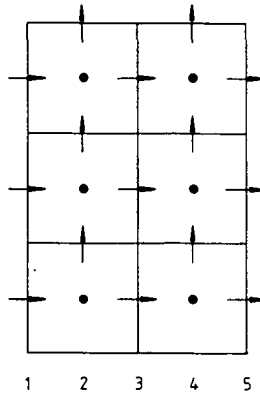


Figure 2.6 The solving process of CHAMPION SGE.

Equations (2.59) and (2.71) to:

$$\phi_P = N \phi_N + S \phi_S + B \quad (2.107)$$

where $N = a_N/a_P$, $S = a_S/a_P$ and $B = \frac{\text{source term} + a_E \phi_E^* + a_W \phi_W^*}{a_P}$ for two-dimensional, steady problems.

The ϕ 's are the in-store values of the ϕ 's. The equation sets are solved with line-by-line SIMPLE scheme (Patankar 1980) and by means of TDMA (Tri-Diagonal-Matrix Algorithm), which will be described as follows (see Figure 2.6):

- Solve momentum equations for u_3 's, v_2 's based on the in-stored values;
- Solve related equations for k , ϵ , H and C at line 2;
- Make uniform adjustment to u_3 's for overall continuity if the flow is parabolic (i.e. the continuity in line 3 must be satisfied);
- Check cell-wise continuity at line 2;
- Adjust p_2 's via pressure correction equation to satisfy cell wise continuity (i.e. the continuity in each cell must be satisfied);
- Adjust v_2 's and u_3 's appropriately according to the pressure correction;
- Make uniform adjustments to u_1 's and u_3 's for overall continuity;
- Iterate the whole procedure above at the same lines until the convergence criterion on the line has been satisfied or the maximum number of the iteration has been reached;
- Shift the control cells to the next-higher-x cells and repeat the whole procedure until the east boundary has been reached; and
- Sweep the whole field based on the values got from last sweep, until the convergence criterion on the field has been satisfied or the maximum number of sweeps has been reached.

2.6 Conclusions

The following paragraphs provide a summary of the more important conclusions which may be extracted from the present chapter:

(1) The nature and origin of turbulence was discussed to demonstrate the major differences between laminar flow and turbulent flow. The properties of turbulent airflow are briefly studied.

(2) Turbulence models have been reviewed in order to select one for the air movement and heat transfer in a room. The predictions of turbulence by computations are classified in turbulent transport models and large eddy simulations. Too much computing time is required by large eddy simulations so that at the present it is not suitable for the airflow modelling. Among turbulent transport models, Reynolds stress models are very complicated and are mainly used as subjects to research turbulence rather than as tools to solve engineering problems. Among the models using Boussinesq hypothesis, the $k-\epsilon$ turbulence model seems to be the most suitable one.

(3) The differential equations of a turbulent flow based on the $k-\epsilon$ model in their finite-domain forms were developed thoroughly. They are the mathematical model built in the computer programs PHOENICS and CHAMPION SGE. In addition, boundary conditions were developed in some detail in the form of wall functions.

(4) The original wall functions for enthalpy, H , used in programs PHOENICS and CHAMPION SGE give too small values of heat exchange coefficient (1.0-3.0 W/m^2K). In comparison with measurements (2.0-5.0 W/m^2K), they are too low. To correct this defect, we have modified the logarithmic form of the wall functions for y^+ in the range between 8 to 40. These improved wall functions lead to better convective heat exchange coefficients (1.5-4.0 W/m^2K).

(5) The two-dimensional computer program CHAMPION SGE was developed from the original one, CHAMPION 2/E/FIX. Now it is a user-friendly program.

CHAPTER 3

EXPERIMENTAL SETUP

Experiments were carried out in a full scale climate room which is $L=5.6$ m long, $W=3.0$ m wide and $H=3.2$ m high as shown in Figure 3.1. The thermal properties of the room enclosure materials are presented in Table 3.1.

The measurements can be classified as the following three types:

- field measurements of air velocity, temperature and contaminant concentration distributions;
- measurements of convective heat exchange on enclosure surfaces; and
- measurements of air-conditioning loads.

The measuring technique will be described in this chapter, whereas the measuring data will be the subject of chapters four and six.

3.1 Field Measurements of Air Velocity, Temperature and Contaminant Concentration Distributions

The venetian blinds near the window can be heated uniformly by electricity in order to simulate solar radiation. There is a cavity above the ceiling and one under the floor in which the temperature can be controlled to simulate the rooms above and below. The floor surface temperature of the space above the room was controlled to be the same as that of the room and the ceiling

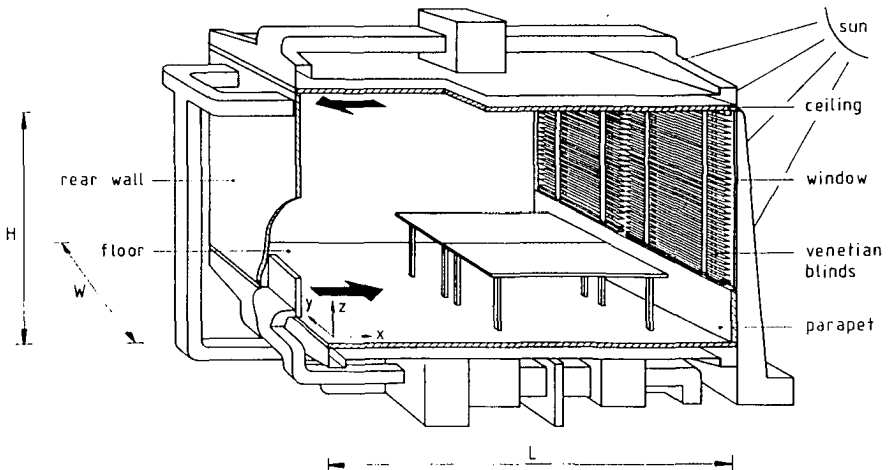


Figure 3.1 The climate room used for measurements.

TABLE 3.1
Room enclosure materials

Enclosure	Thickness m	Density kg/m ³	Specific heat J/kg·K	Thermal conductivity W/m·K
Ceiling	0.175	2300	840	1.9
Floor	0.175	2300	840	1.9
Rear wall	0.140	700	840	0.23
Side walls	0.140	700	840	0.23
Parapet	0.100	30	1470	0.035
Window	Outside glass: thickness 0.6 cm, absorption coeff. 0.018 Inside venetian blinds: slat angle 45°, slat width 5.5 cm the height between two slats 5.0 cm, absorption coeff. 0.3			

surface temperature of the space below the room to be the same as that of the room. When the room air temperature is higher than that of the inside surfaces of rear and side walls, these walls can be electrically heated to ensure the total heat exchange through these walls to be zero. The air temperature outside of the window can be set at a value between 0.0 to 40.0°C. The sensor for the control of the room air temperature was placed in the middle of the occupied zone (x=2.8 m, y=1.5 m and z=0.9 m). The set point of the sensor can be a value between 10.0 to 35.0°C. In order to simulate contaminant, a constant helium source combined with a certain amount of heat can be introduced in the point x=3.7 m, y=0.7 m and z=1.1 m. The constant flow of helium was supplied for a period of one hour.

The field measurements concerned those of airflow patterns, air temperature, velocity and helium concentration fields, enclosure surface temperatures, inlet mass flow, and inlet and outlet air temperatures. The airflow patterns were observed by using smoke. The velocities were measured through hot-wire anemometers and the temperatures by thermo-couples and all of them were connected to a data logger. The anemometers and thermo-couples were positioned in the middle section of the room (y=1.5 m) as shown in Figures 3.2(A) and 3.2(B). The helium concentration was measured by a portable gas monitor and its sampling tubes were placed in the section y=0.7 m as shown in Figure 3.2(C).

The air velocity in the room is quite small and a hot-wire probe can be used only for measurements near the inlets, where the velocity is relative high. The measurement of air velocities below 0.05 m/s with the hot wire anemometers is very difficult because of the calibration of the probes and the impact of free convection on the heat transfer from the probes. The thermo-couples are copper-constantan ones and their error after conversion by the data-logger is about 0.1°C. The smallest scale of the Helium meter is 0.1%. The accuracy of the calibration value for the heat flux meters is within 5%.

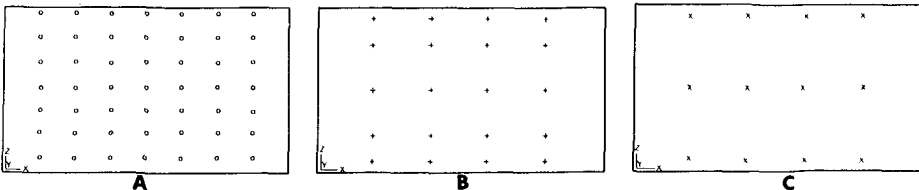


Figure 3.2 Measuring positions. (A) Anemometers in section y=1.5 m; (B) thermo-couples in section y=1.5 m; (C) concentration sampling points in section y=0.7 m.

The field measurements of air velocity, temperature and contaminant concentration distributions, etc. in the room were carried out for mixed convection and natural convection situations.

3.1.1 Mixed convection situations

3.1.1.1 Cooling cases

For cooling, four kinds of ventilation systems were used as shown in Figure 3.3.

- Cooling System 1: An inlet air diffuser with the dimension of 68 cm in height and 50 cm in width was on the floor near the rear wall. Two outlets were in the rear wall near the ceiling. A table, 175 cm long, 145 cm wide and 85 cm high was placed near the window.
- Cooling System 2: The air diffuser was installed on the floor near the window and there were two outlets in the rear wall near the ceiling. In this system, the table can not be placed near the window otherwise the inlet air is confined under the table.
- Cooling System 3: Two vertical inlet units were installed on the floor near the window. The inlet size for both of them was 100 cm in length and 1 cm in width. Two outlets were in the rear wall near the ceiling. The table was located near the window.
- Cooling System 4: Two horizontal inlets in the upper part of the rear wall were used. The inlet size was 25 cm long and 2 cm high each. Two outlets were in the rear wall near the floor.

3.1.1.2 Heating cases

The heating system concerned a mixture of natural convection with cold window surface and forced convection with a hot air supply (1000 W) in the rear wall of the room as shown in Figure 3.4. The heating unit, with a 20 cm wide and 4 cm high air supply slot and two return air slots on its sides, was placed in

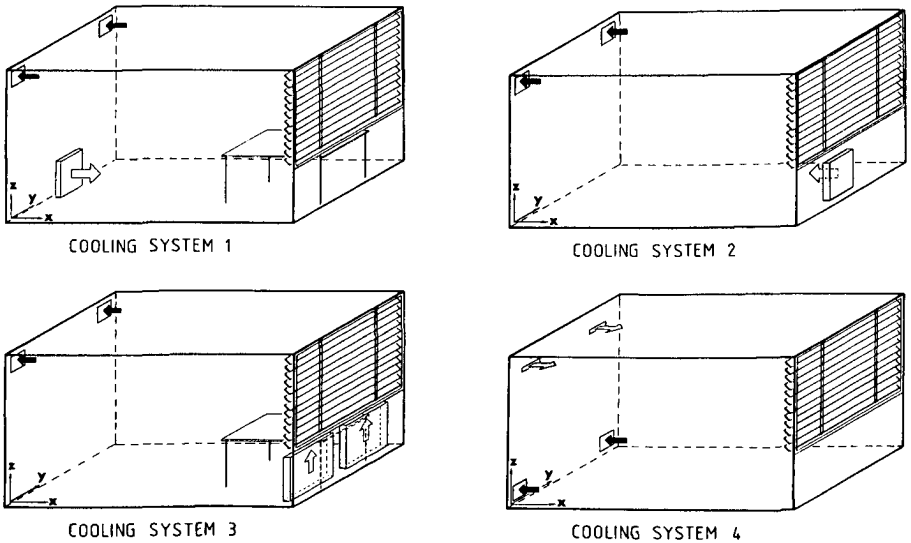


Figure 3.3 The cooling systems of the climate room.

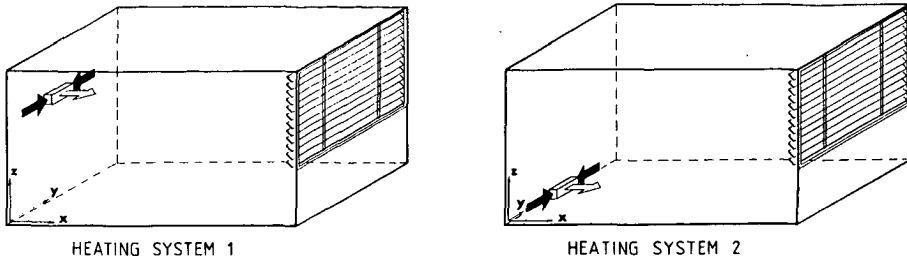


Figure 3.4 The heating systems of the climate room.

different vertical positions of the rear wall. The heating situations are divided into two systems as illustrated in Figure 3.4:

- Heating system 1: The heating unit was in the rear wall at two-third the height of the room; and
- Heating system 2: The heating unit was placed in the rear wall near the floor of the room.

3.1.2 Natural convection situations

The natural convection situation means that no cooling or heating inlets or outlets were used for the measurements. Only the wall surface temperatures and room air temperatures were controlled to be much different from the air temperature outside the window.

3.2 Measurements of Convective Heat Exchanges on Enclosure Surfaces

The convective heat exchange in the climate room was determined in order to validate the improved wall functions.

Twenty heat flux meters were distributed in ceiling, floor and side walls of the room respectively as indicated in Figure 3.5. The uniform distribution of the heat flux meters on the ceiling was used to measure the heat flux fields on the whole ceiling. The one line distribution on the floor was employed to study the feature of the gradually increasing or decreasing heat flow. Two heat fluxes next to each other on the vertical side wall were applied to check each other. These heat flux meters measured the sum of the convective and radiative heat flux on the enclosure surfaces. The surface temperatures, the corresponding air velocities and temperatures were also measured at the points about 10 cm above the heat flux meters.

In order to simulate the airflow and heat exchange mostly occurring in an

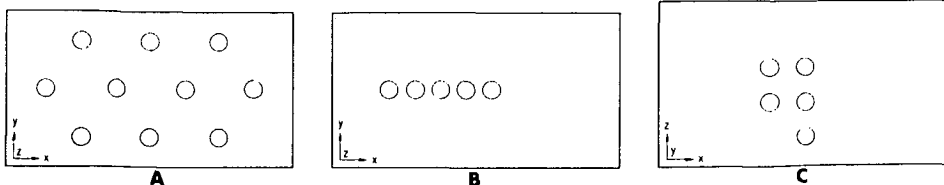


Figure 3.5 The measuring positions of the heat flux meters.
(A) On the ceiling; (B) on the floor; (C) on the side wall.

air conditioned room, different kinds of cooling, heating and natural convection systems as indicated in the former section were employed in this investigation. The ventilation rate was controlled to be 3, 5, 7 and 10 times per hour for the cases using cooling and about one time per hour for using heating units. The ventilation rate used in the present study is defined to be the ratio of the supplied mass flow (m^3/s) from the inlets of the room to the volume of the room (m^3). The heat supply on the venetian blinds was controlled to simulate absorbed solar radiation with a value in the range of 0 to 1000 W. The room enclosure surface temperatures were forced at a value varying between $10^\circ C$ to $30^\circ C$.

The convective heat exchange coefficient is determined from:

$$\alpha_c = q_c / (T_{\text{surface}} - T_{10}) \quad (3.1)$$

where T_{surface} is the surface temperature and T_{10} is the air temperature at the point about 10 cm above the surface. The convective heat flux, q_c , is calculated from:

$$q_c = q_t - q_r \quad (3.2)$$

where q_t is the total heat flux measured by the heat flux meters and q_r is the radiative heat flux. The q_r is determined by the following equation:

$$q_r = \sum_{j=1}^N q_{r_{i,j}} = \epsilon_i \psi_{i,j} (E_{b,i} - E_{b,j}) \quad (3.3)$$

where ϵ_i is the emissivity of the surface, $\psi_{i,j}$ is the radiative heat exchange factor between surfaces i and j , $E_{b,i}$ and $E_{b,j}$ are the emissive power of black body of surfaces i and j respectively. More detailed information will be described in section 5.2.3.2.

3.3 Measurements of Air-Conditioning Loads

The air-conditioning loads of the room with all the cooling systems can be measured. For the measurements, the room enclosure temperatures and air temperatures were initialized to be the same until steady situation (under the steady situation, the inlet air temperature was the same as the outlet air temperature). The venetian blinds then were heated with a constant electrical supply and the room air temperature at the point $x=2.8$ m, $y=1.5$ m and $z=0.9$ m was controlled to be always the same as the initial value and the inlet air mass flow, m , was maintained to be constant. The cooling load, Q , is calculated by the following equation:

$$Q = m C_p \Delta T \quad (3.4)$$

where ΔT is the measured air temperature difference between the outlet and the inlet.

In most cases, the air temperature difference, wall surface temperatures and field air temperature distributions were measured every 15 minutes.

CHAPTER 4

COMPUTATIONS AND VALIDATIONS OF INDOOR AIRFLOW, HEAT TRANSFER AND AIR QUALITY

In this chapter, the computations of air movement and air quality of the climate room by computer programs CHAMPION SGE and PHOENICS will be presented for the air supply systems described in chapter 3. The corresponding measured results will be used for validation.

For the computations of airflow in the room by the computer programs CHAMPION SGE and PHOENICS, the boundary conditions, such as inlet mass flow rate, inlet air temperature, and wall surface temperatures, must be known. The cooling load program ACCURACY is applied to obtain these boundary conditions. ACCURACY calculates the radiative heat exchange between the room enclosure surfaces, the transient heat conduction in the enclosures, and determines the enclosure surface temperatures and air-conditioning load of the room. When the inlet mass flow is fixed, the inlet air temperature which is required by the airflow programs can be calculated from the air-conditioning load. The convective heat exchange between the venetian blinds and the room air can also be calculated in the program ACCURACY and is inserted in the airflow programs as a thermal source near the window. A detailed description of the cooling load program will be discussed in chapter 5.

4.1 Two-Dimensional Calculations and Validations

This section briefly presents the computed results of air movement in a room by the two-dimensional airflow computer program CHAMPION SGE. The three-dimensional results computed by PHOENICS, which are presented in section 4.2, are also employed for the comparison. More results about the two-dimensional computations by CHAMPION SGE can be found in the literature (Chen 1985b, 1986a, Chen and Van der Kooi 1987a).

4.1.1 Method with thermal sources/sinks for heat transfer in the third dimension

Generally speaking, a two-dimensional computer program can only be used in situations which can be reasonably approximated as being two-dimensional. Examples are the cooling system 3 or the natural convection system described in chapter 3. The heat transfer through the side walls (the third dimension) can be ignored, if the thermal conditions in the adjacent rooms are more or less the same. But in many cases, for instance if the side walls are external, the errors caused by the approximation will be large and unacceptable. In order to solve the problem above, a reasonable approximation is to consider the heat transfer through the side walls as additional thermal sources or sinks.

In the governing equation (2.42), S_H is 0 under normal conditions. For each side wall, the additional thermal sources (if the temperatures on the side walls are higher than those in the corresponding grid points) or sinks (if they are lower) can be introduced into the term S_H by the following equation:

$$S_H = \alpha_c (T_s - T_p) A_p \quad (4.1)$$

where T_p is the temperature value in grid P and T_s is the temperature on the side wall. A_p is the cell area and α_c has the physical meaning of a convective heat exchange coefficient.

If the heat transfer in both side walls has to be considered, the total heat source is:

$$S_H = S_{H1} + S_{H2} \quad (4.2)$$

where S_{H1} and S_{H2} are the sources for the two side walls respectively.

It can be assumed that buoyancy is a dominant factor in the heat transfer through the side walls (the third dimension). Therefore, the coefficients, α_c 's, may be computed via (Alamdari and Hammond 1983):

$$\alpha_c = ([b_1(\Delta T/L)^{b_3}]^{b_5} + [b_2(\Delta T)^{b_4}]^{b_5})^{1/b_5} \quad (4.3)$$

where $\Delta T = |T_s - T_p|$, L is the characteristic length scale which is the height of the room, $b_1=1.5$, $b_2=1.23$, $b_3=1/4$, $b_4=1/3$ and $b_5=6$. This formula is originally derived for natural convection.

Let us take the natural convection system described in section 3.1.3 as an example. The room temperature was initialized at 15.0°C by a large ventilation while the outside air temperature on both side walls was 22°C. This resulted in an inside surface temperature of the side walls which was 2°C higher than that of the room air under steady conditions. The air temperature outside the window was controlled at 3.0°C.

The measured and predicted results by CHAMPION SGE with the introduction of an extra source term are shown in Figure 4.1. The agreement between the two-dimensional computations and experiments is fairly good.

The second example is cooling system 3 as described in section 3.1.1. The inlet mass flow of the room was 0.075 m³/s which corresponded with a ventilation rate of five times per hour. The electrical supply on the venetian blinds was 950 W. The air temperature in the middle of the occupied zone was controlled at 23.0°C. The inlet air temperature was 14.9°C according to the measurements and 15.2°C according to the computation by ACCURACY. The reason for the difference is that the measurement was not performed under a real steady condition. The heat obtained from the floor was smaller than that transferred into the ceiling. Therefore, the inlet air temperature required can be higher. A more detailed discussion is given in chapter 6.

The measured and computed results by the CHAMPION SGE code and PHOENICS (3D) code are shown in Figure 4.2. The agreement between the two- and three-dimensional computations and experiments on velocity and temperature fields is rather reasonable. It is assumed that 25 W convective heat was generated

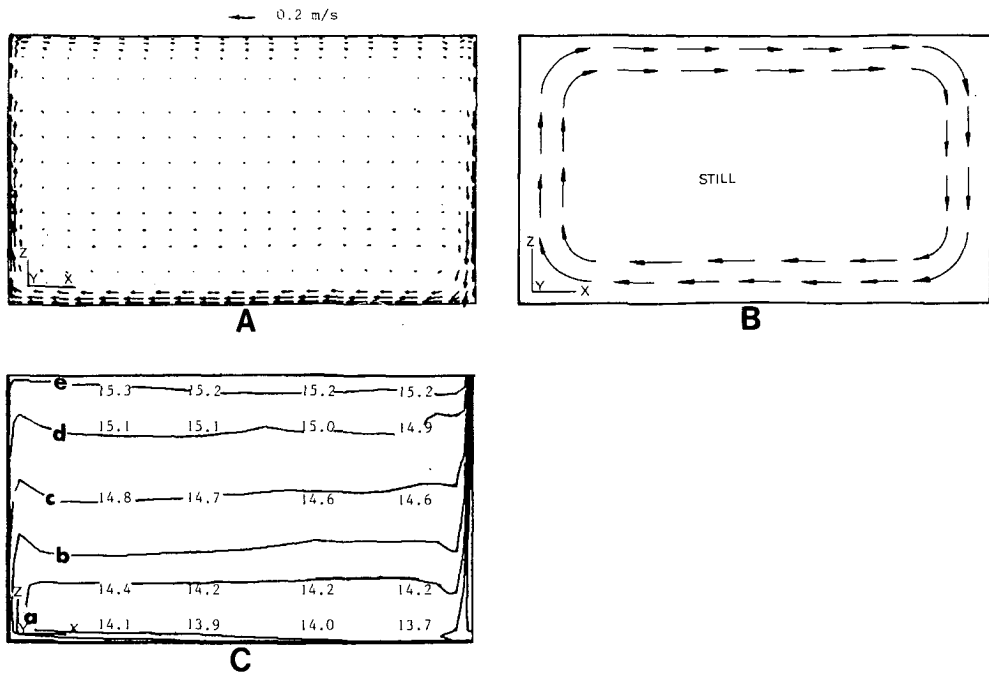


Figure 4.1 The computed and measured results for the natural convection. (A) Computed air velocity distribution by CHAMPION SGE; (B) airflow pattern observed by using smoke; (C) computed (contours) and measured (numerical values) temperature field ($^{\circ}\text{C}$)*. * Contour key for C: a-14.0, b-14.3, c-14.6, d-14.9, e-15.2.

by a human body. This source can be simulated in the three-dimensional computation but not in the two-dimensional computation, because the source is only presented in one point. This causes the difference in the air velocity distributions in the area above the table between the two- and three-dimensional computations. Because each inlet is 1.0 m long and the room width for half of the room is 1.5 m, the inlet air velocity used in the two-dimensional computation is 1.0/1.5 times smaller. As a consequence, this causes a discrepancy in the region near the inlets between the two- and three-dimensional computations. Although there are no air velocity values measured, the airflow pattern observed by smoke shows similar results.

4.1.2 Concentrated method

When the width of the ventilating units is much smaller than the width of the room, like cooling system 1 described in section 3.1.1, two-dimensional computation will cause a very big error. If only the shaded section in Figure 4.3 is considered, all heat transfer through the ceiling, floor, window, rear wall and parapet is concentrated together on the corresponding shaded section. The heat transfer through the side walls can also be set by thermal sources or sinks as treated in section 4.1.1. Because the location of outlets has a small influence on airflow patterns, the two outlets in the system can be replaced by the one in the shaded section. By this method, the heat transfer through the shaded section can be calculated in two ways. The first

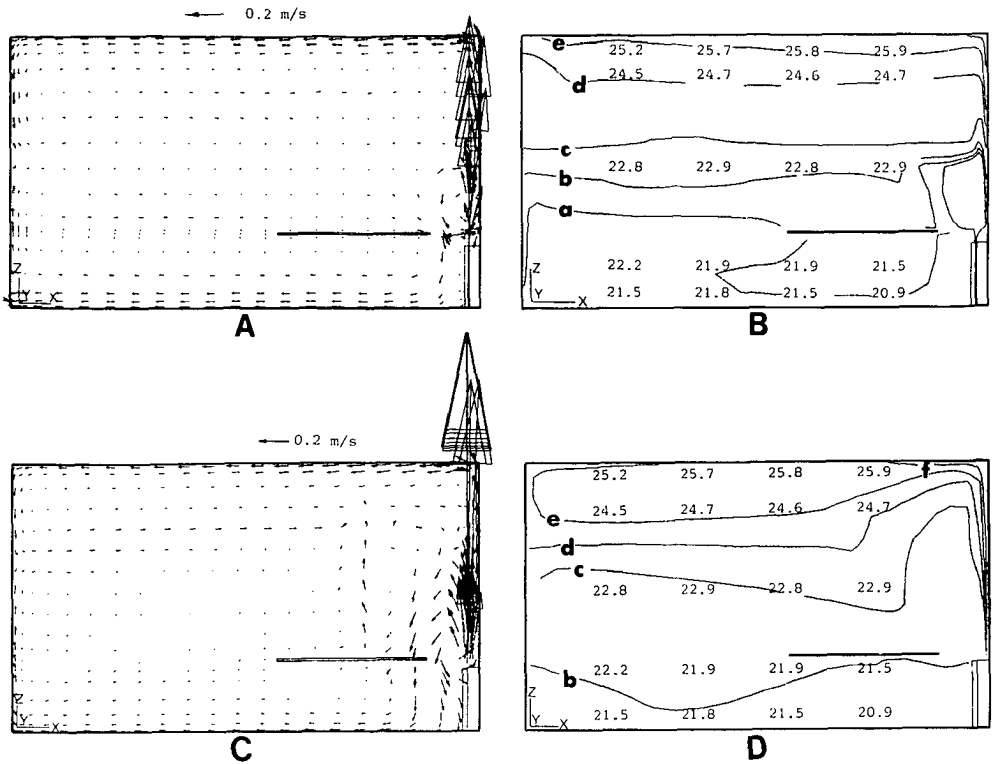


Figure 4.2 The computed and measured results for cooling system 3. (A) Computed air velocity distribution by CHAMPION SGE; (B) temperature field of measurements (numerical values) and computation by CHAMPION SGE (contours) ($^{\circ}\text{C}$)*; (C) computed air velocity distribution by PHOENICS in section $y=1.5\text{ m}$; (D) temperature field of measurements (numerical values) and computation by PHOENICS (contours) in section $y=1.5\text{ m}$ ($^{\circ}\text{C}$)*.

* Contour key for B and D: a-21.0, b-22.0, c-23.0, d-24.0, e-25.0, f-26.0.

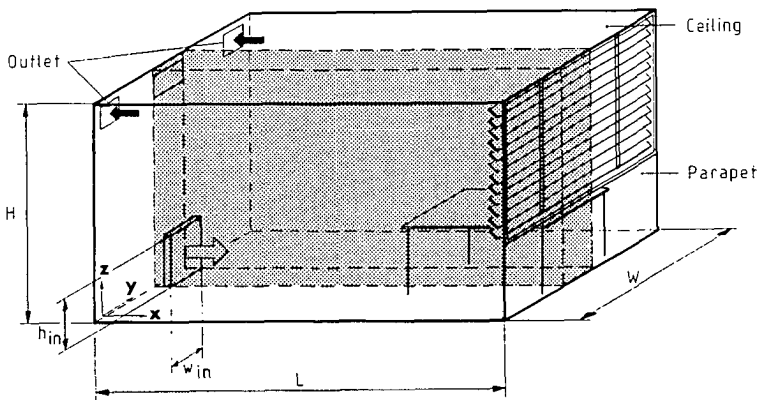


Figure 4.3 Flow and heat transfer are concentrated on the shaded section.

one is to increase the heat exchange coefficients by W/w_{in} times (w_{in} is the width of the inlet.) and the second one is to estimate the total heat transfer on the walls and insert this heat as thermal sources on the boundary cells. In fact, the two methods present the same results. The heat transfer on the side walls can be calculated by the method described in section 4.1.1.

In cooling system 1 as described in Figure 4.3, the inlet mass flow through the cooling unit was $0.105 \text{ m}^3/\text{s}$, which corresponded with a ventilation rate 7 times/hour and an inlet air velocity of 0.37 m/s . A 950 W heat was introduced on the venetian blinds to simulate the solar radiation absorbed by the window. The room air temperature in the middle of the occupied zone was controlled at 23.0°C . The inlet air temperature was 19.6°C according to the measurements and 19.4°C according to the computation by ACCURACY. A contaminant source, 0.5% of the total mass inflow together with a 25 W heat source, was introduced in a point above the table ($x=3.7 \text{ m}$, $y=0.7 \text{ m}$, $z=1.1 \text{ m}$).

The computations by CHAMPION SGE and PHOENICS and the measurements of the velocity and temperature distributions are shown in Figure 4.4. The two-dimensional computational results, compared to the three-dimensional computations and the measurements, were quite reasonable but there were some discrepancies. Although the airflow patterns look similar, the computed air velocities by CHAMPION SGE were almost twice the values of the three-dimensional computation (the three-dimensional one shows fairly good agreement with the measurements which will be discussed in next subsection). These differences were caused by the approximation. In fact, the flow is limited in the shaded section and the inlet velocity remains the same in the concentrated method. This increases the velocity in the room and results in a more uniform temperature distribution. But the limitation of mass transfer in the shaded section makes the temperature gradient in vertical direction larger. Because the two influences compensate each other, the room air temperature distributions are nearly the same as those obtained from the measurements. The concentration distribution near the source point computed by CHAMPION SGE was much different from that of the three-dimensional computation and the measurements.

In brief, this method can only be applied for obtaining preliminary information of airflow and heat transfer in a room.

4.1.3 Adjusted inlet temperature method

For acquiring approximated numerical results by a two-dimensional calculation on temperature and velocity distributions, another method is to keep the inlet opening height and inlet velocity constant and to adjust the inlet temperature to satisfy the energy balance in the room. This, in fact, assumes the inlet openings to be extended over the whole width of the room. In other words, it implies that the mass flow supplied into the room is increased. If the inlet size of cooling system 4 is w_{in} in width and h_{in} in height, the inlet velocity is v_{in} and inlet temperature is T_{in} , this method remains the inlet height and velocity unchanged and adjusts the inlet temperature to be $T_{d,in}$. The $T_{d,in}$ is calculated from the following inflow energy balance equation:

$$(T_{d,in} - T_{out}) \cdot v_{in} \cdot W \cdot h_{in} = (T_{in} - T_{out}) \cdot v_{in} \cdot w_{in} \cdot h_{in} \quad (4.4)$$

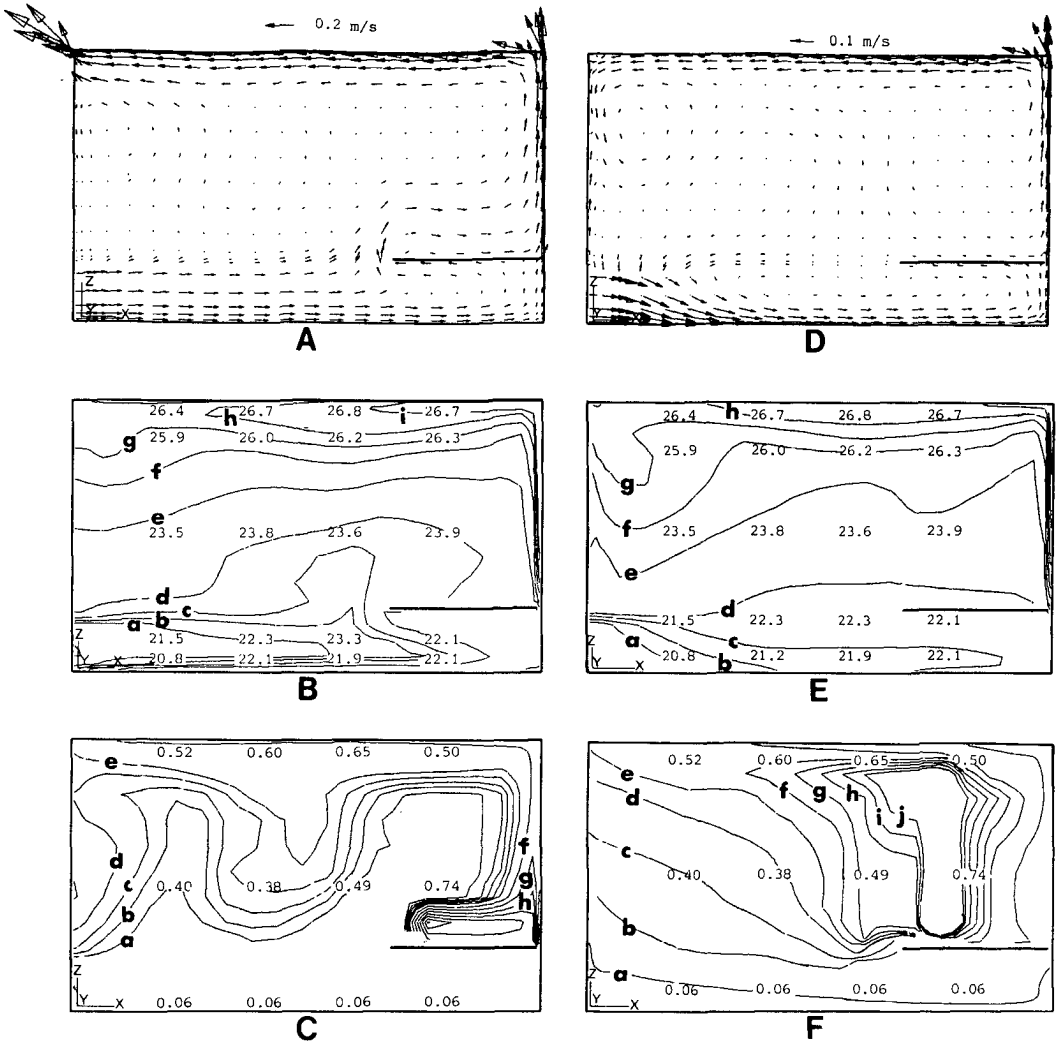


Figure 4.4 The computed and measured results for cooling system 1. (A) Computed air velocity distribution by CHAMPION SGE; (B) temperature field of measurements (numerical values) and computation by CHAMPION SGE (contours) ($^{\circ}\text{C}$)*; (C) concentration field of measurements (numerical values) and computation by CHAMPION SGE (contours) (%)#; (D) computed air velocity distribution by PHOENICS in section $y=1.5$ m; (E) temperature field of measurements (numerical values) and computation by PHOENICS (contours) in section $y=1.5$ m ($^{\circ}\text{C}$)*; (F) concentration field of measurements (numerical values) and computation by PHOENICS (contours) in section $y=1.5$ m (%)#.

* Contour key for B and E: a-20.0, b-21.0, c-22.0, d-23.0, e-24.0, f-25.0, g-26.0, h-27.0, i-28.0.

Contour key for C and F: a-0.1, b-0.2, c-0.3, d-0.4, e-0.5, f-0.6, g-0.7, h-0.8, i-0.9.

or

$$T_{d,in} = T_{out} + (T_{in} - T_{out}) \cdot w_{in} / W \quad (4.5)$$

When $w_{in} = W$ (width of the room), $T_{d,in} = T_{in}$, this becomes a real two-dimensional problem. This method can be explained by assuming that the mixing in the zone near the inlet is so quick that air temperature increases rapidly. Therefore, this method is suitable for the system with a strong inlet induction effect.

The calculated and measured results of the cooling system 4 are illustrated in Figure 4.5. Although the airflow pattern observed by smoke was not presented, it was similar to the computations. The airflow pattern by the two-dimensional computation was in good agreement with that through the inlet section ($y=0.75$ m) by the three-dimensional computation. However, the air velocities in the middle of the room by the two-dimensional computation are at least twice as large as those by the three-dimensional computation. This is because the mass flow supplied in the two dimensional computation is increased. The temperature distribution showed better agreement with that of the three-dimensional computation and the measurements in the middle section ($y=1.5$ m). More information about the difference in different sections will

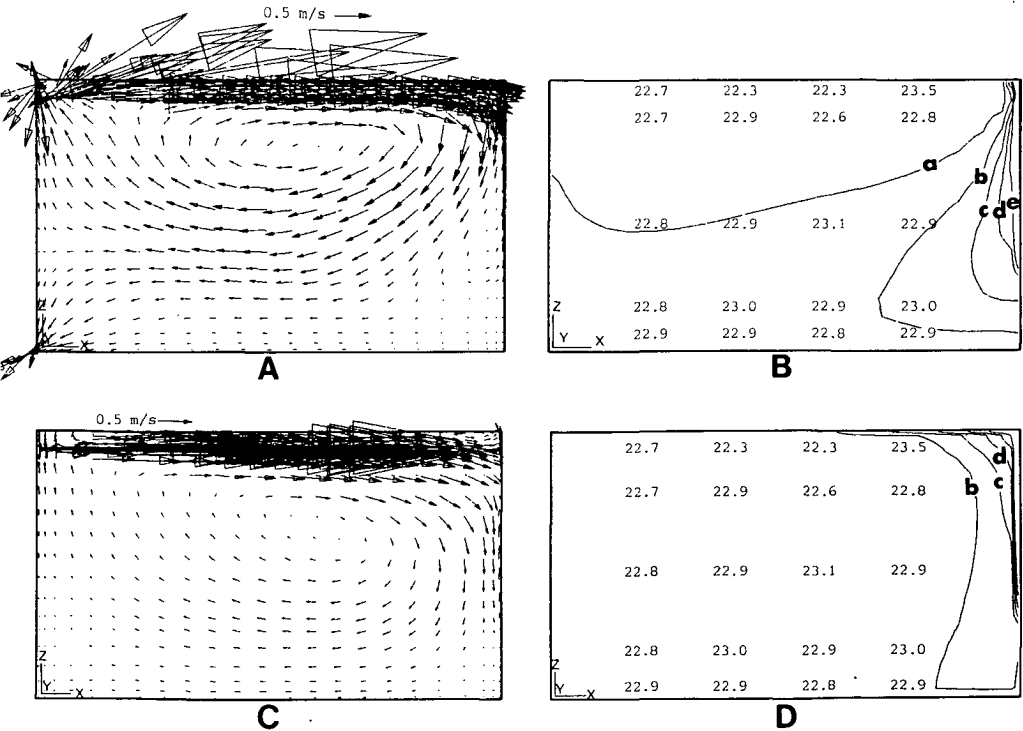


Figure 4.5 The computed and measured results for cooling system 4. (A) Computed air velocity distribution by CHAMPION SGE; (B) temperature field of measurements (numerical values) and computation by CHAMPION SGE (contours) ($^{\circ}\text{C}$)*; (C) computed air velocity distribution by PHOENICS in section $y=0.75$ m; (D) temperature field of measurements (numerical values) and computation by PHOENICS (contours) in section $y=1.5$ m ($^{\circ}\text{C}$)*.

* Contour key for B and D: a-22.0, b-23.0, c-24.0, d-25.0, e-26.0.

be discussed in next section.

This method has also been applied for cooling system 1. Due to the fact that the induction by the inlet air is small in the this system, it will cause very large errors.

It can be concluded that this method can only be used for obtaining initial airflow information in a room where the inlet flow induction is very strong.

4.1.4 Remarks and conclusions of the two-dimensional computations

From the two-dimensional computational results presented above, the following paragraphs summarize the important conclusions and remarks:

(1) The first approximation, which treats the heat transfer through the side walls in the third dimension as thermal sources or sinks in nearly two-dimensional situations, gives fairly good predictions on temperature and velocity distributions of the room.

(2) The concentrated method and the adjusted method are very useful to get general information, such as velocity patterns, temperature distributions. If precise results are required, the numerical predictions are not satisfactory.

(3) The adjusted inlet temperature method is suitable for the system with strong inlet airflow induction.

(4) When the proportion of room width to the inlet width is larger than 5.0, the two methods will cause too big discrepancies between computations and measurements. In this case, three-dimensional computations are required.

(5) The two-dimensional CHAMPION SGE code combined with the methods above only costs 2 minutes CPU time for a grid number 18x27 in an IBM 3083 JX1 computer. Two-dimensional computations are much cheaper compared to three-dimensional computations by PHOENICS which will be discussed in the following section. This is the reason why the approximated methods are studied.

4.2 Three-Dimensional Simulations and Validations

Due to the difficulties mentioned in the former section, it is necessary to simulate the indoor airflow in a room by a three-dimensional program. In this section, the PHOENICS computer program is used for the investigation. The experimental and computational results, temperature and contamination distributions will be reported in four groups:

- (1) different ventilating systems for cooling;
- (2) different ventilation rates;
- (3) different heat gains from the venetian blinds; and
- (4) different heating systems.

More results of computations by PHOENICS and experiments can be found in the literature (Chen 1985a, 1986b, Chen and Van der Kooi 1987b, Chen et al. 1988).

In order to evaluate objectively the effects of ventilation and its influence on indoor air quality and energy saving, two terms, ventilation efficiency (η_V) and temperature efficiency (η_T), are introduced. They are defined as:

$$\eta_V = \frac{C_{out} - C_{in}}{C_{occu} - C_{in}} \quad (4.6)$$

and

$$\eta_T = \frac{T_{out} - T_{in}}{T_{occu} - T_{in}} \quad (4.7)$$

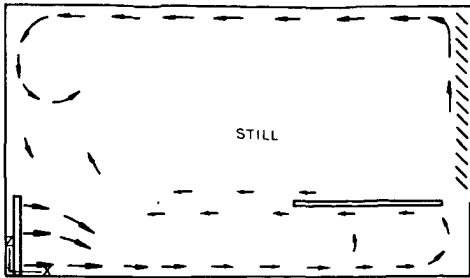
where C_{occu} is the air contaminant concentration in an occupied zone and T_{occu} is the air temperature in an occupied zone. In this section, C_{occu} is the air contaminant concentration at point $x=2.2$ m, $y=0.7$ m and $z=1.6$ m and T_{occu} is the air temperature at point $x=2.2$ m, $y=1.5$ m and $z=1.6$ m, because the measurements presented are carried out only in a few points. It is not possible to obtain a precise average value of the zone of occupation from the measurements.

When room air is perfectly mixed, η_V and η_T are one. For well-organized room air distributions, η_V and η_T have values higher than one. The ventilation efficiency and the temperature efficiency only represent a relative evaluation of an air-conditioning system. If quantitative results, such as the amount of energy saved, are required, the dynamic behaviour of heat transfer and airflow in the room must be considered under real weather conditions. A more detailed description will be presented in chapter 7.

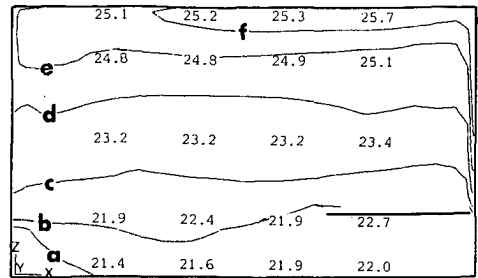
4.2.1 Different ventilating systems for cooling

In this group, the mechanical ventilation rate was controlled at five times/hour ($0.075 \text{ m}^3/\text{s}$) for all four cooling systems. The heat introduced in the venetian blinds was 600 W for cooling systems 1 and 2, and 950 W for cooling systems 3 and 4. The higher the heat on the venetian blinds, the lower the inlet air temperature required. Therefore, the 600 W heat was chosen for cooling systems 1 and 2 to prevent the inlet air from causing a draught in the occupied zone, because it was supplied directly into the lower part of the room through the air diffuser. However, for the cooling systems 3 and 4, where the inlet jets were used to supply air outside the occupied zone, the induction by the jets increased the inlet air temperature and made it possible to use a lower inlet air temperature. This is the reason that the heat on the venetian blinds was controlled at 950 W for these two cooling systems. A constant helium source combined with 25 W heat is introduced in point $x=3.7$ m, $y=0.7$ m and $z=1.1$ m. The 25 W heat is used to simulate the convective heat released from a human body.

The airflow, temperature and helium concentration distributions obtained from the computations and measurements of cooling system 1 are shown in Figure 4.6. The temperature efficiency and the ventilation efficiency are given in Table 4.1. The agreement between the computations and the measurements is good although there are some discrepancies in the temperature and concentration fields. The difference between the computations and the measurements in most cases occurs where the variation in gradient is large. This means that a slight difference in the measuring location can cause a significant error. From Table 4.1, it can be calculated that the heat extracted from the room was smaller than the heat supplied on the venetian



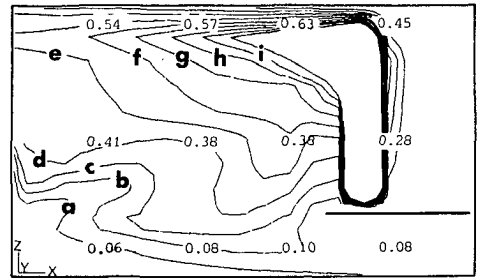
A



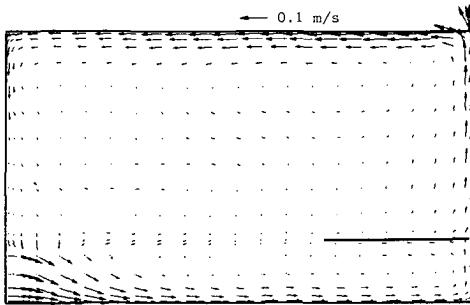
D

	.05	.07	.06	.08	.04	.14	.16
	.03	.04	.03	.03	.00	.03	.04
	.01	.02	.01	.01	.00	.01	.03
	.02	.03	.02	.01	.00	.01	.04
	.02	.03	.02	.02	.00	.01	.04
	.11	.05	.03	.02	.00	.01	.04
Z Y X	.24	.07	.02	.01	.01	.03	.09

B



E



C

Figure 4.6 The computed and measured results for cooling system 1. (A) Airflow pattern observed by using smoke in section $y=1.5$ m; (B) measured air velocities in section $y=1.5$ m (m/s); (C) computed air velocity distribution in section $y=1.5$ m; (D) computed (contours) and measured (numerical values) temperature field in section $y=1.5$ m ($^{\circ}\text{C}$)*; (E) computed (contours) and measured (numerical values) concentration field in section $y=0.7$ m (%)#.

* Contour key for D: a-21.0, b-22.0, c-23.0, d-24.0, e-25.0, f-26.0.
 # Contour key for E: a-0.1, b-0.2, c-0.3, d-0.4, e-0.5, f-0.6, g-0.7, h-0.8, i-0.9.

blinds, because a part of the heat was transferred outside of the window. Figure 4.6 indicates that the inlet discharges the fresh air horizontally across the floor and that the air velocity near the ceiling is large due to the buoyancy effect from the hot venetian blinds. In the remaining part of the room, there is a large stagnant zone and the ventilation efficiency in this case is high (refer to Table 4.1). The reason for this is that the buoyancy affect of the 25 W heat source causes the helium to rise immediately

TABLE 4.1
Measured and computed ventilation and temperature efficiencies
with different ventilation systems*

Systems	Heat on venetian blinds W	T _{in} °C	T _{out} °C	T _{occu} °C	η_T -	Temp. grad. °C/m	C _{in} %	C _{out} %	C _{occu} %	η_V -
1 (meas.)	600	19.7	25.0	23.2	1.51	1.20	0.0	0.51	0.38	1.34
1 (comp.)	600	19.1	25.0	23.4	1.37	1.53	0.0	0.50	0.41	1.22
2 (meas.)	600	19.3	25.0	23.2	1.46	1.53	0.0	0.50	0.40	1.25
2 (comp.)	600	18.7	24.8	23.2	1.36	1.33	0.0	0.51	0.40	1.02
3 (meas.)	950	15.2	24.9	22.9	1.26	1.41	0.0	0.52	0.11	4.73
3 (comp.)	950	14.9	24.9	22.9	1.25	1.32	0.0	0.52	0.13	4.00
4 (meas.)	950	12.5	22.8	22.9	0.99	-0.07	0.0	0.50	0.78	0.64
4 (comp.)	950	12.6	22.9	22.9	1.00	0.04	-	-	-	-

* Ventilation rate is 5 times/hour

upwards to the ceiling. As a result, the helium concentration near the ceiling is very high and it is removed directly through the outlets. This phenomenon is explained by the computed velocity and temperature fields in the section $y=0.7$ m which is shown in Figure 4.7. The concentration distributions in sections $y=0.7$ m (where the helium is introduced), $y=1.5$ m and $y=2.3$ m are shown in Figure 4.8. Of course, the ventilation efficiency depends strongly on the positions of the contaminant source.

The required inlet air temperature of simulation shown in Table 4.1 is lower than that of the measurements. The reason for this is that the measurements are not carried out under a real steady situation or it could be due to discrepancies caused by the computation. Because the ceiling and the floor of the room are of heavy concrete of which the heat capacity is very large, a very long time is needed to reach steady conditions. In a dynamic period, the heat transferred into the ceiling is larger than that obtained from the floor, and therefore, the measured inlet air temperature is higher.

For cooling system 2, the numerical and experimental results are

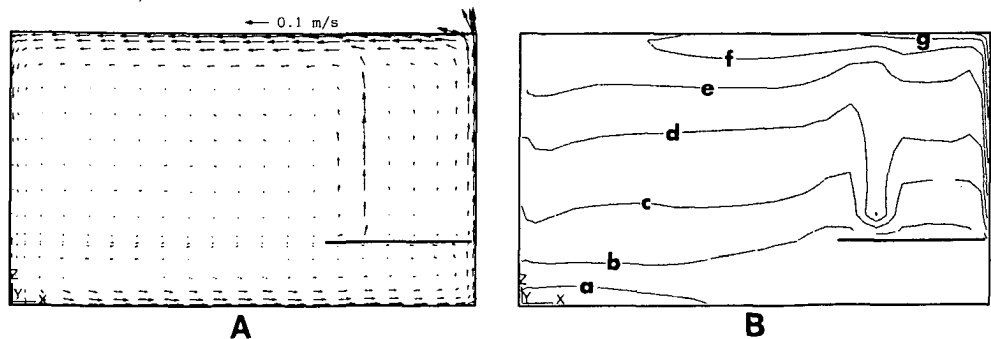
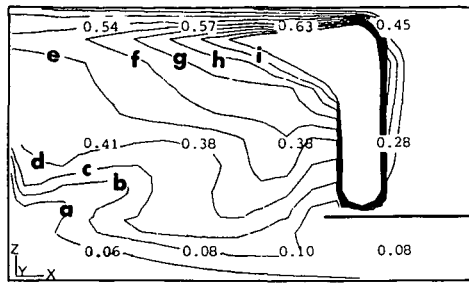
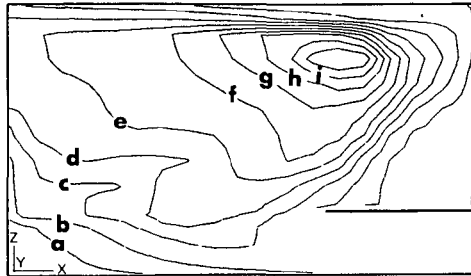


Figure 4.7 The computed results for cooling system 1 in section $y=0.7$ m. (A) Air velocity distribution; (B) temperature field (°C)*.

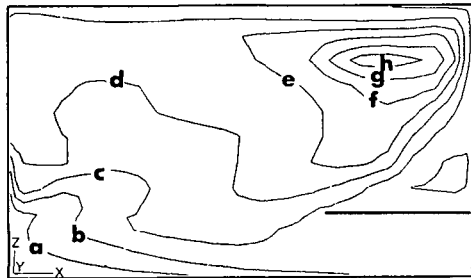
* Contour key for B: a-21.0, b-22.0, c-23.0, d-24.0, e-25.0, f-26.0, g-27.0.



A



B

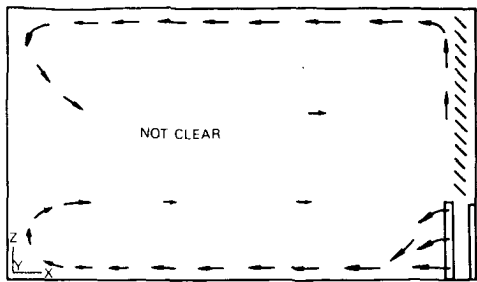


C

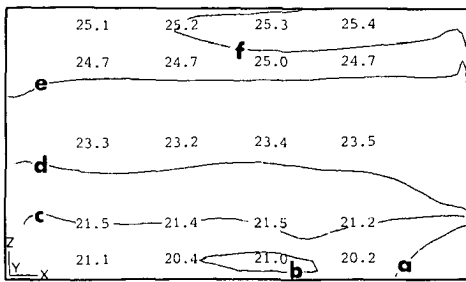
Figure 4.8 The computed and measured concentration distributions in different sections for cooling system 1. (A) Computation (contours) and measurement (numerical values) in section $y=0.7$ m (%)#; (B) computation in section $y=1.5$ m (%)#; (C) computation in section $y=2.3$ m (%)#.

Contour key for A, B, C: a-0.1, b-0.2, c-0.3, d-0.4, e-0.5, f-0.6, g-0.7, h-0.8.

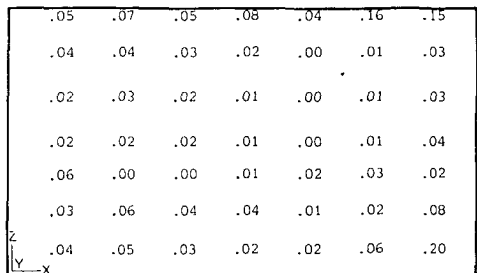
presented in Figure 4.9. The agreement between the computations and the measurements is rather good but there are still some discrepancies. As shown in Figure 4.9, there are two large eddies in the room. One is formed by the air discharge from the inlet air diffuser and the other from the buoyancy produced by the hot window. The measured results indicate that both the hot air near the ceiling and the cold air near the floor can reach to the rear wall so that the two eddies are larger than those of computations. The temperature efficiency, temperature gradient and ventilation efficiency of this cooling system are almost the same as those of cooling system 1. Although the fresh air keeps the lower part of the room very clean, the



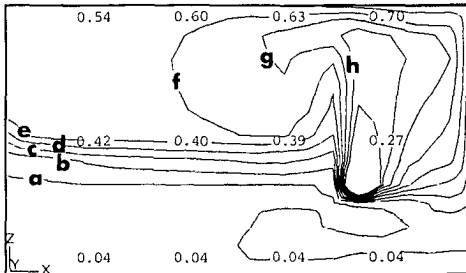
A



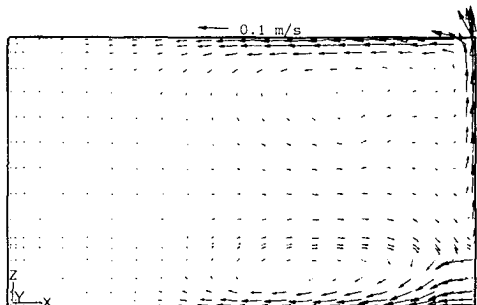
D



B



E



C

Figure 4.9 The computed and measured results for cooling system 2. (A) Airflow pattern observed by using smoke in section $y=1.5$ m; (B) measured air velocities in section $y=1.5$ m (m/s); (C) computed air velocity distribution in the section $y=1.5$ m; (D) computed (contours) and measured (numerical values) temperature field in section $y=1.5$ m ($^{\circ}\text{C}$)*; (E) computed (contours) and measured (numerical values) concentration field in section $y=0.7$ m (%)#.

* Contour key for D: a-20.0, b-21.0, c-22.0, d-23.0, e-24.0, f-25.0.

Contour key for E: a-0.1, b-0.2, c-0.3, d-0.4, e-0.5, f-0.6, g-0.7, h-0.8.

concentration at standing level ($z=1.6$ m) is nearly the same as that in the upper part of the room. For this reason, cooling system 1 is better for acquiring good air quality.

The measured and simulated field results of cooling system 3 are shown in Figure 4.10. The air velocities presented in this figure are those in the section $y=0.7$ m in which the helium is introduced. However, the temperature and concentration fields shown in the figure are those in the middle section

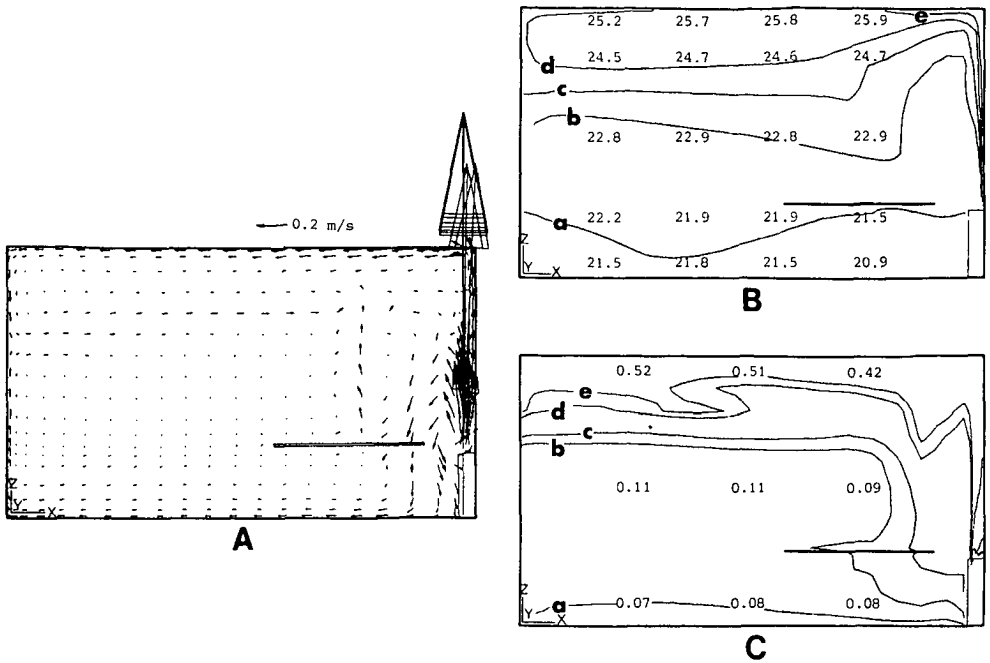


Figure 4.10 The computed and measured results for cooling system 3. (A) Computed air velocity distribution in section $y=0.7$ m; (B) computed (contours) and measured (numerical values) temperature field in section $y=1.5$ m ($^{\circ}\text{C}$)*; (C) computed (contours) and measured (numerical values) concentration field in section $y=1.5$ m (%)#.
 * Contour key for B: a-22.0, b-23.0, c-24.0, d-25.0, e-26.0.
 # Contour key for C: a-0.1, b-0.2, c-0.3, d-0.4, e-0.5.

of the room where the measured results are available. The induction by the inlet air increases the inlet air temperature and will not cause draught after it falls back into the occupied zone of the room. The ventilation efficiency is very high as shown in Table 4.1 and in Figure 4.10. However, the airflow patterns of this cooling system are very sensitive to the inlet air temperature, inlet dimensions and ventilation rate. If the mechanical ventilation rate, for instance, is seven times per hour (i.e. 0.125 kg/s), the ventilation efficiency can drop to 0.79 because the inlet air brings the contaminant directly into the occupied zone. If the opening of the inlet is too large or, in other words, the inlet air velocity is too low, the cold air will drop down directly to the occupied zone and has no induction effect. This will cause a draught.

Cooling system 4 is a very common one. Due to its outlets on the lower part of the room, the cooling system is not good both for saving energy and for obtaining good indoor air quality in summer. This can be explained from the temperature efficiency and the ventilation efficiency shown in Table 4.1. The room air mixture is very good, therefore the air temperature gradient is very small (See Table 4.1 and Figure 4.11). The computed concentration distribution is not available. The calculated air velocity fields and temperature distributions in the section of the inlet and in the middle section are presented in Figure 4.11. The simulated room air temperatures in the section $y=1.5$ m mostly are larger than 22.0°C and smaller than 23.0°C so

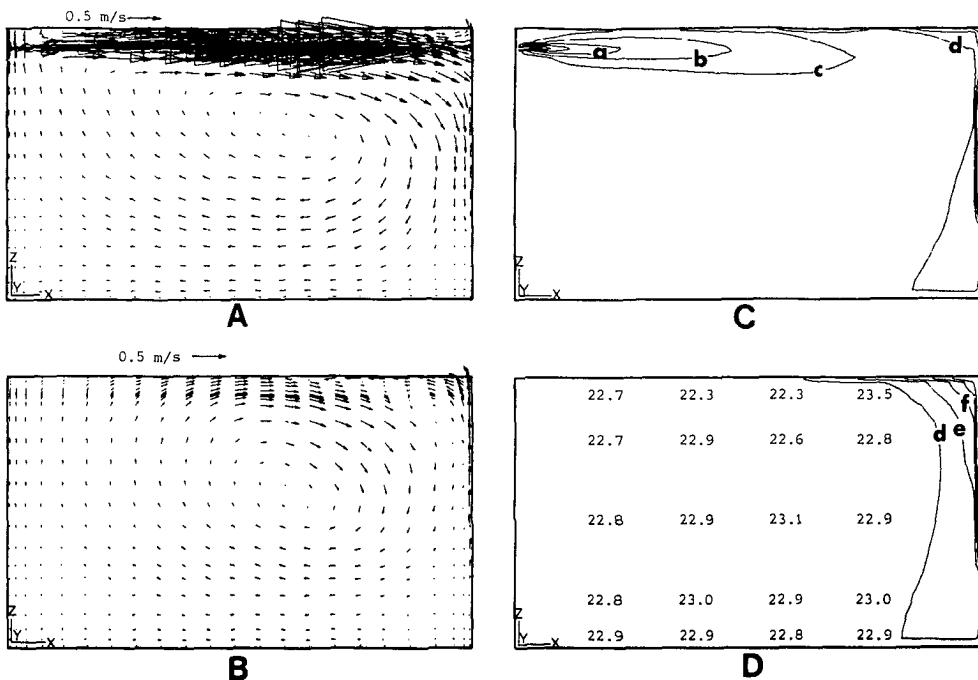


Figure 4.11 The computed and measured results for cooling system 4. (A) Computed air velocity distribution in section $y=0.75$ m (through the inlet); (B) computed air velocity distribution in section $y=1.5$ m; (C) computed temperature field in section $y=0.75$ m ($^{\circ}\text{C}$)*; (D) computed (contours) and measured (numerical values) temperature field in section $y=1.5$ m ($^{\circ}\text{C}$).

* Contour key for C and D: a-20.0, b-21.0, c-22.0, d-23.0, e-24.0, f-25.0.

that no contour for 22.0°C can be drawn in the figure. They are in good agreement with the measured ones.

Among these four cooling systems, cooling system 1 seems the best one both for saving energy and obtaining good indoor air quality in cooling situations. For cooling system 2, a table placed on the middle near the window is not suitable even with a distance of 1.0 m to the window. When the table is placed in this position, the air temperature under the table is less than 20°C . This is not permitted from the comfort aspect. Although cooling system 3 presents the best ventilation effect, it is too sensitive to the inlet air temperature, ventilation rate and inlet geometry. This will cause difficulties in control. The airflow pattern of the cooling system is more complicated and is not easy to observe by using smoke. Cooling system 4 is not good either for energy saving or better air quality in summer. The situations discussed here are concerned with a dominant heat gain from the window. If the inner heat sources in a room are dominant, the results can be different. For example, the ventilation efficiencies might be highly sensitive to the location of pollutant sources and the rate of heat generation at the sources or to physical characteristics of the room and its furnishings. Further research on the sensitivities, such as the influence of the locations of thermal sources, pollutant sources and furnishings on temperature efficiency and ventilation efficiency, seems to be necessary.

4.2.2 Different ventilation rates

Cooling system 1 was used to study the influence of ventilation rate on the ventilation efficiency and temperature efficiency. The heat introduced on the venetian blinds for this group was fixed at 600 W. The study concerned the airflow, temperature fields and helium concentration distributions when the mechanical ventilation rates were controlled at 3 times/hour, 5 times/hour and 7 times/hour.

The computed results presented in Table 4.2 imply that the larger the ventilation rate, the higher the temperature efficiency and the ventilation efficiency and the smaller the temperature gradient. When room ventilation rate increases, the required inlet air temperature increases in cooling situations. According to the definition of temperature efficiency, both $T_{out} - T_{in}$ and $T_{occu} - T_{in}$ become smaller. However, the change rate of $T_{occu} - T_{in}$ is much larger, therefore η_T is higher. This can also be explained by the fact that $d\eta_T/dT_{in} > 0$. But the increase of temperature efficiency does not mean that it saves energy, since the energy consumption of a building also depends on the ventilation rate.

As shown in Figure 4.12, the buoyancy influence in the upper part of the room is the same under these three ventilation rates because the heat gain from the venetian blinds is the same. However, the mechanical ventilation controls air distribution in the lower part of the room. The higher the ventilation rate, the more fresh air is injected into the occupied zone. Therefore, the concentration of contaminant in the zone of occupation is lower so that η_V is higher. This can be seen from the concentration fields and the numerical air velocity distributions illustrated in Figure 4.12.

Although measured results of velocity distributions are not presented in Figure 4.12, they are same as the computed ones.

The measured transient behaviour of the helium concentration of this group is presented in Figure 4.13. The smaller the ventilation rate, the more difficult it is to remove the helium which was used as contaminant.

TABLE 4.2
Measured and computed ventilation and temperature efficiencies
for system 1 with different ventilation rates*

Ventilation rates times/hour	T_{in} °C	T_{out} °C	T_{occu} °C	η_T -	Temp. grad. °C/m	C_{in} %	C_{out} %	C_{occu} %	η_V -
3 (meas.)	16.0	25.6	23.8	1.23	1.68	0.0	0.50	0.39	1.28
3 (comp.)	16.0	25.8	23.5	1.31	1.67	0.0	0.49	0.44	1.11
5 (meas.)	19.7	25.0	23.2	1.51	1.20	0.0	0.51	0.38	1.34
5 (comp.)	19.1	25.0	23.4	1.37	1.53	0.0	0.50	0.41	1.22
7 (meas.)	20.8	24.8	22.9	1.90	1.23	0.0	0.50	0.32	1.56
7 (comp.)	20.7	24.9	23.4	1.56	1.27	0.0	0.48	0.28	1.71

* Heat on the venetian blinds is 600 W

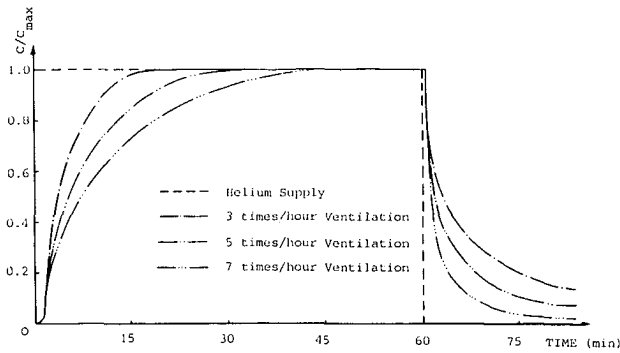


Figure 4.13 The Transient behaviour of the room helium concentration in point $x=2.2$ m, $y=0.7$ m and $z=3.0$ m for cooling system 1 with different ventilation rates.

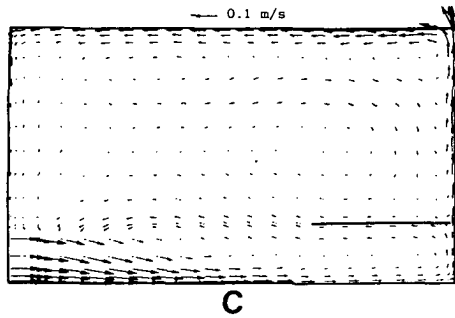
4.2.3 Different heat gains from the venetian blinds

In this group, the mechanical ventilation rate was fixed at 7 times/hour for cooling system 1. The ventilation rate was higher than that used in practice because the major concern was to study the influence of heat gain. If a too small amount of heat was used, it would be very difficult to overcome the influence from other disturbances. In addition, the larger the amount of the heat used, the higher the ventilation rate required to maintain comfort in the zone of occupation. The study concerned the air velocity, temperature and helium concentration distributions when heating amounts of 300 W, 600 W and 950 W were applied to the venetian blinds.

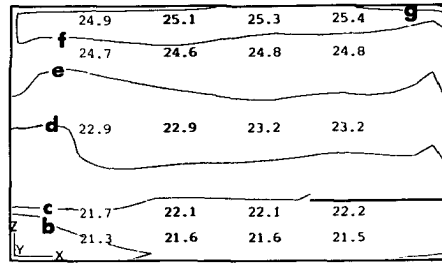
The computed and measured air temperature, concentration fields, and calculated airflow patterns are shown in Figure 4.14. The airflow patterns observed by smoke present similar results. The temperature efficiency and the ventilation efficiency are presented in Table 4.3. If the heat gain from the venetian blinds is larger, the required inlet air temperature is lower and the air movement in the upper part of the room is stronger. The stronger air movement forms a larger eddy. The inlet air, which is of lower temperature, stays in a thin layer on the floor and induces a certain amount of air from the room (Figure 4.14). Due to these two reasons, the mixture in the room is better. As can be seen in the results, the concentration of contaminant in the occupied zone increases so that η_T is smaller.

There is a large difference of temperature efficiency between the computation and the measurement, when the heat on the venetian blinds is 300 W. This is because the temperature in the occupied zone of the computation deviates from that of the measurement.

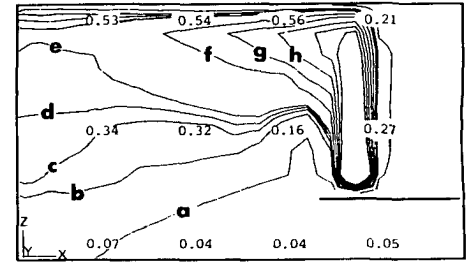
According to the results presented in Table 4.3, it is difficult to find the relationship between the heat gain from the venetian blinds and the temperature efficiencies. This is probably because both the heat on the venetian blinds and the inlet air temperature become dominant factors in the buoyancy term of the momentum equation and are of the same order. As the heat on the venetian blinds becomes larger, $d\eta_T/d(T_{out}-T_{in})$ increases in a similar rate to $d\eta_T/d(T_{occu}-T_{in})$. Therefore, η_T seems to be independent of the heat.



C



F

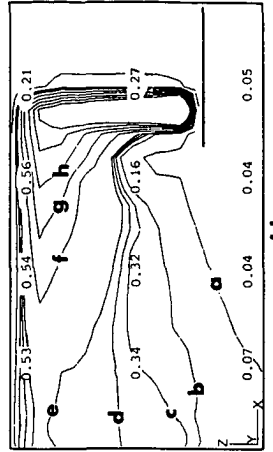
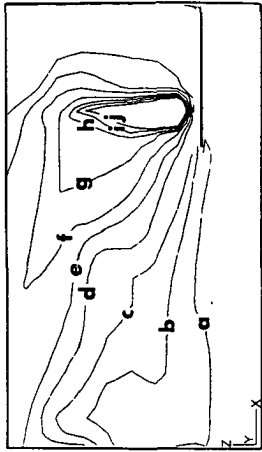
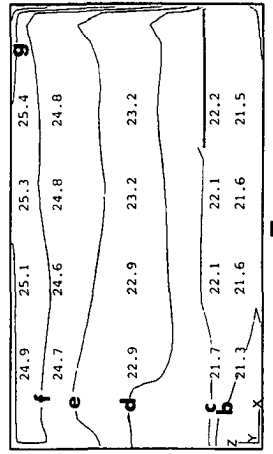
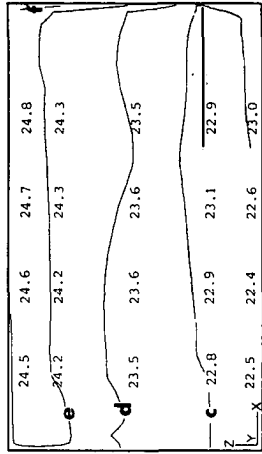
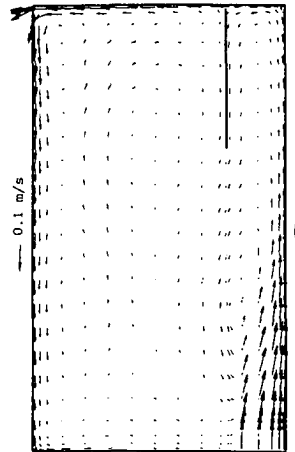
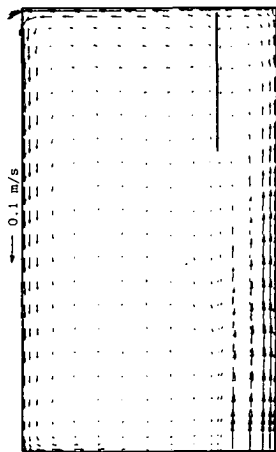


I

Figure 4.12 The computed and measured results for cooling system 1 with different ventilation rates and with 600 W heat gain from the venetian blinds. For (A), (B), and (C), the computed air velocity distributions in section $y=1.5$ m with ventilation rate 3, 5, and 7 times/hour respectively; for (D), (E) and (F), the computed (contours) and measured (numerical values) temperature fields in section $y=1.5$ m with ventilation rate 3, 5, and 7 times/hour respectively ($^{\circ}\text{C}$)*; and for (G), (H) and (I), the computed (contours) and measured (numerical values) concentration fields in section $y=0.7$ m with ventilation rate 3, 5, and 7 times/hour respectively (%)#.

* Contour key for D, E and F: a-20.0, b-21.0, c-22.0, d-23.0, e-24.0, f-25.0, g-26.0, h-27.0.

Contour key for G, H and I: a-0.1, b-0.2, c-0.3, d-0.4, e-0.5, f-0.6, g-0.7, h-0.8, i-0.9.



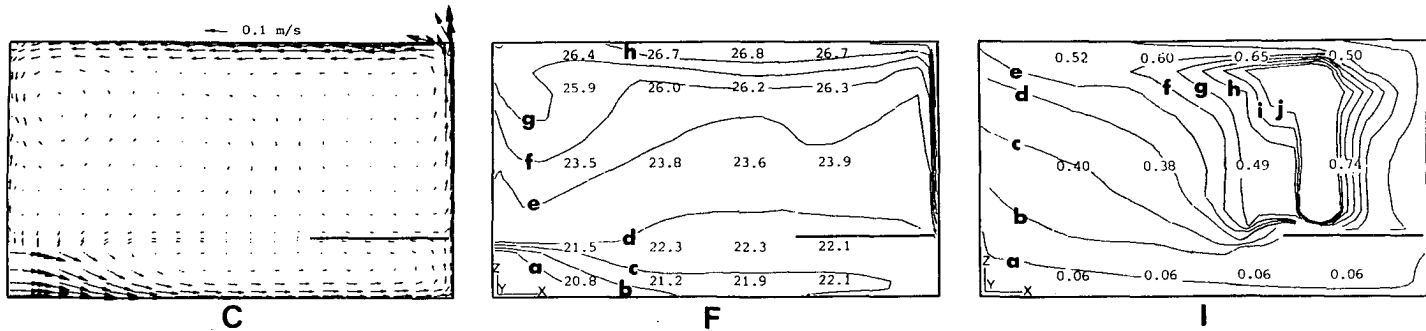


Figure 4.14 The computed and measured results for cooling system 1 with different heat gain from the venetian blinds and with ventilation rate 7 times/hour. For (A), (B), and (C), the computed air velocity distributions in section $y=1.5$ m with heat gain 300, 600, and 950 W respectively; for (D), (E) and (F), the computed (contours) and measured (numerical values) temperature fields in section $y=1.5$ m with heat gain 300, 600, and 950 W respectively ($^{\circ}\text{C}$)*; and for (G), (H) and (I), the computed (contours) and measured (numerical values) concentration fields in section $y=0.7$ m with heat gain 300, 600, and 950 W respectively (%)#.

* Contour key for D, E and F: a-20.0, b-21.0, c-22.0, d-23.0, e-24.0, f-25.0, g-26.0, h-27.0.

Contour key for G, H and I: a-0.1, b-0.2, c-0.3, d-0.4, e-0.5, f-0.6, g-0.7, h-0.8, i-0.9, j-1.0.

TABLE 4.3
Measured and computed ventilation and temperature efficiencies
for system 1 with different heat gains from the venetian blinds*

Heat on the venetian blinds W	T _{in}	T _{out}	T _{occu}	η_T	Temp. grad. °C/m	C _{in}	C _{out}	C _{occu}	η_V
	°C	°C	°C	-	%	%	%	%	-
300 (meas.)	21.3	24.1	23.6	1.22	0.68	-	-	-	-
300 (comp.)	21.7	24.0	22.7	2.30	0.67	0.0	0.53	0.30	1.76
600 (meas.)	20.8	24.8	22.9	1.90	1.23	0.0	0.50	0.32	1.56
600 (comp.)	20.7	24.9	23.4	1.56	1.27	0.0	0.48	0.28	1.71
950 (meas.)	19.6	27.1	23.8	1.79	1.72	0.0	0.50	0.38	1.32
950 (comp.)	19.4	26.9	23.7	1.74	1.67	0.0	0.49	0.37	1.32

* Ventilation rate is 7 times/hour

4.2.4 Different heating systems

The heating systems 1 and 2 which were described in chapter 3 were used to study the air velocity and temperature distributions of the room in winter. The initial room air and wall temperatures were 14.4°C and the air temperature outside the window was controlled to be 3.0°C. 1000 W heat was then introduced into the room by the heating unit in a step function form.

The computations by PHOENICS and the measurement of the velocity and temperature distributions of the heating system 1 and the heating system 2 in the section $y=1.5$ m are shown in Figure 4.15. The results are those after the heating unit worked for 11 hours. According to the computations by ACCURACY and the measurements, at that moment the surface temperature of window glass was 10°C for both systems and the side wall temperatures were about 18.5°C for heating system 1 and 20.0°C for heating system 2. The agreement of the velocity profiles between the measurements and computation is reasonable but there are some discrepancies in the temperature distribution near the heating unit as shown in Figure 4.15. This discrepancy probably is caused by the differences between the numerical and experimental boundary conditions with respect to inlet turbulence parameters. There were no measured inlet turbulence parameters available and the computations were based on estimated values. On the other hand, the temperature gradients near the inlet are very high so that slight differences in measuring positions could cause large errors.

The vertical temperature gradient of heating system 1 is larger than that of heating system 2. This causes an extra amount of heat to be transferred into the ceiling and resulting a lower room air temperature. This also results in side wall temperatures of heating system 1 about 1.5°C lower than those of heating system 2.

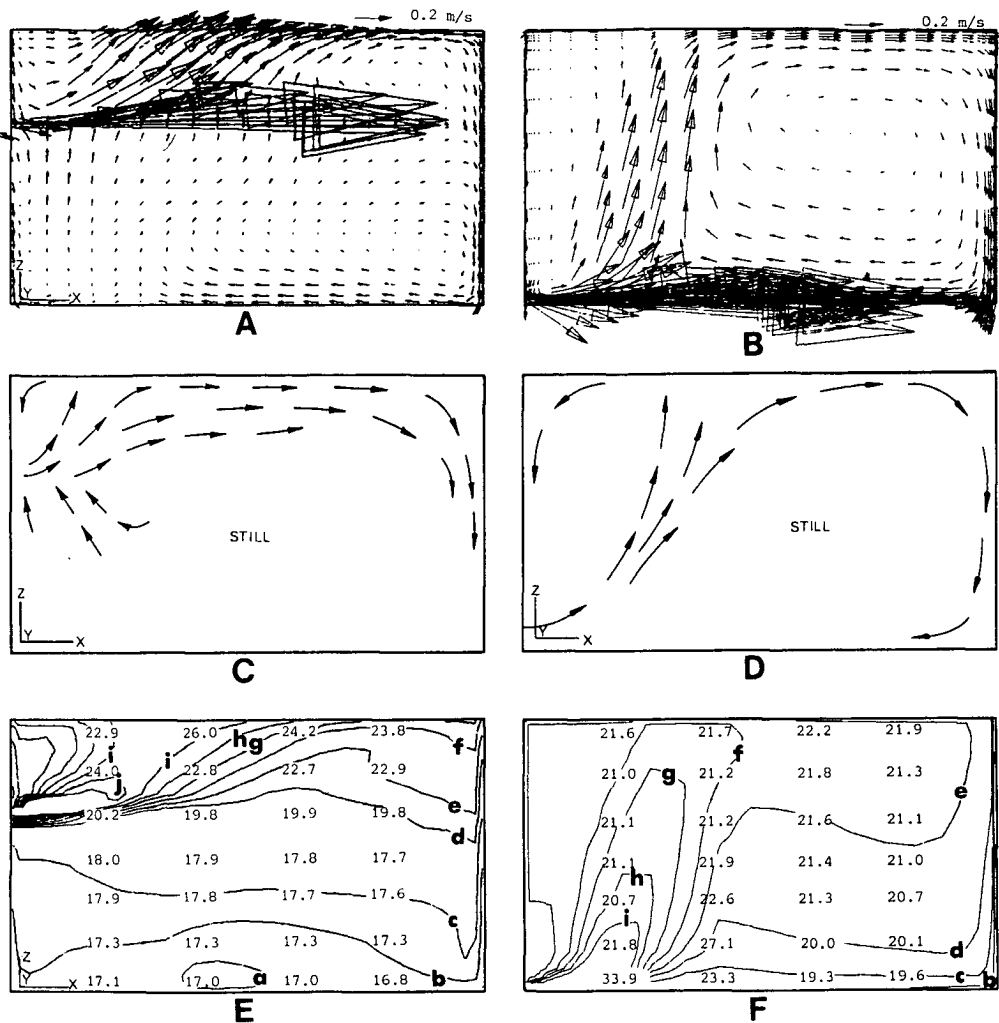


Figure 4.15 The computed and measured results of heating system 1 and heating system 2 in section $y=1.5$ m. For (A) and (B), computed air velocity distributions of heating system 1 and heating system 2; for (C) and (D), airflow pattern of heating system 1 and heating system 2 observed by using smoke; for (E) and (F), computed (contours) and measured (numerical values) temperature field of heating system 1 and heating system 2 ($^{\circ}\text{C}$)*.
 * Contour key for E and F: a-17.0, b-18.0, c-19.0, d-20.0, e-21.0, f-22.0, g-23.0, h-24.0, i-25.0, j-26.0.

4.2.5 Remarks and conclusions of the three-dimensional computations

The following paragraphs provide a summary of the most important conclusions and remarks which may be extracted from the three-dimensional computations:

(1) The agreement between most of the computations by the three-dimensional program PHOENICS and the measurements is acceptable for practical applications.

(2) The computations using computer program PHOENICS are very expensive. In the situations discussed above, the CPU time on an IBM 3083 JX1 computer is about 80 minutes in case of the calculation is started with uniform initial field values and with a total grid number of $18 \times 18 \times 23$. When the computation uses the field results of a similar case as initial values, about 20 minutes CPU time is required, which it is still too expensive.

(3) The temperature and ventilation efficiencies of cooling systems 1 and 2 are very high. They seem to be the best ones both for saving energy and for obtaining a good air quality in cooling situations. However, cooling system 2 is slightly poorer than cooling system 1. Cooling system 3 presents a higher ventilation efficiency but is difficult to control. Cooling system 4 is a representative for commonly used systems where room air is perfectly mixed. Its temperature efficiency and ventilation efficiency are very low.

(4) Inlet sizes and locations seem to be very important for the temperature and velocity distributions. For cooling situations, cooling system 4 gave a much more uniform temperature distribution than the other cooling systems. The vertical temperature differences in the other cooling systems were about 4 to 5°C. Nevertheless, the vertical temperature differences in the occupied zone of these systems were small, and as a result, they met comfort requirements.

(5) If room heat gain and ventilation rate are the same, the required inlet air temperature of the four cooling systems is different. In cooling situations, the inlet air temperature of cooling systems 1 and 2 can be higher than that of cooling system 4. This has to be considered in building energy analysis.

(6) According to the results for cooling system 1, the higher the ventilation rate, the larger the temperature efficiency and the ventilation efficiency and the smaller the temperature gradient. However, one should realize that the energy consumption also depends on the ventilation rate. Obviously, it is easier to remove contaminants in cases with a higher ventilation rate.

(7) The larger the amount of heat introduced in the venetian blinds for cooling system 1, the lower the ventilation efficiency and the larger the temperature gradient. The influence on temperature efficiency is small.

(8) Heating system 2 is better than heating system 1 in winter because the vertical temperature difference is smaller and the air temperature in the occupied zone is higher.

(9) It should be pointed out that the situations discussed here are with a dominant heat gain from the window. If the inner heat sources in a room are dominant, the results, which include temperature efficiency, can be different. The ventilation efficiencies might be highly sensitive to the location of pollutant sources and the rate of heat generation at the sources or to physical characteristics of the room and its furnishings. Further research on the sensitivities, such as the influence of the locations of thermal sources, pollutant sources and furnishings on temperature efficiency and ventilation efficiency, seems to be necessary.

CHAPTER 5

AIR-CONDITIONING LOAD MODELLING

5.1 Review of Air-Conditioning Load Predictions

The air-conditioning load computation can be divided into the following major study topics: heating load and cooling load.

According to the calculation methods, air-conditioning load modelling is divided into two procedures. The first one, manual method, is normally used in initial design situations. In this case, the calculation of the maximum heating load and cooling load will be sufficient.

However, the extensive analysis, such as energy requirement of the air-conditioning system, must be calculated for a period of time. The calculation will be impossible without the aid of a computer. Therefore, the extensive analysis is also used to generate coefficients for the manual method. Such a complex method by means of a computer is normally named as the computer method. Of course, this classification is not very appropriate, since even the simplest methods today are commonly programmed for a computer.

In this section, some manual and computer methodologies will be discussed.

5.1.1 Heating load

Because the temperature difference between indoor and outdoor is large in winter, most manual methods given to estimate heating load (ASHRAE 1979, 1981) assume a steady-state condition for heat loss through the boundary surfaces and an outdoor design temperature that is not the most severe on record (97.5% value). When there is justification to use the median of extremes outdoor design temperature, McQuiston (1984) suggested that new data were required for basements, slab floors, and crawl spaces. It is suggested that the overall heat transfer coefficients calculated by Mitalas (1982) should be used in this purpose.

When an analysis on heating load is required, the computer method must be applied. The method considers the transient heat transfer behaviour and heat storage of the enclosures. This is very similar to the one used in cooling load computations and therefore will be discussed in next section.

5.1.2 Cooling load

The manual method in ASHRAE Fundamentals-1972 (ASHRAE 1972) is the Total Equivalent Temperature Differential Method (TETD). In this method, various components of space heat gain were added together to get an instantaneous total rate of space heat gain, which was then converted to an instantaneous space cooling load through the use of weighting factors. This method considered the heat storage of the enclosures and the lag of heat transfer. The cooling load calculated in this way is much smaller than that obtained

from the traditional method in which the heat gain is regarded as cooling load. In ASHRAE Fundamentals-1972 (ASHRAE 1972), the transfer function method which now forms the biggest portion of the computer method was introduced. In fact, the transfer function method and TETD method are similar in principle, the former one employed entirely different weighting factors (called coefficients of room transfer functions) in converting heat gain to cooling load. ASHRAE Fundamentals-1981 (ASHRAE 1981) used the methodology and basic equations of the transfer method to generate cooling load factors (CLF) for each component of the space cooling load. Consequently, the calculation procedure in ASHRAE Fundamentals-1981 is no longer a two step process. Values of the space cooling load components are calculated directly, through use of CLF's which include the effect of time lag due to thermal storage.

The transfer function method, worked on extensively in the last decade was used as a base to generate new tables for the manual method and is extended for hour by hour energy analysis computations. Among these researches, the response factor method (Mitalas and Stephenson 1967), the z-transfer method (Stephenson and Mitalas 1971), the frequency response method (Muncey 1981, Chen 1983), the state-space method (Jiang 1982), etc., which have been reviewed by Kusuda (1985), are very successful and will be introduced in the following.

In the late 60's and early 70's, Stephenson and Mitalas presented the response factors and z-transfer factors methods. It was hailed as cornerstone of building thermal analysis making it possible to numerically invert the difficult Laplace transform functions for these multi-layer heat conduction problems. Thermal response factors and z-transfer factors are the results of an exact solution of the heat conduction equations, unlike the approximate solutions, such as the finite difference or the finite element approaches. The response factors and z-transfer factors, once computed for given sets of multilayer structures, can be used over and over again to evaluate the heat flux and surface temperature by simple algebraic equations applied to the past time history of boundary condition with the same accuracy as the exact solution. They do not have the problem associated with the stability criteria inherent to many of the finite difference approaches that result from the inappropriate selection of increase for the time and space coordinates.

The frequency method is another approach to building thermal simulation. It involves the employment of frequency domain analysis. This requires solving heat conduction equations in the frequency domain instead of the conventional time domain by using the Fourier transforms instead of the Laplace transforms. The merits of the frequency domain analysis are in its mathematical elegance, its ability to show graphically the effect of thermal mass and its ease of handling the periodic heat transfer problems (such as the annual cycle of earth contact heat transfer). The method is however well suited for the micro-computer solution of heat conduction analysis problems in multi-layer structures. Chen (1983) revealed previously that the relationship between the frequency response factors and thermal response factors is that of Fourier transform. Therefore, the difference between the two methods is in mathematical treatments.

The state-space method is based on the idea of modern control theory. Jiang (1982) gave a very comprehensive theoretical background for the network solution approach, which in essence provides a bridge between the thermal response factor concept and the finite-difference solution approach in the form of state-space formula.

Usually at least 40 terms of response factors are required to obtain accurate results but only 4 to 10 terms of z-transfer factors are sufficient. Hence the z-transfer factors method saves more computing time. Although the

frequency method has merits in frequency domain analysis, it is very difficult to break down real weather data into a set of periodic functions. Therefore, it is not very suitable to be used for cooling load computations. The state-space method requires too much computing time. It can be concluded that the z-transfer factor method is the most suitable one for the present study.

The accuracy of those different methods has been validated in experimental efforts (Mast 1972, Burch et al. 1974, McBride et al. 1975, Peavy et al. 1975, Kusuda and Bean 1981, Kusuda et al. 1981). A lot of programs based on these theories have been constructed, such as NBSLD (Kusuda 1976), BLAST (Hittle 1979), RESPl (Van Weele 1983), and ACCURACY (Chen 1987d, 1987e, 1988). Besides, there are a lot of cooling load computer programs which are based on finite-difference method or network method, such as KOELA and KOELB (Förch 1983). Gadgil et al (1979) have demonstrated that the majority of the large mainframe programs are equivalent, yielding practically the same results. Both transfer function method and finite difference method are regarded as computer methods.

The accurate room cooling load calculation requires the precise assessment of the room surface temperatures, which are influenced significantly by the incident solar radiation through the windows as well as by the mutual infrared radiative heat exchange among surfaces. These involve not only the surfaces of walls, ceiling, floor and windows, but also the radiation of lighting fixtures, electric appliances, radiant panel or fin tube radiant heaters. It is an extremely difficult mathematical process for the direct beam solar radiation and complex convective heat exchange among the complicated room surface geometry encountered in the actual buildings. It is also a non-linear process because the convective and radiative heat transfer coefficients are functions of the surface temperature itself. Moreover the room air temperature varies from floor to ceiling due to buoyancy or imperfect mixing. Many computer programs mentioned above deal with this detailed room surface heat transfer, using what is commonly referred to as the room energy balance method. The room energy balance method entails the simultaneous solution of a matrix equation involving the room surface radiative heat exchange, internal heat generation, infiltration, conductive heat gain and solar heat gain. That is, the heat exchange rate in a wall is:

$$q_i = \alpha_{ci}(T_{ir} - T_i) + \sum_{\substack{j=1 \\ j \neq i}}^N \alpha_{rij} (T_j - T_i) + R_i \quad (5.1)$$

where N is the number of surfaces in the room, q_i is the rate of heat conducted into surface i at the inside surface at time t , T_{ir} is the room air temperature, α_{ci} is the convective heat exchange coefficient at interior surface i . α_{rij} is the radiative heat exchange coefficient between interior surface i and interior surface j . T_i and T_j are the average temperatures of interior surfaces i and j at time t respectively, and R_i is the solar radiation through windows and radiation from lights, appliances and occupants which are re-absorbed by the surface i at time t .

In the present study, the q_i is calculated by the z-transfer factor method (Stephenson and Mitalas 1971):

$$q_{i_n} = \sum_{j=0}^M Z1_j T_{o_{n-j}} - \sum_{j=0}^M ZA_j T_{i_{n-j}} - \sum_{j=1}^M ZB_j q_{i_{n-j}} \quad (5.2)$$

where $Z1_j$, ZA_j and ZB_j are the z-transfer factors; M is the term number of the z-transfer factors, n is the current time step, T_o and T_i are outside and inside surface temperatures of the wall respectively.

The cooling load (Q) is given by:

$$Q = \sum [\alpha_{ci}(T_i - T_{ir}) A_i + \rho C_p V_i (T_{io} - T_{ir})] + C \quad (5.3)$$

where A_i is the area of surface i , V_i is the ventilation/infiltration through surface i and C is the convective part of the solar radiation through the windows, and radiation from lights, equipment and occupants converted into the room air at time t . Because such a rigorous approach for calculating space cooling load is very complicated, the procedure is always performed by computers.

The approximated room transfer function method, or weighting factor method, for cooling load computations is simpler than the room energy balance method. The approach of the weighting factor was intended to reduce the lengthy calculations required by the room energy balance procedure. In the weighting factor method, the conduction and infiltration heat gain/loss through the envelope elements and the internal heat gains are pre-calculated on an hourly basis for a given room temperature and stored as time series. The weighting factor approach, however, is not at all suitable, for evaluating the precise effect of building thermal mass on the affection of indoor temperature fluctuation around the thermostat set point, due to night time setback or intermittent operation of the heating/cooling system. Besides, its accuracy depends on the generation method of the weighting factors. It may be got from measurements (Shan 1985) or computations by the room energy balance equations method (ASHRAE 1981). If the structure of a room is greatly different from a standard room which is used to obtain the weighting factors, the discrepancy will be larger.

In the present study, heating load and cooling load are calculated in the same way with the room energy balance equations. Therefore, the terms, air-conditioning load and space load, are used later on for both heating load and cooling load.

5.1.3 Air-conditioning load components

Besides the general features of the air-conditioning load calculation and the computational method of heat transmission through walls mentioned above, the space air-conditioning load due to solar radiation through fenestration areas, lighting, appliances, occupants and infiltration must be discussed.

5.1.3.1 Solar radiation through fenestration area

One of the manual methods for the calculations of fenestration heat transfer is to use a glass load factor (GLF). The GLF is based on a steady-state heat transfer in winter and on the ASHRAE solar heat gain factor (SHGF) concept (ASHRAE 1981) for summer. The SHGF or GLF concepts were found to be the most widely used for manual calculations. For ease of use, the glass load factors developed include the convective component of heat transmission.

Consideration of shading coefficients (SC) and solar distribution led to some new information (Horridge et al. 1983, Woodson et al. 1983, Todorović 1984, 1985). Woodson et al (1983) thoroughly studied the solar characteristics of several shading devices and these data allow the SC to be readily obtained (ASHRAE 1981). Todorović (1984, 1985) proposed a detailed calculating method for the solar distribution in a room.

In the computer method, many programs calculate the heat gain through the fenestration area first and convert this into the air-conditioning load via weighting factors (Kimura 1977). This calculation, of course, is an approximated one and is very similar to the manual method. However, the air-conditioning load computer programs available in Delft University of Technology, such as KOELA, KOELB (Förch 1983) and ACCURACY (Chen 1987d, 1987e, 1988), are based on the energy balance in the fenestration area, which is constructed into the room energy balance equations.

5.1.3.2 Infiltration

Air-leakage models used to predict infiltration generally can be categorized under three main topics, namely, air-change method, the crack method, and empirical modelling methods.

The air-change method is based on the constant rate method and is limited in validity to average buildings under average conditions (ASHRAE 1981, Ross et al. 1982).

The crack method attempts to correlate air leakage to the driving pressure difference across each building component according to the orifice equation. The resultant data exist today as the basis of the ASHRAE crack method (ASHRAE 1981). The accuracy of the method depends on the accuracy of air-leakage data for individual building components, which may vary due to installation practices or manufacturing tolerance, and wind pressure. Identification of all the cracks in a building is also a problem. Modifications of the crack-method approach are numerous.

Empirical models exist in varying degrees of complexity. The most simple one may be to assume that infiltration is a linear function of wind velocity and the temperature difference between indoor air and outdoor air. The first documented research for this purpose is that of Bahnfleth et al. (1957) and Coblentz and Achenbach (1963). Sophisticated simulation methods are available, such as British gas multi-cell model (Alexander and Etheridge 1980).

An application guide for infiltration calculation has been presented recently (Liddament 1986). However, infiltration in commercial buildings is much more complicate. Recent research on this field is very active both on computational and experimental sides such as those by Feustel and Kendon (1985), Afonso et al. (1986), Parker (1986) and Yoshino (1986).

5.1.3.3 Lights, appliances and occupants

It is essential to estimate the space air-conditioning load caused by lights, appliances and occupants because they may be the major space load components. The calculation of these load components is not straight-forward. The most common used method is first to calculate the heat gain from lights, appliances and occupants and then to convert this into air-conditioning load via air-conditioning load factors or weighting factors (Kimura 1977), z-transfer functions (Ball 1983) and heat exchange procedures (Ball and Green 1983). The latent heat gain caused by appliances, occupants and infiltration is simply calculated in a direct way (ASHRAE 1981, Kimura 1977). More accurate computations which consider the moisture absorption and desorption have been studied recently by Fairey and Kerestecioglu (1985).

5.2 Description of the Computer Program ACCURACY

The study of air movement and heat transfer in buildings by numerical approaches has been active for near twenty years and has successes to its credit. However, consideration of the unsteady heat transfer of buildings in combination with the air movement in a room is still an unexplored territory. The research activities on both fields are quite isolated. They must be coupled, in order to obtain more accurate results, to reveal the overall physical phenomena. This implies that the combination of an airflow program with a cooling load program can be used to estimate more accurate boundary conditions for airflow simulations and to consider the influence of the indoor airflow and temperature distribution on room energy consumption and comfort.

The ACCURACY computer code has been developed in order to meet this need. The name ACCURACY is the acronym for A Cooling-load Code Using Room Air Currents (the final Y is added for euphony) (Chen 1987d, 1987e, 1988, Chen and Van der Kooi 1988). It is capable of calculating the fluid and thermal parameters of room air and building enclosures such as air velocity, air temperature distributions, inside and outside wall temperatures, air-conditioning load and heat fluxes, etc. It can be extended for energy analysis. In this section, the mathematical fundamentals and the computational technique employed in the computer program ACCURACY will be introduced.

5.2.1 Solar radiation

From the viewpoint of air-conditioning, solar radiation gives an important contribution to space heating in winter and gives rise to a considerable amount of air-conditioning load in summer. Consequently solar radiation must be treated as thermal energy in air-conditioning. Subsequent consideration must be given to the characteristics of solar radiation for estimating the rate of solar radiation absorbed by or transmitted through various building materials. The computer program ACCURACY calculates solar radiation in three ways.

5.2.1.1 ASHRAE method

Solar radiation under a cloudless sky. The intensity of solar radiation received on the earth by building surfaces at any time and at any location must be estimated for the calculation of air-conditioning load. The key value for estimating the intensity of solar radiation for given conditions is the direct normal solar radiation I_{DN} . The ASHRAE (1975) used the following expression to give direct normal solar radiation:

$$I_{DN} = A \cdot \exp(-B/\sin(\text{SALT})) \quad (5.4)$$

where SALT is the solar altitude, A is the apparent solar constant and B is the atmospheric solar constant.

The diffuse component of solar radiation is insignificant on clear days but relatively large under turbid sky conditions. In air-conditioning practice, therefore, diffuse radiation is important for the estimation of air-conditioning load calculations.

ASHRAE calculates the diffuse sky radiation for a cloudless condition (BS) from:

$$BS = C \cdot I_{DN} / CN^2 \quad (5.5)$$

where C is the sky diffuse factor, CN is the clearness number, normally with a value between 0.85-1.2.

When a tilted surface of a building receives reflected radiation from the ground, the radiation is considered diffuse. The amount of such diffuse radiation (BG) can be expressed by:

$$BG = \rho_g (BS + I_{DN} \sin(SALT)) \quad (5.6)$$

where ρ_g is the ground reflectivity.

Solar radiation under a cloudy sky. Hour by hour calculation of the air-conditioning load of a space is needed for estimating annual energy requirements, and therefore, solar radiation data in direct and diffuse components on hourly basis must be prepared. Often, cloud cover observations are made every hour at major weather stations by experienced observers who estimate the amount of cloud on a scale of 0 to 10 and indicate the type of cloud in four different layers. Kimura and Stephenson (1969) analyzed 1967 Canadian data for observed solar radiation with respect to the cloud cover data, type of cloud, and the calculated solar radiation under a cloudless condition at the same solar time. Based on their analysis, a methodology was developed by ASHRAE for calculating the cloudy day solar radiation. The factor called CCF (cloud cover factor) is used to modify the total solar radiation on a horizontal surface for a cloudless sky condition with the observed cloud cover data for a cloudy sky condition. The value of CCF is first defined as follows:

$$CCF = I_{THC} / I_{TH} \quad (5.7)$$

where I_{THC} is the total solar radiation on a horizontal surface under a cloudy sky of given cloud amount and type of cloud and I_{TH} is the total solar radiation calculated for a horizontal surface under a cloudless sky at the same solar hour as I_{THC} . I_{THC} is the sum of direct radiation I_{DH} and diffuse radiation I_{dH} on a horizontal surface under a cloudless sky:

$$\begin{aligned} I_{TH} &= I_{DH} + I_{dH} \\ &= I_{DN} \sin(SALT) + BS \end{aligned} \quad (5.8)$$

The cloud cover factor CCF is determined as a function of cloud cover (CC) in the second order polynomial:

$$CCF = P + Q \cdot CC + R \cdot (CC)^2$$

where P, Q, and R are coefficients and CC is updated from the amount of cloud (ASHRAE 1975).

The approach ASHRAE used to calculate the direct solar radiation on a horizontal surface under a cloudy sky, I_{DHC} , is expressed as follows:

$$I_{DHC} = I_{TH} \cdot K (1-CC/10) \quad (5.9)$$

where

$$K = \sin(\text{SALT}) / (C + \sin(\text{SALT})) + (P-1) / (1-Y) \quad (5.10)$$

The C and P in the equation are coefficients and the Y is calculated from (ASHRAE 1975):

$$Y = 0.309 - 0.137 \sin(\text{SALT}) + 0.394 (\sin(\text{SALT}))^2 \quad (5.11)$$

Furthermore, direct solar radiation on a tilted surface under a cloudy sky, I_{DC} , can be given by the following expression:

$$I_{DC} = I_D \cdot I_{DHC} / I_{DH} \quad (5.12)$$

where the direct radiation on a surface under consideration for a cloudless sky I_D is:

$$I_D = \begin{cases} I_{DN} \cos(\eta) \\ 0 \end{cases} \quad \text{if } \cos(\eta) \leq 0 \quad (5.13)$$

$\cos(\eta)$ in the equation is the cosine of the incident radiation on the surface under consideration:

$$\cos(\eta) = \cos(WT) \sin(\text{SALT}) + \sin(WA) \sin(WT) \cos(W) + \cos(WA) \sin(WT) \cos(S) \quad (5.14)$$

Here WA is the azimuth angle of the surface under consideration (positive if west of south and negative if east of south). WT is the tilt angle of the surface under consideration from the horizontal surface, zero for the horizontal surface and $\pi/2$ for the vertical walls. $\cos(W)$, and $\cos(S)$ are the direction cosines of direct solar beam and are calculated as follows:

$$\cos(W) = \cos(\delta) \sin(h) \quad (5.15)$$

$$\cos(S) = \sqrt{1 - (\sin(\text{SALT}))^2 - (\cos(W))^2} \quad (5.16)$$

where h is hour angle and δ is declination angle.

Diffuse radiation from the sky for a cloudless sky I_d is:

$$I_d = BS \text{ for a horizontal surface} \quad (5.17)$$

$$I_{ds} = BS \cdot Y \text{ for a vertical surface} \quad (5.18)$$

where $Y = 0.55 + 0.437 \cos(\eta) + 0.313 (\cos(\eta))^2$, if $\cos(\eta) \geq -0.2$, $Y = 0.45$ (ASHRAE 1975).

The diffuse reflected radiation from the ground for a vertical surface, I_{df} , is:

$$I_{df} = BG/2 \quad (5.19)$$

and the diffuse radiation on a horizontal surface under a cloudy sky, I_{dHC} , is:

$$\begin{aligned} I_{dHC} &= I_{THC} - I_{DHC} \\ &= I_{TH} (CCF - K(1 - CC/10)) \end{aligned} \quad (5.20)$$

The diffuse radiation from the sky on a vertical surface under a cloudy sky, I_{dcs} , is:

$$I_{dcs} = I_{ds} \cdot I_{dHC} / BS \quad (5.21)$$

The diffuse reflected radiation from the ground on a vertical surface under a cloudy sky, I_{dcf} , is:

$$I_{dcf} = I_{df} \cdot I_{dHC} / BS \quad (5.22)$$

5.2.1.2 Dutch weather data

The global radiation, I_{THC} , is observed in the Dutch weather stations but the amount of cloud is not available. This means that the cloud cover, CC, is unknown in Dutch weather data. The computer program ACCURACY uses Equation (5.6) to calculate CCF and Equation (5.8) to update CC back. The rest is the same.

5.2.1.3 Short reference year weather data

Besides normal reference year weather data and real weather data, it will be more economical to use a short reference year weather data for yearly energy consumption computations. The Dutch short reference year weather data (Van Paassen 1981, Liem and Van Paassen 1986) were built in the computer program ACCURACY. Liem and Van Paassen analysed various weather variables and gave their relations by mathematical equations. The relations were determined by polynomials and hourly weather data were generated by a random generator.

The dutch short reference year is divided into four seasons. Each season has 14 days. Hourly variables, such as direct solar radiation on a horizontal surface, diffuse solar radiation, air temperature, absolute humidity, wind speed and direction, solar azimuth and sun rise and sun set time, etc., are available.

5.2.2 Transient heat conduction through walls

The air-conditioning load very much depends on the amount of heat entering into or coming out of the surfaces that enclose an occupied space. This amount of heat varies with time because all of the natural changes, both outdoor and indoor, give rise to thermal effects on a time dependent basis. Furthermore the heat capacity of the building structure is significant. Building elements such as walls and slabs play an important role in damping and delaying the effects of heat flow. In this subsection, the computational method used in ACCURACY for the transient heat conduction behaviour in walls and slabs will be discussed.

5.2.2.1 Basic equations of heat conduction

According to the Fourier's law, the governing equation of one-dimensional unsteady state heat conduction in a homogeneous wall shown in Figure 5.1 is:

$$\frac{\partial T}{\partial t} = a \frac{\partial^2 T}{\partial x^2} \quad (5.23)$$

where $a = \lambda / (C_p \rho)$, thermal diffusivity of the material. The partial differential equation can be re-written in the form of imaginary space by the rules of Laplace transform, making $L[T(x,t)] = \theta(x,s)$ as following:

$$a \frac{\partial^2 \theta(x,s)}{\partial x^2} = s \theta(x,s) \quad (5.24)$$

where s is the Laplace operator. The boundary conditions can be written as:

$$\theta(0,s) = 0 \quad (5.25)$$

and

$$\theta(1,s) = f(s) \quad (5.26)$$

Then the solution of Equation (5.24) is expressed by (Kimura 1977):

$$\theta(x,s) = f(s) \frac{\sinh(x\sqrt{s/a})}{\sinh(l\sqrt{s/a})} = f(s) r_{T1}(x,s) \quad (5.27)$$

where

$$r_{T1} = \frac{\sinh(x\sqrt{s/a})}{\sinh(l\sqrt{s/a})} \quad (5.28)$$

$r_{T1}(x,s)$ is the Laplace transform of the impulse response of the temperature at x against the surface temperature excitation at $x=l$ and is called the transfer function. In general the transfer function may be defined as the Laplace transform of the impulse response. The transfer function could also be interpreted as the solution when excitation is given as a delta function in the original space, i.e. $f(s)=1$ as one of the boundary conditions.

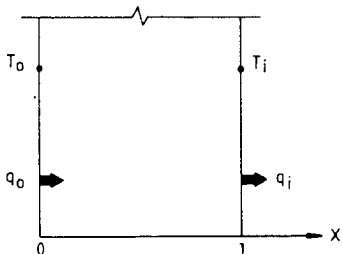


Figure 5.1 A homogeneous wall.

5.2.2.2 S-transfer function for a multilayer wall

The surface temperatures and heat flow of the building elements which form the enclosure are also important in evaluating comfort and radiation exchange between the surfaces on a time-dependent basis. Therefore, we are particularly interested in the temperature and heat flow at both surfaces of a wall.

When the temperature excitation is given on both surfaces at $x=0$ and $x=1$ in the expression $T(0,t)$ and $T(1,t)$ simultaneously, and when $\psi_{q0}(x,t)$ and $\psi_{q1}(x,t)$ stand for the impulse response of the heat flux at x against the surface temperature excitation at $x=0$ and $x=1$ respectively, the heat flux at both surfaces can be expressed as in the following convolution expression:

$$q(0,t) = \int_0^{\infty} \psi_{q0}(0,\tau) \theta(0,t-\tau) d\tau + \int_0^{\infty} \psi_{q1}(0,\tau) \theta(1,t-\tau) d\tau \quad (5.29)$$

$$q(1,t) = \int_0^{\infty} \psi_{q0}(1,\tau) \theta(0,t-\tau) d\tau + \int_0^{\infty} \psi_{q1}(1,\tau) \theta(1,t-\tau) d\tau \quad (5.30)$$

Let $r_{q0}(x,s) = L[\psi_{q0}(x,t)]$
 $r_{q1}(x,s) = L[\psi_{q1}(x,t)]$ (5.31)
 $\phi(0,s) = L[q(0,t)]$
 $\phi(1,s) = L[q(1,t)]$

The relationship between the temperatures and heat flows on both surfaces of the wall can be expressed as follows according to Equations (5.29) to (5.31):

$$\begin{bmatrix} \phi(0,s) \\ \phi(1,s) \end{bmatrix} = \begin{bmatrix} r_{q0}(0,s) & r_{q1}(0,s) \\ r_{q0}(1,s) & r_{q1}(1,s) \end{bmatrix} \begin{bmatrix} \theta(0,s) \\ \theta(1,s) \end{bmatrix} \quad (5.32)$$

where

$$\begin{aligned} r_{q1}(0,s) &= \frac{-\lambda\sqrt{s/a}}{\sinh(l\sqrt{s/a})} \\ r_{q1}(1,s) &= -\lambda\sqrt{s/a} \cdot \frac{\cosh(l\sqrt{s/a})}{\sinh(l\sqrt{s/a})} \\ r_{q0}(0,s) &= \lambda\sqrt{s/a} \cdot \frac{\cosh(l\sqrt{s/a})}{\sinh(l\sqrt{s/a})} \\ r_{q0}(1,s) &= \frac{\lambda\sqrt{s/a}}{\sinh(l\sqrt{s/a})} \end{aligned} \quad (5.33)$$

Furthermore, Equation (5.32) can be rewritten as (Kimura 1977):

$$\begin{bmatrix} \theta(0, s) \\ \phi(0, s) \end{bmatrix} = \begin{bmatrix} A(s) & B(s) \\ C(s) & D(s) \end{bmatrix} \begin{bmatrix} \theta(1, s) \\ \phi(1, s) \end{bmatrix} \quad (5.34)$$

where

$$\begin{aligned} A(s) &= \frac{\tau_{q1}(1, s)}{\tau_{q0}(1, s)} = \cosh(l\sqrt{s/a}) \\ B(s) &= \frac{1}{\tau_{q0}(1, s)} = \frac{\sinh(l\sqrt{s/a})}{\lambda\sqrt{s/a}} \\ C(s) &= \tau_{q1}(0, s) - \frac{\tau_{q1}(1, s)}{\tau_{q0}(1, s)} \cdot \tau_{q0}(0, s) = -\lambda\sqrt{s/a} \cdot \sinh(l\sqrt{s/a}) \\ D(s) &= \frac{\tau_{q0}(0, s)}{\tau_{q1}(1, s)} = \cosh(l\sqrt{s/a}) \end{aligned} \quad (5.35)$$

The physical meaning of Equation (5.34) is that it gives responses of temperature and of heat flow at one surface when both excitations of temperature and heat flow at the other surface affect the thermal system of a wall section as characterised by the transfer matrix. The square matrix on the right side of Equation (5.34) is called the transmission matrix, [H] for the wall.

The transmission matrix for a multilayer wall is the product of the transmission matrices for the various layers combined in the order in which they occur in the wall. Thus, for a wall of M layers (see Figure 5.2):

$$[H] = [H_1][H_2][H_3] \cdots [H_M] \quad (5.36)$$

Equation (5.34) can be re-arranged in the following forms when temperatures θ_0 and θ_M are given:

$$\begin{bmatrix} \phi_0 \\ \phi_M \end{bmatrix} = \frac{1}{B} \begin{bmatrix} D & -1 \\ 1 & -A \end{bmatrix} \begin{bmatrix} \theta_0 \\ \theta_M \end{bmatrix} \quad (5.37)$$

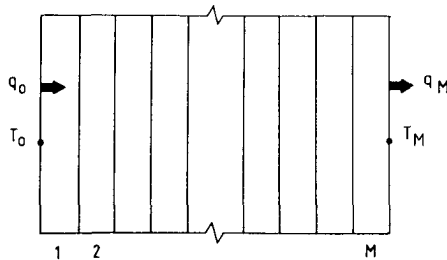


Figure 5.2 A multilayer wall.

5.2.2.3 Z-transfer function for a multilayer wall

In order to solve Equation (5.37), the excitation should be given as imaginary function which can be transformed easily into the Laplace imaginary form, although the calculation process in the convolution can still be complicated. The advanced way of convolution is represented by so-called Z-transform, which is often used in the numerical control in random process (Jury 1964).

In general the Laplace transform of $f(t)$, a function of time t , is expressed by definition as:

$$\theta(s) = \int_0^{\infty} f(t) \exp(-st) dt \quad (5.38)$$

When $f(t)$ is sampled at regular intervals of Δ , the output of the sampling device is a train of pulses. The Laplace transform of this output signal is:

$$\theta(s) = f(0) + f(\Delta) \exp(-s\Delta) + f(2\Delta) \exp(-2s\Delta) + \dots \quad (5.39)$$

If z is substituted for $\exp(s\Delta)$, the transform of the output from the sampler is:

$$f(z) = f(0)z^0 + f(\Delta)z^{-1} + f(2\Delta)z^{-2} + \dots \quad (5.40)$$

This polynomial in z^{-1} is the z-transform of the function $f(t)$. The main advantage of this type of transform is that it can be obtained simply by sampling the function at regular intervals: the successive outputs are the coefficients of successive powers of z^{-1} in the z-transform (Stephenson and Mitalas 1971).

The z-transfer function associated with a particular s-transfer function for a multilayer wall calculated by Stephenson and Mitalas (1971) is in the way to choose an input function that has a known Laplace transform and z-transform (this usually means either a step function or a ramp function). The Laplace transform of the corresponding output is the Laplace transform of the input multiplied by the s-transfer function. This output is converted into a function of z and is divided by the z-transform of the input. The quotient is the z-transfer function that corresponds to the s-transfer function. The following presents the details.

Table 5.1 gives the Laplace transforms and z-transforms for a few simple functions of time which was illustrated by Stephenson and Mitalas (1971). The choice of the input function is equivalent to choosing a function for interpolating between the discrete values given by the z-transform coefficients. The use of the step function is equivalent to representing the input by a staircase approximation, whereas the ramp function is equivalent to linear interpolation. It is important to remember that the resulting z-transfer function will have poles at the zeros of the z-transform of the input, because the output has to be divided by the z-transform of the input. Because the t^2 function produces an unstable result, this method is presented, therefore, for the case of a ramp input. (The results are equivalent to the response factors used by Mitalas (1968) and Kusuda (1969)).

The following discussion is concerned with the transfer function A/B , but the same approach can be used for any of the transfer functions that occur in Equation (5.37). For a ramp input the Laplace transform of the output is $A/(s^2B)$. This function can be expressed in the form of a sum as:

TABLE 5.1
Short table of equivalent Laplace and Z-transforms

f(t)	F(s)	F(Z)
1	1/s	$\frac{1}{1 - z^{-1}}$
t	1/s ²	$\frac{\Delta}{z(1 - z^{-1})^2}$
t ²	2!/s ³	$\frac{\Delta^2(1 + z^{-1})}{z(1 - z^{-1})^3}$
e ^{-at}	$\frac{1}{s + a}$	$\frac{1}{1 - e^{-a\Delta} z^{-1}}$

$$\frac{A}{s^2 B} = \frac{c_0}{s^2} + \frac{c_1}{s} + \sum_{n=1}^{\infty} \frac{d_n}{s + \beta_n} \quad (5.41)$$

where $s = -\beta_n$ are the roots of $B=0$. The coefficients c_0 , c_1 and d_n can be determined by the following formulas.

$$c_0 = [(A/B)]_{s=0} \quad (5.42)$$

$$c_1 = \left[\frac{d}{ds}(A/B) \right]_{s=0} = \left[\frac{B \frac{dA}{ds} - A \frac{dB}{ds}}{B^2} \right]_{s=0} \quad (5.43)$$

and

$$d_n = \left[\frac{A}{s^2 \frac{dB}{ds}} \right]_{s=-\beta_n} \quad (5.44)$$

Each of the terms in Equation (5.41) can be transformed into an equivalent z-transform by using the equivalent pairs of transforms in Table 5.1. Thus:

$$O(z) = \frac{c_0 \Delta}{z(1-z^{-1})^2} + \frac{c_1}{1-z^{-1}} + \sum_{n=1}^{\infty} \frac{d_n}{1 - e^{-\beta_n \Delta} z^{-1}} \quad (5.45)$$

When all those terms are added together, the denominator of the sum is:

$$z(1-z^{-1})^2 \prod_{n=1}^{\infty} (1 - e^{-\beta_n \Delta} z^{-1}) \quad (5.46)$$

The ratio of the output/input is the z-transfer function for the system. Assuming that such a transfer function, $K(z)$, can be found and that it can be expressed as the ratio of two polynomials in z^{-1} , i.e.:

$$K(z) = \frac{E(z)}{D(z)} = \frac{a_0 + a_1 z^{-1} + a_2 z^{-2} + \dots + a_j z^{-j}}{b_0 + b_1 z^{-1} + b_2 z^{-2} + \dots + b_p z^{-p}} = \frac{O(z)}{I(z)} \quad (5.47)$$

so that $D(z)$, the denominator of $O(z)/I(z)$, can be obtained from Equation (5.46):

$$D(z) = \prod_{n=1}^{\infty} (1 - e^{-\beta_n \Delta} z^{-1}) \quad (5.48)$$

$D(z)$ depends only on the roots of B and thus is the same for all transfer functions that have the same denominators in their s -transfer function counterparts.

Equation (5.48) shows that $b_0=1$ and $b_1 = -\sum_{n=1}^{\infty} e^{-\beta_n \Delta}$. (The other coefficients of $D(z)$ are found by multiplying the factors together.) There is an infinite set of roots of $B=0$ lying along the negative real axis.

The values of the various 'a' coefficients in the numerator polynomial $E(z)$ can be found by summing the numerators of the different components of $O(z)$ after they have been multiplied by the appropriate expressions to give them all a common denominator. It is more convenient, however, to proceed in a slightly different way. The function:

$$L^{-1}\left[\frac{A}{s^2 B}\right] = c_0 t + c_1 + \sum_{n=1}^{\infty} d_n e^{-\beta_n t} \quad (5.49)$$

can be evaluated for $t=\Delta, 2\Delta, \dots$ to give the coefficients O_1, O_2, \dots of $O(z)$. But by definition:

$$O(z) \cdot D(z) = I(z) \cdot E(z) \quad (5.50)$$

so that

$$E(z) = \frac{D(z)}{I(z)} \cdot O(z) \quad (5.51)$$

Hence,

$$E(z) = \frac{z(1-z^{-1})^2}{\Delta} \prod_{n=1}^{\infty} (1 - e^{-\beta_n \Delta} z^{-1}) \cdot O(z) \quad (5.52)$$

As $O_0=0$ the coefficient of z^{+1} in $E(z)$ is zero and the first term in $E(z)$ is

$$a_0 = \frac{1}{\Delta} (c_0 \Delta + c_1 + \sum_{n=1}^{\infty} d_n e^{-\beta_n \Delta}) \quad (5.53)$$

Here values of β_n are used to get progressively each successive values of a .

The computer code ACCURACY uses either square pulses or triangle pulses as input function $I(z)$ so that the z -transfer function obtained from ACCURACY is for square or triangle pulses. The program for obtaining the z -transfer

factors (Mitalas and Arseneault 1970) was modified as a part of the subroutines used in ACCURACY.

A similar method is used for the determination of the z-transfer functions of D/B and l/B. The heat flux on both sides of surfaces q_0 and q_M can be obtained from the following expression, viz.

$$q_{0n} = \sum_{j=0}^N ZD_j T_{0n-j} - \sum_{j=0}^N Zl_j T_{Mn-j} - \sum_{j=1}^N ZB_j q_{0n-j} \quad (5.54)$$

$$q_{Mn} = \sum_{j=0}^N Zl_j T_{0n-j} - \sum_{j=0}^N ZA_j T_{Mn-j} - \sum_{j=1}^N ZB_j q_{Mn-j} \quad (5.55)$$

where ZD_j , Zl_j , ZA_j and ZB_j are the z-transfer factors; ZD_j , Zl_j and ZA_j are the coefficients a_j in Equation (5.47) for D/B, l/B and A/B and ZB_j are the coefficients b_j in Equation (5.47); N is the term number of the z-transfer factors, n is current time step, T_0 , T_M , q_0 and q_M are temperatures and heat flux indicated in Figure 5.2.

5.2.3 Heat transfer on surfaces of enclosure

The heat exchange on the outside and inside surfaces of walls and windows are very important in air-conditioning load computations. They should be built up before the overall energy balance equation for a room is set up. The convection between the surfaces and the air adjacent to it and the radiation from the sun, ground and sky, etc., take place at the same time on the exterior surfaces of buildings. The radiation among the inside surfaces and convection between inside surfaces and room air near the surfaces play a very important role in the energy computations. In this subsection the combination of the radiation, convection and conduction on walls and windows which was used in ACCURACY will be discussed.

5.2.3.1 Convective heat exchange coefficients

In the calculation of heat gain or loss through walls, convective heat exchange coefficients should be used. The values of the convective heat exchange coefficients are usually higher for the outside surfaces of exterior walls than for the inside, because the air movement along the outside surface is higher. They will be discussed successively in this section.

Convective heat exchange coefficient on the outside surface of an exterior wall. Sato et al. (1972) and Ito et al. (1972) considered that the principal factors governing the convective heat transfer are wind speed and direction in relation to the geometry of the surface. First the following formula is used to reveal the relationship between wind speed, U, and airflow velocity near the surface, u:

$$\begin{aligned} u &= 0.25U && \text{(for } U > 2) && \text{if the surface is windward;} && (5.56) \\ u &= 0.5 && \text{(for } U \leq 2) \end{aligned}$$

$$u = 0.3 + 0.05U \quad \text{if the surface is leeward.} \quad (5.57)$$

Because the relationship between convective heat exchange coefficient and airflow velocity near the surface is found to be fairly consistent and independent of either the wind direction relative to the surface or the surface location of the building, this breakdown is necessary for the estimation of the convective heat exchange coefficient, especially when the air temperature near the surface is different from the ambient dry bulb temperature. The convective heat exchange coefficient α_c is calculated from (Kimura 1977):

$$\alpha_c = 3.5 + 5.6u \quad (5.58)$$

Convective heat exchange coefficient on an inside surface. The inside convective heat exchange coefficient is quite variable due to a number of different causes. The computer code ACCURACY uses the formulae which were got from the measurements and the computations using the improved wall functions. The detailed information was described in sections 2.4.2 and 2.4.3.

5.2.3.2 Radiative heat exchange coefficients

The radiative heat exchange between enclosure surfaces is complicated. In practice, these enclosure surfaces are considered as grey bodies. The radiative heat exchange $Q_{i,j}$ between surface i to j is calculated from:

$$Q_{i,j} = \epsilon_i \psi_{i,j} (E_{b,i} - E_{b,j}) A_i \quad (5.59)$$

where ϵ_i is the emissivity of the surface, $\psi_{i,j}$ is the radiative heat exchange factor between surfaces i and j , A_i is the area of the surface i , and $E_{b,i}$ and $E_{b,j}$ are the emissive power of black body for surfaces i and j respectively.

Hoornstra (1986) presented the formula to calculate the radiative heat exchange factor $\psi_{i,j}$ in which the multiple reflection of the radiative heat exchange in a room was considered. If the view factor from surfaces i to p is $F_{i,p}$, $F_{i,p} E_{b,i} A_i$ is the amount projected on the surface p (See Figure 5.3).

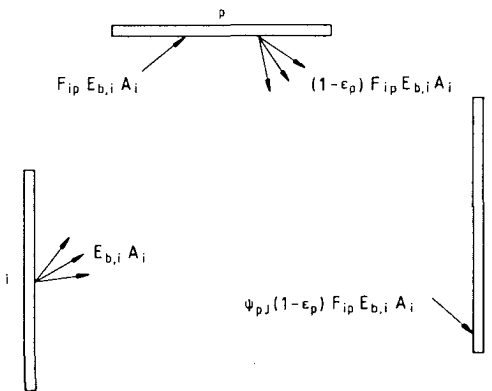


Figure 5.3 Multiple radiation among grey body walls.

Then the reflection absorbed by surface j is expressed as:

$$\psi_{p,j} \rho_p F_{i,p} E_{b,i} A_i \quad (5.60)$$

where ρ_p is the reflectivity of surface p. The direct radiation from surface i absorbed by surface j is:

$$a_j F_{i,j} E_{b,i} A_i \quad (5.61)$$

where a_j is the absorptivity of surface j.

Considering the multiple reflections from all the room surfaces, therefore, the total radiation from surface i absorbed by surface j is:

$$\psi_{i,j} E_{b,i} A_i = a_j F_{i,j} E_{b,i} A_i + \sum_{p=1}^N \psi_{p,j} \rho_p F_{i,p} E_{b,i} A_i \quad (5.62)$$

where N is the room surface number.

For all surfaces of the room, Equation (5.62) can be written as the following matrix equation:

$$\begin{bmatrix} \psi_{1,1} & \cdots & \psi_{N,1} \\ & \cdots & \\ \psi_{1,N} & \cdots & \psi_{N,N} \end{bmatrix} = \text{diag}(a) \begin{bmatrix} F_{1,1} & \cdots & F_{N,1} \\ & \cdots & \\ F_{1,N} & \cdots & F_{N,N} \end{bmatrix} + \begin{bmatrix} \psi_{1,1} & \cdots & \psi_{N,1} \\ & \cdots & \\ \psi_{1,N} & \cdots & \psi_{N,N} \end{bmatrix} \text{diag}(\rho) \begin{bmatrix} F_{1,1} & \cdots & F_{N,1} \\ & \cdots & \\ F_{1,N} & \cdots & F_{N,N} \end{bmatrix} \quad (5.63)$$

After re-arrangement by the relations:

$$a_i = \epsilon_i; \rho_i = 1 - \epsilon_i \quad (5.64)$$

the matrix can be expressed as:

$$[\psi] = \{[I] - [F] \cdot \text{diag}(1 - \epsilon)\}^{-1} \cdot [F] \cdot \text{diag}(\epsilon) \quad (5.65)$$

From the practical point of view it is very convenient that the rate of radiative heat transfer from one surface to the other is expressed in the form:

$$Q_{i,j} = \alpha_{r_{i,j}} (T_i - T_j) A_i \quad (5.66)$$

where T_i and T_j are the temperatures of surface i and surface j respectively. $\alpha_{r_{i,j}}$ is defined as radiative heat exchange coefficient from surfaces i to j. A_i is the area of surface i. Equation (5.66) can be arranged to yield:

$$\begin{aligned}\alpha_{r_{i,j}} &= \epsilon_i \psi_{i,j} \sigma_0 \left(\frac{T_i^4 - T_j^4}{T_i - T_j} \right) \\ &= \epsilon_i \psi_{i,2} \sigma_0 \theta\end{aligned}\quad (5.67)$$

where σ_0 is Stefan-Bolzman constant and $\theta = T_i^3 + T_i^2 T_j + T_i T_j^2 + T_j^3$. When the difference between T_i and T_j is not too large ($0.7 \leq T_i/T_j \leq 1.4$), θ can be simplified as

$$\theta = 4[(T_i + T_j)/2]^3 \quad (5.68)$$

5.2.3.3 Absorptivity, transmissivity and reflectivity of a window

Since a considerable part of the space load is caused by solar radiation through glass windows, various types of shading devices are being used to reduce the heat from the sun through windows. The method of estimating the absorptivity, transmissivity and reflectivity of a window for solar radiation, which was used in ACCURACY, will be discussed.

Single sheet of glass. A part of radiation incident upon the glass surface is transmitted through the glass, a part of it absorbed by the glass and the remainder reflected back towards the space where it comes from. The value of these three components can be expressed by the surface reflectance and the absorption coefficient in the glass to be concerned. The absorptivity A_g , reflectivity R_g and transmissivity T_g of a sheet of glass can be written as (Oegema 1970):

$$T_g = \frac{1}{2} \left[\frac{t_t^2 a}{1 - a^2 r_t^2} + \frac{t_l^2 a}{1 - a^2 r_l^2} \right] \quad (5.69)$$

$$R_g = \frac{1}{2} \left[r_t + r_l + \frac{t_t^2 a^2 r_t}{1 - a^2 r_t^2} + \frac{t_l^2 a^2 r_l}{1 - a^2 r_l^2} \right] \quad (5.70)$$

$$A_g = 1 - T_g - R_g \quad (5.71)$$

where r_t and r_l are the surface reflectance for vertical and horizontal parts of the radiation respectively, a is the absorption coefficient of the glass and t_t and t_l are the surface transmission for vertical and horizontal parts of the radiation respectively.

The diffusion on the sky and reflection from the ground must also be updated. The view factors for sky and ground normally are taken as 0.5 respectively. Therefore the absorptivity a_g , reflectivity r_g and transmissivity t_g of the sheet of glass for the diffuse radiation from the sky can be obtained by integrating A_g , R_g and T_g respectively over the sky area. The transmissivity, absorptivity and reflectivity of the ground reflection is the same as those of diffuse from sky for a single glass window.

Single layer venetian blinds. The venetian blinds are widely used to intercept mainly direct solar radiation. Parmelee and his co-workers (1952, 1953) derived a set of formulas to calculate the absorptivity, reflectivity and transmissivity of slat-style venetian blinds. If L is a factor to identify whether or not part of the direct solar radiation transmits through the slat assembly, the transmissivity T_v , and the absorptivity A_v and reflectivity R_v for direct solar radiation can be expressed by the following formulas. For $L \geq 0$,

$$T_v = L + (1 - L) \left[F_1(1 - a) + \frac{F_2 F_3(1 - a)^2}{1 - F_2^2(1 - a)^2} + \frac{F_1 F_2^2(1 - a)^3}{1 - F_2^2(1 - a)^2} \right] \quad (5.72)$$

$$A_v = a(1 - L) \left[1 + \frac{F_2(1 - a)}{1 - F_2(1 - a)} \right] \quad (5.73)$$

$$R_v = 1 - T_v - A_v \quad (5.74)$$

For $L < 0$

$$T_v = (1 - a)F_4 + \frac{F_3 F_5(1 - a)^2}{1 - F_2^2(1 - a)^2} + \frac{F_1 F_2 F_5(1 - a)^3}{1 - F_2^2(1 - a)^2} \quad (5.75)$$

$$A_v = a + \frac{a F_5(1 - a)}{1 - F_2(1 - a)} \quad (5.76)$$

$$R_v = 1 - T_v - A_v \quad (5.77)$$

where a is the absorptivity of slat surface and $F_1, F_2, F_3, F_4,$ and F_5 are the form factors of the venetian blinds (Parmelee et al. 1952, 1953).

The absorptivity a_{vs} , transmissivity t_{vs} and reflectivity r_{vs} for the diffuse radiation from the sky can be obtained by integrating A_v, T_v and R_v respectively on the sky area and the absorptivity a_{vf} , transmissivity t_{vf} and reflectivity r_{vf} for the ground reflection by integrating from the ground area.

Multilayer window. When a window structure has more than one layer, the overall absorptivity, the overall transmissivity and the overall reflectivity must be considered taking multiple repetitions of absorption, transmission and reflection by each layer as shown in Figure 5.4.

Oegema (1970) developed the formulas to calculate the overall absorption, transmission coefficients for multilayer windows. For the window shown in Figure 5.4, the overall coefficients can be expressed by the summation of infinite series as follows.

For direct radiation, the overall transmission coefficient T^0 is:

$$T^0 = T_{vg} + t_{vg} R_v r_g + t_{vg} R_v r_g^2 r_v + \dots$$

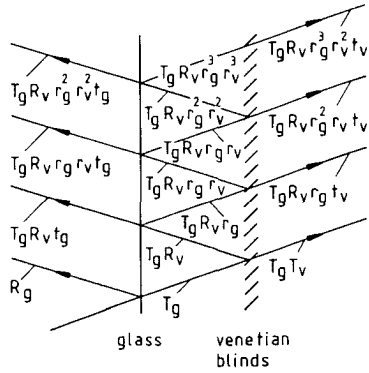


Figure 5.4 Reflection, absorption and transmission in a window with outside glass and inside venetian blinds.

$$= T_v T_g + \frac{t_v T_g R_v r_g}{1 - r_g r_v} \quad (5.78)$$

Similarly, the overall absorption coefficients for the direct radiation for glass A_g^0 and for venetian blinds A_v^0 are:

$$A_g^0 = A_g + \frac{a_g T_g R_v}{1 - r_g r_v} \quad (5.79)$$

$$A_v^0 = T_g A_v + \frac{t_g R_v a_r}{1 - r_g r_v} \quad (5.80)$$

The similar method can be applied for the reflection R^0 .

For diffuse radiation from the sky and reflection from the ground, the overall transmission coefficients t_s^0 and t_f^0 , the overall absorption coefficients of glass a_{gs}^0 and a_{gf}^0 and the overall absorption coefficients of the venetian blinds a_{vs}^0 and a_{vf}^0 are determined in a similar procedure.

The formulas to calculate the overall absorption and transmission coefficients for the windows with the following structure were also built in the computer program ACCURACY.

- outside venetian blinds inside glass;
- double glass;
- outside double glass and inside venetian blinds;
- double glass with venetian blinds between the glass; and
- outside venetian blinds and inside double glass.

5.2.3.4 Shadow factor

A portion of the air-conditioning load on buildings comes from solar radiation. To improve the accuracy of load assessment, it is necessary to know how much of a building is shaded and how much lies exposed to the sun's rays. Tseng-yao Sun's algorithm (1968) has been used in the computer program

ACCURACY to find the ratio of the sunlit and shaded area of a given window where the shadows are cast by various combinations of overhang and side fins.

5.2.3.5 Thermal balance on the outside surface of a wall

Radiation and convection always takes place in a mixed mode on the surfaces of a wall. The heat conduction in the wall is an unsteady one as has been discussed in section 5.2.2. The heat exchange at the outside surface and the inside surface of the wall or slab is different, their nature will be studied in this and next subsections.

At the outside surface of a building, there are always two components of heat, the one coming into and that leaving the surface. The temperature of the surface is such that the heat balance is to be maintained. The thermal state of a wall is presented in Figure 5.5.

The heat balance equation at the outside surface can be expressed as follows:

$$q_s + q_{oex} = q_{oc} + q_o \tag{5.81}$$

where q_s is solar radiation absorbed by the outside surface, q_{oex} is extra heat flux pressed on and absorbed by the outside surface, q_{oc} is overall convective heat transfer from the outside surface to the ambient air and q_o is the heat conduction flux at the outside surface into the wall.

The left hand side of Equation (5.81) is the heat coming into the surface and right-hand side is the heat going out of the outside surface. The above terms can be expressed as follows:

$$q_s = a_{oD} I_{Dc} + a_{od} (I_{dcs} + I_{dcf}) \tag{5.82}$$

where I_{Dc} , I_{dcs} , and I_{dcf} are direct, diffuse and ground reflection components of solar radiation under a cloudy condition upon the outside surface respectively; a_{oD} and a_{od} are the absorptivities of the outside surface for direct and diffuse radiation respectively.

$$q_{oc} = \alpha_{oc} (T_o - T_a) \tag{5.83}$$

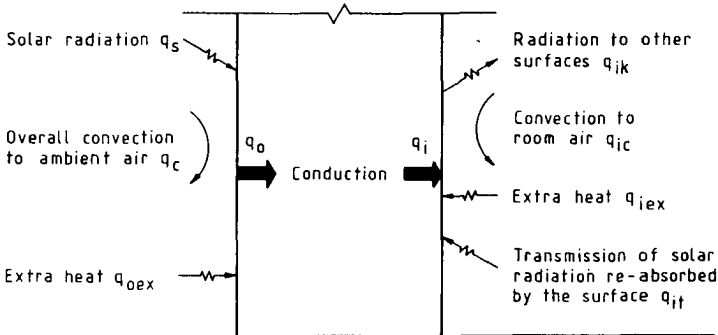


Figure 5.5 Heat exchange in an exterior wall.

where T_o is the outside surface temperature (K), α_{oc} is the overall outside surface heat exchange coefficient which considers the heat exchange by atmospheric radiation, earth radiation, wall surface radiation and convection between the outside wall surface and the ambient air.

$$q_o = q_{o,n} = \sum_{j=0}^M ZD_j T_{o,n-j} - \sum_{j=0}^M ZI_j T_{i,n-j} - \sum_{j=1}^M ZB_j q_{o,n-j} \quad (5.84)$$

where ZD_j , ZI_j , and ZB_j are the z-transfer factors as described in Equation (5.54); M is the term number of the z-transfer factors; $T_{o,n-j}$ and $T_{i,n-j}$ are the outside and inside surface temperatures at time $(n-j)\Delta t$.

5.2.3.6 Thermal balance on the inside surface of a wall

The radiation occurring on the inside surface of a wall takes place among the inside surfaces of a room and the convection occurs between the inside surface and the air near the surface. In general the inside surface temperature of the wall is different from the room air temperature near the surface and this is particularly evident during early morning hours in the case of intermittent operation of air-conditioning. As a matter of fact, the surface temperatures are determined by convective heat transfer to or from the room air near the surface and radiative heat exchange between the surfaces. Using the time series notation on an unsteady state basis, the heat balance at the inside surface as shown in Figure 5.5 is:

$$q_i + q_{iex} + q_{it} = \sum_{\substack{k=1 \\ k \neq i}}^N q_{ik} + q_{ic} \quad (5.85)$$

where q_i is the heat conduction flux at the inside surface from the outside surface, q_{iex} is extra heat pressed on and absorbed by the inside surface, q_{it} is the solar radiation transmission through the windows of the room re-absorbed by the inside wall surface. q_{ik} is the radiation transfer from the inside surface i to the other inside surface k, and q_{ic} is the convective heat transfer to the room air near the surface. The above terms can be expressed as follows:

$$q_i = q_{i,n} = \sum_{j=0}^M ZI_j T_{o,n-j} - \sum_{j=0}^M ZA_j T_{i,n-j} - \sum_{j=1}^M ZB_j q_{i,n-j} \quad (5.86)$$

where ZI_j , ZA_j and ZB_j are the z-transfer factors.

q_{it} is calculated from direct, diffuse and reflected solar radiation and the overall transmissivities of each window.

$$q_{ik} = \alpha_{r_{i,k}} (T_i - T_k) \quad (5.87)$$

where $\alpha_{r_{i,k}}$ is the radiative heat exchange coefficient from the surface i to surface k as described in section 5.2.3.2, T_k is the temperature on inside surface k .

$$q_{ic} = \alpha_{ic}(T_i - T_{ri}) \tag{5.88}$$

where α_{ic} is the inside convective heat exchange coefficient, T_{ri} is the room air temperature near the inside surface i .

5.2.3.7 Thermal balance on the outside layer of a window

Due to the fact that the heat capacity of a window is very small, it can be ignored in the computation of air-conditioning load. Therefore, z-transfer functions are unnecessary to be used for window structure enclosures. But some window structures are rather complicated as shown in Figure 5.6 in which the window has three layers. Because a window may be the combination of venetian blinds and glasses, solar radiation can be reflected, absorbed and transmitted in any layer of the window. The determinations of the reflectivity, absorptivity, and transmissivity for direct radiation, diffuse radiation from the sky and reflection from the ground for many kinds of windows have been discussed in subsection 5.2.3.3. In this and the next subsections the window with three layers as shown in Figure 5.6 is taken as an example to establish the heat balance equations.

Very similar to the heat transfer on the outside surface of a wall, the heat balance equation on the outside layer of the window can be expressed as:

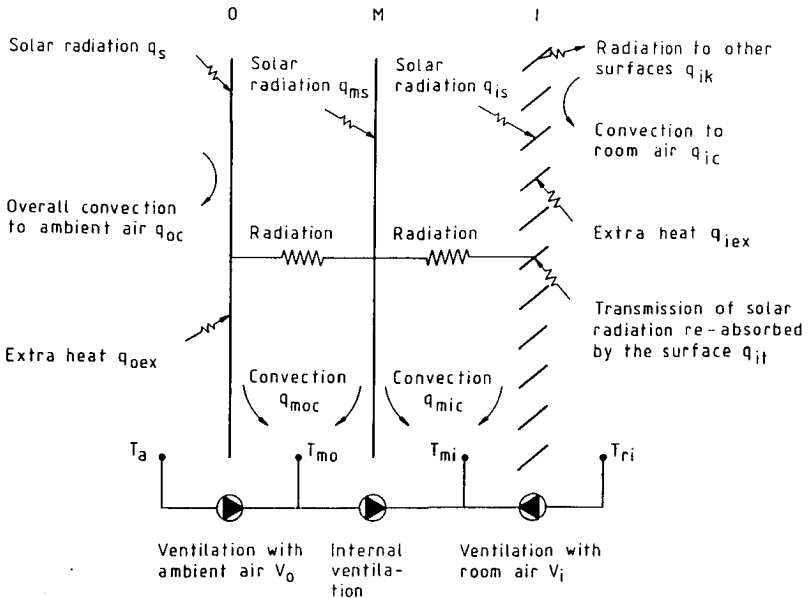


Figure 5.6 Heat exchange in an exterior window.

$$q_s + q_{oex} = q_{oc} + q_o \quad (5.89)$$

The left hand side of Equation (5.89) is the heat coming into the surface and right-hand side is the heat going out of the outside surface. Besides the similar terms discussed in section 5.2.3.5, the rest term, q_s , can be rewritten as follows:

$$q_s = S_D a_{oD} I_{Dc} + S_s a_{os} I_{dcs} + S_f a_{of} I_{dcf} \quad (5.90)$$

where I_{Dc} , I_{dcs} , and I_{dcf} are direct, diffuse and ground reflection components of solar radiation under a cloudy sky condition upon the outside surface respectively; S_D , S_s and S_f are the shade ratios of the window for I_{Dc} , I_{dcs} , and I_{dcf} respectively; and a_{oD} , a_{os} and a_{of} are the absorptivity of the outside surface for I_{Dc} , I_{dcs} , and I_{dcf} respectively. q_o is the sum of the convective heat released to the air between layer O and layer M and the radiative heat transferred to middle layer M:

$$q_o = \alpha_{oi}(T_o - T_{mo}) + \alpha_{or}(T_o - T_m) \quad (5.91)$$

where α_{oi} is the inside convective heat exchange coefficient of the outside layer; T_{mo} is the air temperature between outside layer (o) and middle surface (m); T_m is the middle layer temperature; and α_{or} is the radiative heat exchange coefficient from outside layer to the middle layer.

5.2.3.8 Thermal balance on the inside layer of a window

The heat balance equation on the inside layer (i) of the window as shown in Figure 5.6 can be expressed as:

$$q_{is} + q_i + q_{iex} + q_{it} = \sum_{k=1}^N q_{ik} + q_{ic} \quad (5.92)$$

where q_{is} solar radiation absorbed by the inside window surface. It is determined from:

$$q_{is} = S_D a_{iD} I_{Dc} + S_s a_{is} I_{dcs} + S_f a_{if} I_{dcf} \quad (5.93)$$

where a_{iD} , a_{is} and a_{if} are the absorptivity of the inside layer for I_{Dc} , I_{dcs} , and I_{dcf} respectively.

$$q_i = \alpha_{io}(T_{mi} - T_i) + \alpha_{ir}(T_m - T_i) \quad (5.94)$$

Other terms of Equation (5.92) are similar to those of Equation (5.85).

5.2.4 The influence of indoor air temperature distributions

Most available normal cooling load computer programs are based on the one-air-point model, which means that the values of the whole temperature field in a room are assumed to be uniform. In many air-conditioned rooms with a high ventilation rate, this kind of treatment can be accepted because the room air temperatures are the same. However, if this one-air-point model is applied to an air-conditioned room with a low ventilation rate or with natural convection or to big industrial halls and theatres, a large error in the energy consumption will result. This is due to the presence of a vertical temperature difference in room air. The vertical temperature difference is generated from buoyancy and plays an important role in the computations of an air-conditioning load.

In order to study the influence of the vertical temperature difference with room air, Van der Kooi and his co-workers (1983, 1985, 1987) developed three improved methods for the computation of air-conditioning loads (See Figure 5.7): (1) adjusting the convective heat-exchange coefficient near the inside wall surface, (2) introducing constant temperature differences between the middle point of the room and the air layers adjacent to ceiling and floor, and (3) using more air points, each representing a part of the room and mutually connected by adjustable mass flows. The first method gives unrealistic physical results, since the adjusted heat exchange coefficients have to be negative sometimes in order to calculate the right heat flux into the ceiling, floor, and wall surfaces. The second method requires that temperature differences are obtained from measurements, and they are not always available. Van der Kooi and Chen (1987) demonstrated in a previous paper that, for situations with a varying air-conditioning load, the constant-temperature method gave results different from the measured ones, because the temperature differences change with time. In the third method, the results are noted to depend critically on the mass flow pattern used. These mass flows are usually obtained from measurements. The more-air-points model with 9 or 16 points cannot be applied to describe the complicated airflow structure in a room because more points are needed (See chapter 4 for details). These methods, therefore, cannot account precisely for the influence of room air movement and temperature distribution on room energy consumption.

Since the early 1970s, many computer programs have been written for the calculation of heat transfer and fluid flow. A much greater reliability on the calculation of fully turbulent flow was obtained by introducing the $k-\epsilon$ model (Harlow and Nakayama 1968, Launder and Spalding 1974) which has been discussed in chapter 2. For the computations in a room, the inputs required by an airflow program are enclosure surface temperatures, inlet and outlet

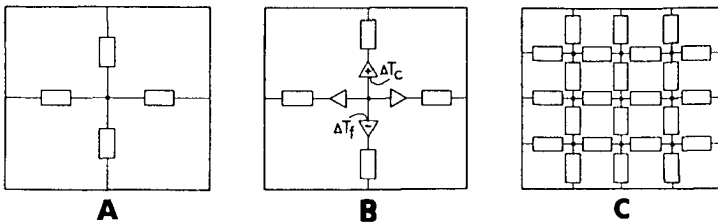


Figure 5.7 Indoor air temperature models. (A) One point model; (B) constant temperature difference model; (C) more points model.

locations, mass flow rate, the temperature of air supply, etc. These can be obtained from the outputs of a cooling load program. However, the outputs of the airflow program, such as room air velocity, temperature and contamination distributions and convective heat exchange coefficients, are a part of the inputs for the cooling load program. Therefore, the combination of a normal cooling load program with an airflow program can be used to study the influence of the indoor airflow, temperature distribution on room energy consumption.

The computer code ACCURACY was developed based on the idea of combining a cooling load program with an airflow program in order to find a better agreement between computed and measured results of room air-conditioning load and temperatures. The concentration of contamination, air velocity and temperature distributions can be also predicted with this program for evaluating comfort.

The main difference between ACCURACY and other cooling load programs is that the former considers transient temperature distributions of room air. This temperature distributions can be obtained from an airflow computer program hourly, such as PHOENICS or CHAMPION SGE. However, it is too expensive to get the time-dependent airflow and temperature distributions of a room from an airflow computer program based on the $k-\epsilon$ turbulence model. This is due to the properties of the fluid and turbulence governing equations as well as the numerical method, which requires a large amount of grid numbers to give a good prediction as indicated in chapter 4. For three-dimensional computations, a grid number $18 \times 18 \times 23$ is required for the air-conditioned room. This is equivalent to approximately 80 minutes CPU time in an IBM 3083-JX1 computer for a steady situation. For these reasons, a direct combination between a cooling load program and the airflow program will be unacceptable for practical use.

It has been demonstrated by Chen and Van der Kooi (1987b) that under a forced convection situation, the airflow pattern seems to be independent of time if the inlet airflow mass is maintained to be constant and heat introduced on the venetian blinds does not change very much, although there may be a great change in the air temperature of the room. This is explained by examining the governing equations of the airflow programs PHOENICS and CHAMPION SGE which were described in chapter 2:

$$\frac{\partial}{\partial t}(\rho\phi) + \text{div}(\rho\vec{V}\phi - \Gamma_{\phi}\text{grad}\phi) = S_{\phi} \quad (2.48)$$

where ϕ stands for any one of the variables: l , V_i , k , ϵ , H and C .

The temperature and concentration equations have no direct influence on the transient, convective, and diffusive terms of the velocity components. If the thermal boundary conditions can be estimated somehow, the buoyancy contribution to the source terms of the velocities and the turbulent parameters, such as Γ_{ϕ} , can be determined for typical situations. This means that a number of airflow distributions can be pre-calculated in an airflow program under different kinds of boundary conditions, such as various kinds of inlet mass flow and different heat gains from windows, etc. When a simulation of annual energy consumption is required, the computer program searches for one of the airflow patterns pre-calculated as the airflow distribution at the moment according to the corresponding thermal boundary conditions. A computation on the hourly room air temperature distribution is necessary because the thermal boundary conditions may vary significantly and

this may be obtained from the corresponding flow pattern based on the energy equation:

$$\frac{\partial}{\partial t}(\rho H) + \text{div}(\rho \vec{V}H - \Gamma_H \text{grad} H) = 0 \quad (5.95)$$

where

$$H = \frac{C}{P} T \quad (5.96)$$

In this case, the temperature is considered to be an auxiliary variable and has no direct influence on flow fields, since the convergence is very fast. When the simulation of contamination concentration is required, it can be obtained using the concentration equation:

$$\frac{\partial}{\partial t}(\rho C) + \text{div}(\rho \vec{V}C - \Gamma_C \text{grad} C) = 0 \quad (5.97)$$

This equation can be solved with the same procedure as the energy equation (5.95), but because the normal air-conditioning load calculation is based on a one-hour time step, the transient term can be ignored. For some kinds of contaminant, such as tobacco smoke, the time step has to be divided as small as one minute and the transient term then must be taken into consideration. Furthermore, they are solved in two different time steps in ACCURACY. For example, the time step for temperature is one hour and for concentration is one minute in the computations for a room. The "staggered grid" and the upwind scheme, which are employed in the airflow programs PHOENICS and CHAMPION SGE, are used here for Equations (5.95) and (5.97) in ACCURACY. The finite domain form of Equations (5.95) and (5.97) is:

$$\phi_P = \frac{a_E \phi_E + a_W \phi_W + a_N \phi_N + a_S \phi_S + a_H \phi_H + a_L \phi_L + a_T \phi_P + S_0}{a_P} \quad (2.59)$$

where ϕ stands for any one of T and C.

The finite-domain equations are solved by the Gauss-Seidel method in ACCURACY.

5.2.5 Room energy balance equations

The cooling load computer program ACCURACY was constructed to meet such kind of requirements as predictions of heat extraction and room temperatures. In order to maintain comfort in a room, positive or negative heat must be supplied to or removed from the room by various means. The amount of heat removed for this purpose is known as cooling load (air-conditioning load). When room temperature is a function of time, the heat removed is called heat extraction.

5.2.5.1 Heat gain components

The components of the air-conditioning load of the room should be discussed first before the room energy balance equation of a room is built. The common components in a room are:

- (1) the heat from lights;

- (2) the heat from occupants;
- (3) the heat from appliances;
- (4) the heat from infiltration;
- (5) the heat transfer through windows; and
- (6) the heat transfer through walls, ceiling, floor, etc.

Terms (1) to (4) can be calculated via the methods discussed in subsection 5.1.3. Terms (5) and (6) have been described in sub section 5.2.3.

5.2.5.2 Heat balance of a room

If the whole room air is taken as a control volume, the heat balance of the room means that the sum of the input and output heat of the control volume is the energy gain of the control volume. The input heat components are:

- the heat exchange from the enclosures (such as walls, windows, etc.),

$$N \sum_{i=1}^N q_{ic} A_i$$
, where A_i is the area of region i ;
- the heat from lights, occupants, appliances and infiltration,
 $H_L + H_P + H_A + H_I$; and
- the internal ventilation between room air and window gaps is $\sum_{i=1}^N V_i (T_{mi} - T_{ri}) A_i$; where V_i is mass flow flux of region i , T_{mi} is the gap air temperature.

The output component is the heat extraction, H_{ex} and the energy gain of the control volume is:

$$\frac{\rho V_R C_p [T_R(n) - T_R(n-1)]}{\Delta t}$$

where V_R is the room air volume, Δt is the time interval and n is current time and T_R is the room air temperature at the controlled point.

Therefore the heat balance for the room is:

$$\frac{\rho V_R C_p [T_R(n) - T_R(n-1)]}{\Delta t} = \sum_{i=1}^N q_{ic} A_i + H_L + H_P + H_A + H_I + \sum_{i=1}^N V_i (T_{mi} - T_{ri}) A_i - H_{ex} \quad (5.98)$$

If the heat extraction is to be calculated, Equations (5.85) and (5.92) are required to calculate wall enclosure surface temperature T_i , i.e.:

$$q_i + q_{iex} + q_{it} = \sum_{k=1}^N q_{ik} + q_{ic} \quad \text{for walls} \quad (5.85)$$

$$q_{is} + q_i + q_{iex} + q_{it} = \sum_{k=1}^N q_{ik} + q_{ic} \quad \text{for windows} \quad (5.92)$$

where q_{ic} can be written as:

$$q_{ic} = \alpha_{ic} (T_i - T_R) - \alpha_i \Delta T_{ri} \quad (5.99)$$

because

$$T_{ri} = T_R + \Delta T_{ri} \quad (5.100)$$

where ΔT_{ri} is the temperature difference between the controlled point and the point near wall surface i .

All equations are related and form a set of simultaneous equations and may be expressed in matrix form as shown below:

$$[M] \cdot [T] = [q] + [\alpha \Delta T] \quad (5.101)$$

where

$$[M] = \begin{bmatrix} \alpha_{1c} + \sum_{k=1}^N \alpha_{r1,k} & -\alpha_{r1,2} & -\alpha_{r1,3} & \dots & -\alpha_{r1,N} \\ -\alpha_{r2,1} & \alpha_{2c} + \sum_{k=1}^N \alpha_{r2,k} & -\alpha_{r2,3} & \dots & -\alpha_{r2,N} \\ \dots & \dots & \dots & \dots & \dots \\ -\alpha_{rN,1} & -\alpha_{rN,2} & \dots & -\alpha_{rN,N-1} & \alpha_{Nc} + \sum_{k=1}^N \alpha_{rN,k} \end{bmatrix} \quad (5.102)$$

$$[T] = \begin{bmatrix} T_1 \\ T_2 \\ \vdots \\ \vdots \\ T_N \end{bmatrix} \quad (5.103)$$

$$[q] = \begin{bmatrix} q_{1,coming} + \alpha_{1c} T_R \\ q_{2,coming} + \alpha_{2c} T_R \\ \vdots \\ \vdots \\ q_{N,coming} + \alpha_{Nc} T_R \end{bmatrix} \quad (5.104)$$

$$[\alpha \Delta T] = \begin{bmatrix} \alpha_{1c} \Delta T_{r1} \\ \alpha_{2c} \Delta T_{r2} \\ \vdots \\ \vdots \\ \alpha_{Nc} \Delta T_{rN} \end{bmatrix} \quad (5.105)$$

The $q_{i,coming}$ in Equation (5.104) is:

$$q_{i,coming} = q_i + q_{iex} + q_{it} \quad \text{for walls} \quad (5.106)$$

$$q_{i,coming} = q_{is} + q_i + q_{iex} + q_{it} \quad \text{for windows} \quad (5.107)$$

Equation (5.101) is so-called room energy balance equation.

5.2.5.3 Determination of the heat extraction of a room

According to Equations (5.98) and (5.100), the heat extraction, H_{ex} , is expressed as:

$$H_{ex} = \sum_{i=1}^N q_{ic} A_i + H_L + H_P + H_A + H_I + \sum_{i=1}^N V_i (T_{mi} - T_R - \Delta T_{ri}) A_i - \frac{\rho V_R C_p [T_R(n) - T_R(n-1)]}{\Delta t} \quad (5.108)$$

The computer program can consider the room air temperature difference ΔT_{ri} in five ways: (1) The method with uniform room air temperature in which no air temperature difference in the room is considered, (2) The method with fixed room air temperature difference in which constant air temperature differences in the room are introduced, (3) The method assuming room air temperature difference proportional to air-conditioning load, (4) The method using airflow currents in which transient air temperature distributions in the room are calculated, and (5) The method with room air temperature difference function in which the room air temperature differences are treated as the functions of air-conditioning load, ventilation rate, etc.

The method with uniform room air temperature. This method corresponds to the one-air-point-model. This means:

$$\Delta T_{ri} = 0 \quad (i=1,2,\dots,N) \quad (5.109)$$

The method with fixed room air temperature difference. This method introduces directly the constant temperature differences between the air near the enclosure surfaces and the control point of the room (such as middle point of the occupied zone) into ACCURACY. That is:

$$\Delta T_{ri} = C_i \quad (i=1,2,\dots,N) \quad (5.110)$$

where C_i is constant.

When no airflow pattern is available, this can be useful for initial computations since ACCURACY runs as fast as normal cooling load programs which were constructed from the room energy balance method (like method 1). This method can also be applied for a room with natural convection in which the vertical temperature difference does not change very much.

The method assuming room air temperature difference proportional to air-conditioning load. The method is based on the assumption that room air temperature differences are proportional to the air-conditioning load of the room (Nielson 1982), i.e.:

$$\Delta T_{ri} = C_i Q \quad (i=1,2,\dots,N) \quad (5.111)$$

where Q is air-conditioning load and C_i is a constant proportional factor.

However, the relationship between the air-conditioning load and the room air temperature differences not a linear one. This method in which a constant proportional factor is used will still give a certain discrepancy in air-conditioning load predictions.

The method with room air temperature difference function. Although room air temperature and contamination distributions can be calculated from airflow patterns in ACCURACY as discussed in subsection 5.2.4, it is too expensive to be used for hour-by-hour air-conditioning load calculations. Because hourly indoor air temperature distributions and contaminant fields are not required for annual energy analysis, it is sufficient if non-linear functions for the room air temperature differences can be estimated.

The computer program ACCURACY assumes that this function is related to the air-conditioning load (Q) and the ventilation rate ($Vent$), etc. of the room. That is:

$$\Delta T = f(Q, Vent) \quad (5.112)$$

This function is generated from the airflow patterns which are calculated based on different kinds of ventilation rates and heat gains. Normally less than 10 airflow patterns are sufficient to be used to approximate indoor air distributions under a certain air supply system for cooling situations.

The method using airflow patterns. If hour-by-hour room air temperature and contamination distributions are required, those have to be computed from the airflow patterns pre-calculated in an airflow program.

ACCURACY employs Equation (2.59) to calculate the room air temperature distributions using the corresponding airflow patterns. The air temperature near a wall surface, T_{ri} , is updated from the related air temperature distributions as shown in Figure 5.8(B). Then the room air temperature differences, $\Delta T_{ri} = T_{ri} - T_R$, are set in the energy balance equations for calculating heat extraction as shown in Figure 5.8(A).

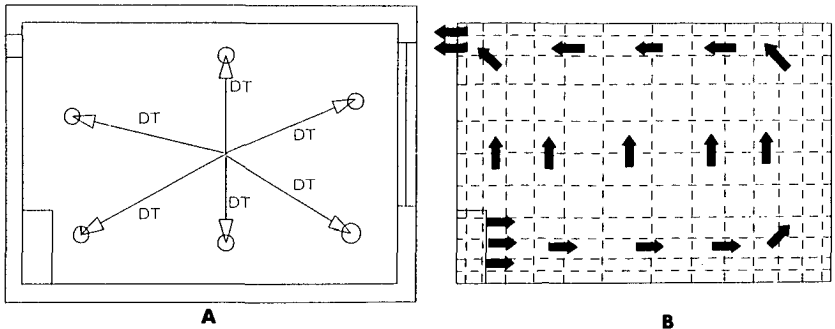


Figure 5.8 Program ACCURACY uses airflow patterns. (A) Temperature differences are considered in the program; (B) the temperature differences are calculated from airflow patterns.

5.2.5.4 The solving procedure of ACCURACY

As mentioned above, the most significant difference in air-conditioning load determinations between ACCURACY program and other cooling load programs is that the former one considers room air temperature difference ΔT_{ri} . Therefore, before introducing an overview on the whole solving procedure, the treatment of ΔT_{ri} in ACCURACY will be described.

The method with uniform room air temperature and the method with fixed room air temperature difference. In these two methods, ΔT_{ri} is known ($\Delta T_{ri}=0$ or $\Delta T_{ri}=C_i$) and no computation for ΔT_{ri} is required.

The method assuming room air temperature difference proportional to air-conditioning load and the method with room air temperature difference function. Based on the airflow computations by an airflow program or measurements, the proportional factors or the function can be pre-determined. However, ΔT_{ri} is a function of air-conditioning load in both methods and iteration between Equations (5.101) and (5.111) or Equations (5.101) and (5.112) is necessary. This is the reason why these two methods are more expensive than the first two methods.

The method using airflow patterns. In this method, the temperature difference, ΔT_{ri} , is obtained from Equation (5.95). However, the solutions of Equation (5.95) need thermal boundary conditions which are provided in the room energy balance equation (5.101). Iterations between Equations (5.101) and (5.95) are necessary for obtaining convergent results.

It is clear that the first four methods can be regarded as the simplified cases of the fifth method. The solving procedures are very similar and the fifth method will be used as an example.

A diagram for the computer program ACCURACY, is shown in Figure 5.9 and the iterations are carried out by the fifth method in the following way:

(1) Use Equations (5.101) and (5.108) for calculating inside surface temperature T_i and heat extraction H_{ex} which are based on guessed temperature differences ΔT_{ri} (for the first iteration, $\Delta T_{ri}(n-1)$ can be used) (See Figure 5.8A).

(2) Use T_i and H_{ex} obtained from step (1) and Equations (5.95) and (5.100) for calculating room temperature distribution T_{ri} and ΔT_{ri} (see Figure 5.8B).

(3) Iteration between step (1) and (2) are necessary until

$$\max \left| (\Delta T_{ri})_{\text{iteration no. } j} - (\Delta T_{ri})_{\text{iteration no. } j-1} \right| \leq \delta \quad (5.113)$$

where δ is a small positive value.

(4) Calculate the concentration distributions, etc. and move to the next time step.

When the heat introduced into or extracted from the room is known, the determination of room air temperature becomes necessary. For example, it is a typical case when air-conditioning system is off or air-conditioning capacity

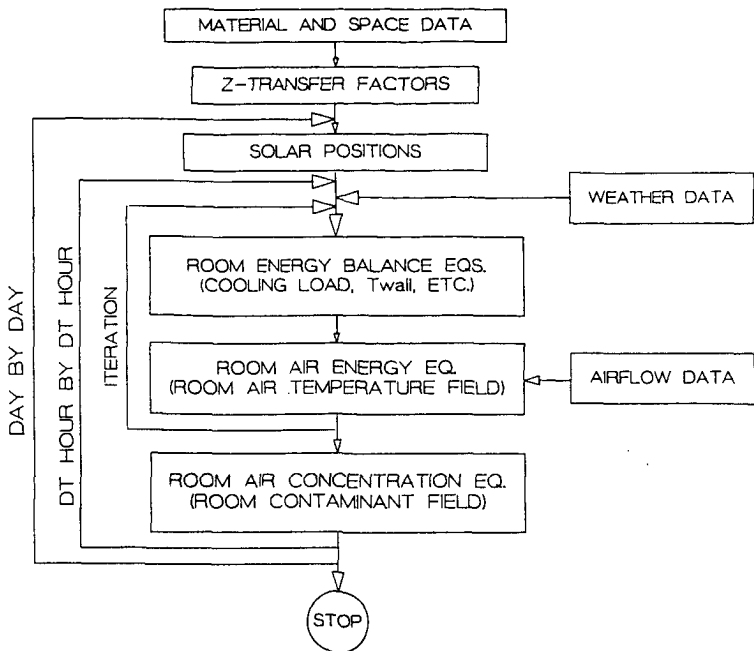


Figure 5.9 The diagram for ACCURACY.

is too small. This prediction can be performed by changing Equation (5.101). A more detailed description can be found in the report (Chen 1987b).

5.2.5.5 The heat extraction of a room and a cavity

In many modern buildings, there is often a cavity above the false ceiling of a room and the predictions of air-conditioning loads or air temperatures of the room and the cavity are related and must be solved together. The computer program ACCURACY is built for this purpose. The cavity is considered as another room which can be located above, under or next to the room. The program can be used to predict heat extraction or air temperature in the room or the cavity. In the computer code ACCURACY, the heat transfer in the cavity is treated in the same way as that in the room. Suppose the room is divided into N_R regions and the cavity into N_C regions, according to matrix equation (5.101), it follows:

$$\begin{bmatrix} M_R & 0_1 \\ 0_2 & M_C \end{bmatrix} \begin{bmatrix} T_R \\ T_C \end{bmatrix} = \begin{bmatrix} q_R \\ q_C \end{bmatrix} + \begin{bmatrix} \alpha \Delta T_R \\ \alpha \Delta T_C \end{bmatrix} \quad (5.114)$$

where M_R , M_C , T_R , T_C , q_R , q_C , ΔT_R and ΔT_C are M , T , q and ΔT in the room and the cavity respectively. The matrices 0_1 and 0_2 are used to reveal the thermal relationship between the room and the cavity. They are really zero only when the room and the cavity are separated. More detailed information is given in literature (Chen 1987d).

5.2.5.6 Other remarks

Another improvement in ACCURACY is that the convective and radiative heat exchange coefficients in the [M] matrix of Equation (5.101) or Equation (5.114) can be modified. The program re-sets the coefficients if the change is large. In cases where radiative heat exchange coefficients vary rapidly, such as when the radiant panels for heating are switched on and off, these values are recalculated in the program according to the surface temperatures, view factors and multiple reflections.

5.2.6 The program structure of ACCURACY

A computer simulation of heat transfer in buildings should be a general-purpose program that can be easily adapted for a solution of the particular problem. The common core of the program must be a highly efficient and constantly maintained item of software with which the user can communicate only in carefully controlled ways. At the same time, the program must provide a subroutine in which the program user who needs other facilities that are not provided within the common core can form the required coding structure. The computer program ACCURACY has been constructed to meet those requirements. The present program was developed for personal computers and is written in FORTRAN 77.

The user-friendly computer program ACCURACY has three elements, as shown in Figure 5.10: (1) STATIC, which provides problem-defining data, (2) DYNAMIC, which is attached to the main part of the program, SOLVER, assisting the latter to complete the simulation tasks, and (3) SOLVER, which is the central equation solver. STATIC is used for static input data and works with the help of a group data input subroutines. All variables in the program are equipped with default values that are set in BLOCK DATA. A user requires only minor changes for his need. It is convenient to use the data input subroutines by simply CALL-ing them instead of modifying them. The STATIC finishes its work before SOLVER takes off. The information it transmits is therefore one of "once-for-all" characters. For many problems, this is not adequate such as when the user may want to add into or to extract from the SOLVER more dynamic information which cannot be defined in STATIC, or to modify any variable or parameter in a particular time step, or to offer printout frequency during some especially interesting parts of the process. Therefore, there is often a need for the simulator of a special process to provide coding that interacts with SOLVER during its operations. This function is performed by the DYNAMIC work station.

The SOLVER contains approximately 7000 FORTRAN statements. It is equipped with all equations given in section 5.2. The SOLVER first receives the static

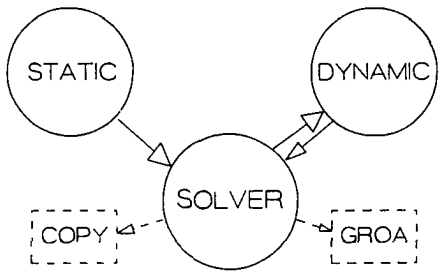


Figure 5.10 The structure for ACCURACY. COPY stores the numerical results as it appears in screen and GROA is the Graphical Representation Of ACCURACY.

input data from subroutine STATIC, and performs the job associated with DYNAMIC. The user has, and needs to have, no direct contact with SOLVER. As far as he is concerned, it is a mathematical apparatus embodying the relevant laws of physics and providing solutions of variables which have been activated by the commands supplied by STATIC.

5.3 Conclusions

The prediction methods of air-conditioning load are discussed briefly. Based on the review of the response factor method, the z-transfer factor method, the frequency analysis method and the state space method which are used for the computations of unsteady heat conduction, the z-transfer method seem to be the most suitable one for air-conditioning load computations.

The room energy balance method, although it is very complicated, presents very accurate results. For precise computations of air-conditioning load, it should be employed.

The new user-friendly, personal computer program, ACCURACY, has been constructed for energy analysis, room air temperature and contamination field predictions. The program is a coupling of a cooling load program and an airflow program. For obtaining better accuracy in air-conditioning load computations, the ACCURACY program is based on the room energy balance method and uses z-transfer functions and window energy balance equations for heat transfer through enclosures. The computer program also involves the solution, in finite-domain form, of three dimensional, transient equations for the conservation of energy and contamination concentration using airflow patterns, which are pre-calculated from dedicated computer programs, such as PHOENICS (3D) and CHAMPION SGE (2D). The influence of room air supply system on the temperature distribution and indoor air quality, and subsequently on the energy consumption can be calculated by ACCURACY.

ACCURACY also calculates indoor convective and radiative heat exchange coefficients. The coefficients will be reset in the room energy balance equations when they have a large variation.

CHAPTER 6

COMPUTATIONS AND VALIDATIONS OF AIR-CONDITIONING LOAD AND ROOM AIR TEMPERATURE

The capacities of ACCURACY will be demonstrated by applying it to two different situations: cooling conditions and heating conditions.

6.1 Cooling Situation

In the first case, the cooling system 1 as described in chapter 3 was used. The inlet-mass-flow for the room was 0.126 kg/s (a ventilation rate of seven times per hour), which corresponds to an inlet airflow Reynolds number of 11400. The Reynolds number is based on the bulk velocity and the equivalent diameter of the inlet. A 950 W of heat (a step function) was uniformly distributed on the venetian blinds. The initial temperature and the temperature in the middle of the occupied zone (the height is 0.9 m) were controlled at 23.0°C. A concentrated helium source, 0.5% of the total ventilation rate, in a step function form, is supplied into the room after the heat was supplied for 16 hours (at point $x=3.7$ m, $y=0.7$ m and $z=0.9$ m). The concentration source was maintained for one hour.

6.1.1 Cooling load predictions

The cooling load is calculated by ACCURACY in five ways: (1) without considering air temperature differences in the room, (2) by introducing constant air temperature differences in the room, (3) by assuming that the room air temperature differences are proportional to cooling load, (4) by applying the room air temperature difference function method to reveal the non-linear relationship between the temperature differences and the cooling load, and (5) by using an airflow pattern for computing the transient air temperature differences in the room.

As illustrated by Figure 6.1, the cooling load showed a very significant discrepancy between the measured and the computed results using the above methods (1) and (2) for the dynamic period. The third method presented a better result, however, the agreement was very good when the fourth and the fifth methods were employed. The final two methods presented almost the same results.

When the heat was introduced on the venetian blinds, a vertical room air temperature difference was generated as shown in Figure 6.2. Because the air temperature in the middle of the occupied zone was controlled to be a constant, the air temperature difference between the point near the ceiling and the controlled point was much bigger than that between the point near the floor and the controlled point. This resulted in more heat being transferred into the ceiling than that being obtained from the floor. In the first method, where the normal one-air-point model was used, this thermal behaviour

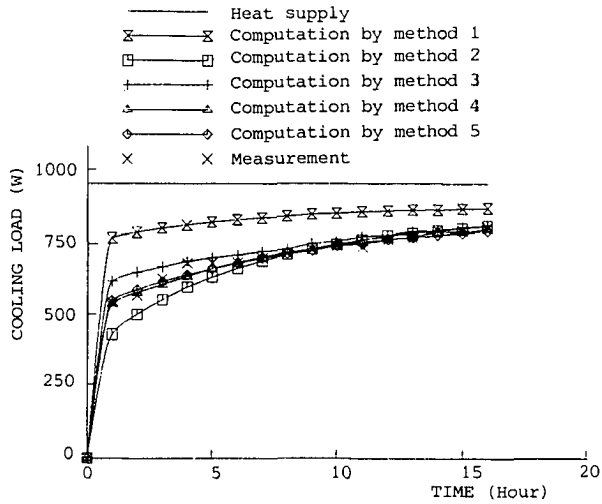


Figure 6.1 The cooling load of cooling system 1 measured and computed by ACCURACY.

cannot be simulated. The extra heat was considered to be a part of the cooling load, and it gave a too high value for the computed results in the initial hours. A too low computed cooling load was obtained from the second method, because the vertical temperature difference used was obtained from the steady situation (i.e., $t=16$ hour) and this value was too high to be used for the initial hours (see Figure 6.3). The too large temperature difference set at the beginning for the computation resulted in excessive heat being transferred into the ceiling. As a consequence, a smaller computed cooling load was obtained. Therefore, the temperature difference set in the cooling load program must be a transient one in order to obtain reliable results.

The third method assumes that the vertical room air temperature difference is proportional to the air-conditioning load (heating load or cooling load) of the room. However, the relationship between the cooling load and the room air temperature difference for this case was not a linear one as indicated in Figure 6.4. A constant proportional factor used for this case still gave a too small temperature difference. As shown in Figure 6.1, it

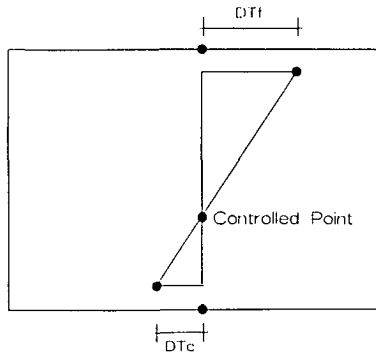


Figure 6.2 The temperature gradient in the room.

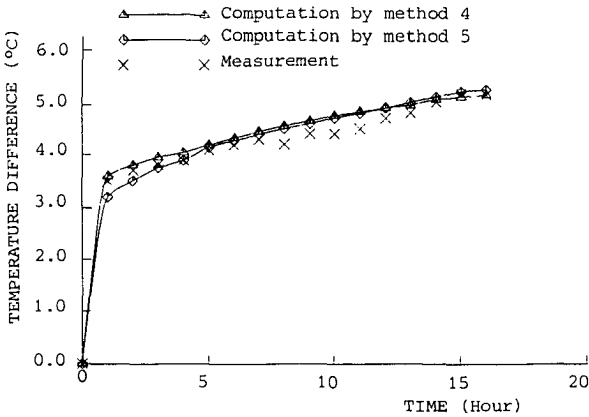


Figure 6.3 The temperature difference between the air points near the ceiling and the floor in cooling system 1 after the heat was introduced on the venetian blinds.

nevertheless still gave a little higher value although the computed result by this method was better than that obtained from the first and the second methods. The proportional factor can be either measured directly from the room or calculated once from an airflow program.

In the fourth method, the non-linear temperature difference functions presented in Figure 6.4 were calculated from the computational temperature distributions as shown in Figure 4.14. The non-linear functions under a ventilation rate of seven times per hour for this case were determined by curve fitting:

$$\Delta T_{\text{ceiling}} = 0.036 + 6.99 \times 10^{-3} \cdot Q - 2.72 \times 10^{-6} \cdot Q^2$$

$$\Delta T_{\text{floor}} = 0.026 - 1.83 \times 10^{-3} \cdot Q + 5.55 \times 10^{-7} \cdot Q^2$$

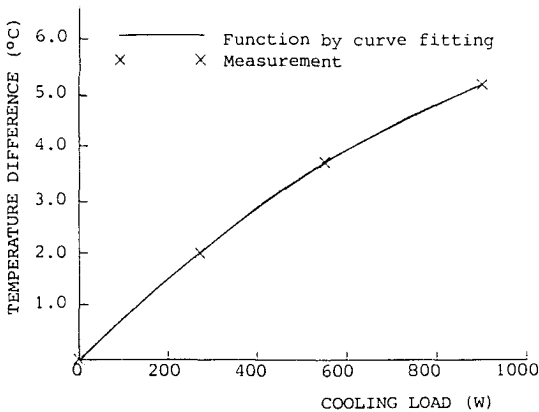


Figure 6.4 The relationship between cooling load and temperature difference in cooling system 1.

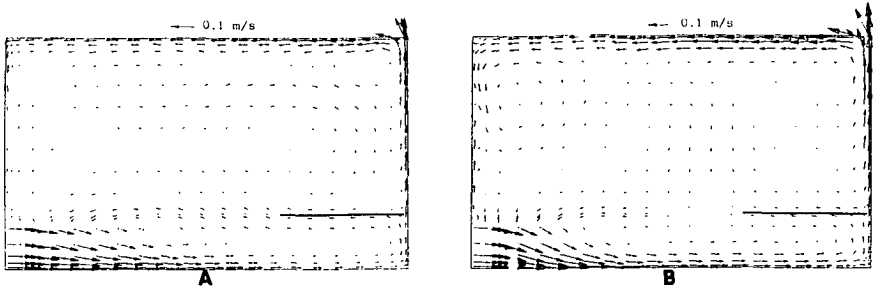


Figure 6.5 The airflow patterns of cooling system 1 precomputed by PHOENICS. (A) for $350 \text{ W} \leq \text{cooling load} \leq 750 \text{ W}$ (B) for $750 \text{ W} < \text{cooling load} \leq 1050 \text{ W}$.

$$\Delta T_{\text{window}} = 0.036 + 6.99 \times 10^{-3} \cdot Q - 2.72 \times 10^{-6} \cdot Q^2$$

$$\Delta T_{\text{walls}} = 0.047 + 2.10 \times 10^{-3} \cdot Q - 1.07 \times 10^{-6} \cdot Q^2$$

$$\Delta T_{\text{parapet}} = 0$$

where Q is cooling load.

The predicted cooling load was good because the computed transient temperature differences of the room agreed with the measured ones (Figure 6.3).

The transient temperature differences in the fifth method were calculated from airflow patterns, which were pre-calculated by PHOENICS (Figure 6.5). Due to the computed transient temperature differences of the room were in good agreement with the measured ones (Figure 6.2), the computed cooling load was the same as the measured one.

The thermal conditions of the rooms above and below were controlled to be the same as those of this climate room both in the measurements and the computations. At steady state, the heat obtained from the floor was the same as that transferred into the ceiling in all the five methods. As a result, the cooling loads computed were almost the same under the steady situation, because all heat supplied has to be removed.

Because in this case the supplied mass flow was a constant and cooling load is related to the supplied mass flow and the inlet and the outlet air temperatures, it is more clear to describe the energy requirement of this room by the inlet air temperatures. The results of measurements and the computations by the five methods are illustrated in Figure 6.6. The discrepancies were very significant when the first and the second methods were used, because the outlet air temperatures are different.

The computing time used by these five methods in an IBM 3083-JX1 mainframe computer and an IBM PC(AT) for one month hourly-simulation of the cooling system 1 is given in Table 6.1. The computing performance index of the IBM PC(AT) to IBM PC is 7.7. Clearly, the method using flow patterns is much more expensive. However, the cost very much depends on the amount of grid points used. The grid points used are related with airflow patterns and room geometry. The influence of the grid number on the computations of air-conditioning load is small.

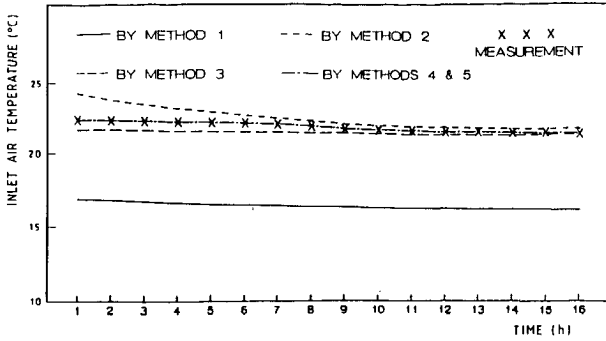


Figure 6.6 Supplied air temperatures under different computational methods.

The storage required by ACCURACY for the computation with the grid number 18x18x23 is less than 500 kilobytes on a personal computer.

6.1.2 The calculations of room air temperature and contamination distributions

The fifth method also computes the room air temperature and contaminant distributions and consequently, the temperature efficiency and ventilation efficiency can be evaluated. Figure 6.7 shows the distribution in the middle section ($y=1.5$ m) at $t=16$ hours. The agreement in most of the measuring points between the measured data and the calculated values by ACCURACY was good. The differences are less than 0.5 K. These results are acceptable for practical applications. They are nearly the same as that obtained by calculating it directly from the airflow program PHOENICS. When ACCURACY gives hourly room air temperature distributions and cooling load for a one-month period, it costs 279 seconds CPU time in the IBM mainframe. However, when this is done using the 3D airflow program, it costs 10 minutes CPU time in the IBM mainframe for calculating the temperature distributions at each time step.

The computed and measured concentration field after the helium source was bled in for one hour (step function) is presented in Figure 6.8. The

TABLE 6.1
Computing time

Cases	Methods	IBM mainframe (second)	IBM PC (AT) (minute)
Cooling	(1) Without differences	2.46	6
	(2) With constant differences	2.46	6
	(3) Proportional factor	6.20	14
	(4) Non-linear function	6.20	14
	(5) With airflow pattern grid number 6x11x17 With airflow pattern grid number 18x18x23	30.43 279	60 -
Heating	(1) Without differences	2.88	7
	(2) With constant differences	2.88	7

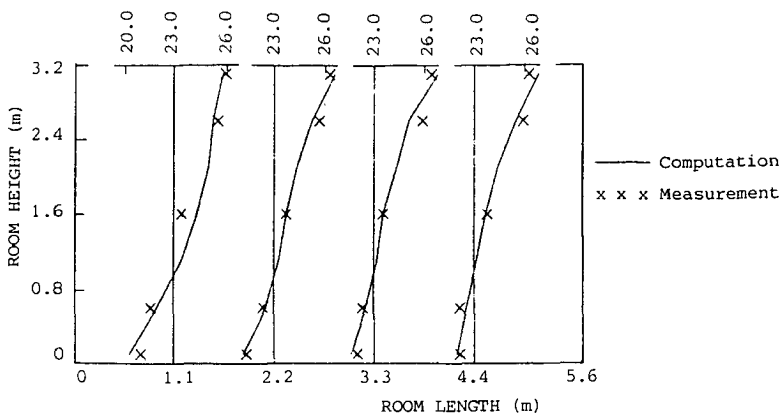


Figure 6.7 The room air temperature distribution of cooling system 1 in section $y=1.5$ m ($^{\circ}\text{C}$).

agreement between the computation and the measurement is fairly good except in the places near the source. Because the room time constant for the helium concentration was very small, the transient concentration of helium in the point near the ceiling had to be simulated with a time step of one minute. The comparison between the computed and the measured results for the transient response is shown in Figure 6.9. The measured values were higher than the computed ones in this case. This is probably due to the large gradient of concentration near the measuring point so that the measured values were very sensitive to the sampling position.

6.2 Heating Situation

The second case is the heating system 1 as described in chapter 3. It concerned a mixture of natural convection with a cold window surface and forced convection with a hot air supply on the rear wall at two-thirds the height of the room and the outlet at the same height. The outside air temperature of the window was 3.0°C , and initial room temperature was 14.4°C .

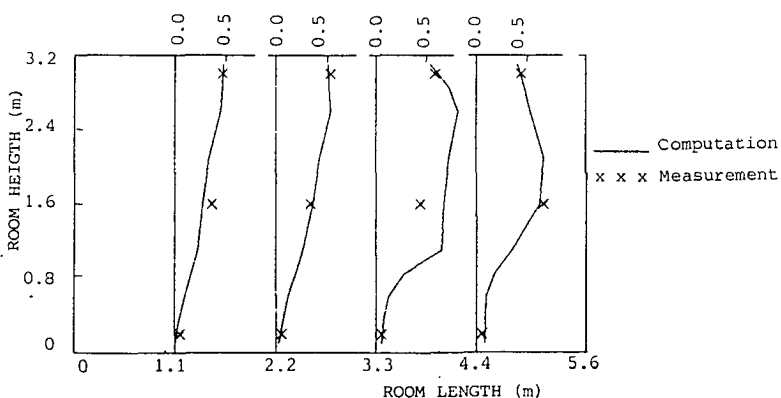


Figure 6.8 The room contamination distribution of cooling system 1 in section $y=0.7$ m (%).

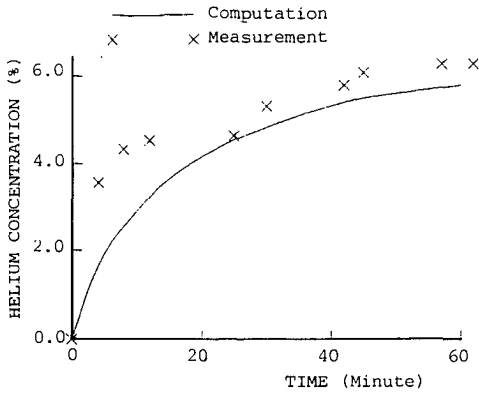


Figure 6.9 The contamination concentration of cooling system 1 in point $x=3.3$ m, $y=0.7$ m, $z=3.0$ m.

The heater capacity was 1000 W (also a step function).

We have noted that there is no difference in air-conditioning load calculations between a heating case and a cooling case. In order to get better computational results, the fourth or the fifth methods used above should be employed for this situation. Because the heating load in this heating case is a constant (1000 W), the temperature difference between the air points near the ceiling and the floor is also a constant (See Figure 6.10). Therefore, method two with constant temperature differences can be used. The air temperatures in the middle point of the room, which are computed by this method, are in good agreement with the measured ones (Figure 6.11). Another calculation based on the normal one-air-point model (method one) was used for comparison in Figure 6.11. It gives a very large discrepancy with the measurements.

The required CPU time in the IBM 3083-JX1 computer is 2.88 seconds (Table 6.1) for one-month hourly room air temperature predictions by introducing constant room temperature differences. It takes 7 minutes to do this computation in the IBM PC(AT).

With such a heating system, there is always a very large vertical temperature difference in the room, which makes it uneconomical. As has been discussed in section 4.2.4, heating system 2 is better in winter.

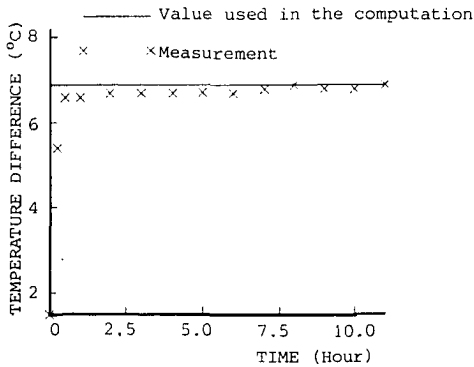


Figure 6.10 The temperature difference between the air points near the ceiling and the floor in heating system 1.

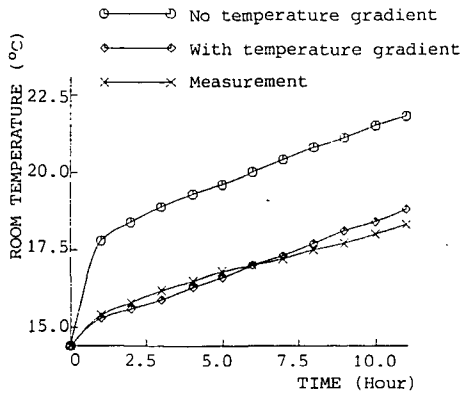


Figure 6.11 The computed and measured air temperatures of heating system 1 in the middle point of the room.

6.3 Further Remarks

From the results given above, it can be concluded that when there is no air temperature difference in a room, normal cooling load computer programs (method one) are sufficient for obtaining accurate results. However, if the room air temperature differences are large, normal cooling load computer programs have to be improved with respect to the following two points:

(1) If the room air temperature differences are not functions of time, the one-air-point model with constant temperature differences (method two) will give good predictions. The constant temperature differences should either be calculated from an airflow program once or directly measured in the room.

(2) If the room air temperature differences are transient, there are three choices:

- The air temperature differences can be approximated to be proportional to the room air-conditioning load (method three). However, if the differences are not linear to the air-conditioning load, the predicted results will deviate from the measured results. The proportional factors are calculated from the relationship between air-conditioning load and room temperature differences which can be obtained from measurements or from an airflow program.
- The best way is to calculate the room air temperature differences as the function of air-conditioning load and ventilation rate (method four), but the determination of the function requires temperature distributions under different thermal conditions.
- The third choice is to update the transient air temperature differences from the corresponding airflow patterns (method five). This method shows not only the most accurate air-conditioning load predictions but also the air temperature fields and contaminant distributions at each time step. Unfortunately, it is very expensive.

The proportional method only requires one computation with an airflow program for a typical situation to obtain the proportional factors. The room

air temperature difference function method needs calculations for more situations so the latter method is more expensive.

6.4 Conclusions

The cooling load programs using a normal one-air-point model seem to be suitable for a room without temperature differences. When the room temperature differences are constant, these can be used directly in ACCURACY for air-conditioning load computations. However, when the temperature differences are transient functions, an improved method is to assume that the room air temperature differences are proportional to the air-conditioning load and the best way is to determine the temperature differences as functions of air-conditioning load and ventilation rates, etc. If hourly room air temperature fields or minutely room contaminant distributions are required, the airflow patterns pre-calculated in an airflow program have to be employed.

For the first two methods, ACCURACY uses the same computing time as normal cooling load computer programs which are based on the room energy balance equations. The method, which uses proportional factors for obtaining temperature differences from the cooling load, is 2.3 to 2.5 times more expensive than the normal one-air-point model. For practical applications, this method presents rather good results. The room air temperature difference function method costs the same as the proportional factor method in air-conditioning load prediction, but it needs much more computing time in airflow predictions. This is because more typical situations of airflow computations are required. The computations using room air currents are expensive and their costs greatly depend on the numerical grid points used in an airflow program. In all the computations discussed in this chapter, the cost required by an airflow program is excluded.

ACCURACY considers the influence of room air temperature distributions on its air-conditioning load or room air temperature predictions and also calculates contamination distribution. This improvement is necessary for the investigation of the energy saving and comfort of indoor environment in different air supply systems.

It can be seen that room air temperature and contamination distributions calculated from airflow patterns are much cheaper than those computed directly from an airflow program.

CHAPTER 7

PREDICTIONS OF BUILDING ENERGY CONSUMPTION

7.1 Theories of Building Energy Analysis

7.1.1 Methodology of building energy analysis

Often it is necessary to estimate energy requirements and fuel consumption of HVAC systems for short or long term operation. The procedures for estimating energy requirements vary considerably in degree of sophistication. However, they have three common elements: (1) space load calculation, (2) secondary equipment load computation and (3) primary equipment energy requirements computation. The space load is the amount of heat added to or extracted from a space to maintain thermal comfort and the computations of the space load have been discussed extensively in chapters 5 and 6. The secondary refers to equipment that distributes the heating, cooling or ventilating medium to the conditioned spaces. The primary refers to central plant equipment that converts fuel or electricity to heating or cooling effect.

There are many kinds of methods available for the energy analysis. They can be classified as (1) single measure methods, (2) simplified multiple measure methods and (3) detailed simulation methods (ASHRAE 1985). The single measure methods use only one measure, such as annual degree days. They may be appropriate only for simple systems and applications. In the simplified multiple measure methods, the accuracy is improved by using more information, such as the number of hours anticipated under particular operating conditions. Among these methods, the bin-method is best known (ASHRAE 1985). The most elaborate methods perform energy balance calculations hourly over a given analysis period, typically one year. These are called as detailed simulation methods.

The single measure methods and simplified multiple measure methods are not good enough for accurate energy analysis and therefore, they will not be discussed in this chapter.

Figure 7.1 describes a simulation model and shows the basic function of each major model element on an input and/or output basis. Based on this model, many computer programs are written for the building energy analysis (BLAST 1979, DOE-2 1981, ASHRAE 1980, NECAP 1975, ESP-I 1978, ENERK (Van Paassen 1986)). Among these programs, most based on the method of hour-by-hour prediction in all the three elements. The hour-by-hour prediction in all the three elements is very expensive, if the weather data of a full reference year are employed. When the prediction is applied to optimize a system for best solution of energy saving, many computations are required for comparing various alternative designs of buildings and installation. In order to reduce the computational time, they are two possibilities. The first one is to use short reference year weather data (Van Paassen 1981, Liem and Van Paassen 1986). In section 5.2.1, the Dutch short reference year weather data, which

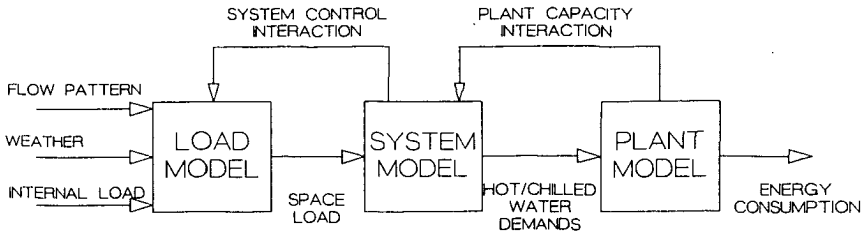


Figure 7.1 The model for energy estimation.

are used in the computer program ACCURACY, has been briefly discussed. It is also possible to optimize the computer algorithm used in the secondary equipment and the primary equipment to reduce the computing costs (Van Paassen 1986). This is classed as the second one. In the following section, the optimized algorithm, which was used in the computer program ENERK, will be introduced.

7.1.2 The fundamentals of the energy analysis program ENERK

The computer program ENERK breaks down the energy consumption simulation into two parts. One part is for space load calculation and the other for the combined predictions of the secondary equipment load and the primary equipment energy requirements. Based on an hour-by-hour calculation of the indoor temperature and the space loads, which were obtained from a cooling load program such as ACCURACY, ENERK calculates the annual energy consumption in the following steps:

- calculating the probability of the joint occurrence of specific values of the space load (Q), the outdoor temperature (T) and the humidity (X);
- determining the energy consumption of the plant for all kinds of values of the temperatures and the humidities of the outside air and the space loads of the room;
- giving the annual energy consumption by the combination of the values of the load probability matrix and the energy matrix of the plant.

The space load of the room can be characterized by the probability distribution matrix of multi-variables, $P(Q, T, X)$. It gives the probability of the joint occurrence of Q to $Q+\Delta Q$, T to $T+\Delta T$ and X to $X+\Delta X$. In the computations presented here, the space load only is divided into two parts, one for heating and the other for cooling. Therefore, only the probabilities P^+ and P^- are calculated for each of the seven sections in the psychrometric chart shown in Figure 7.2. Then the temperatures and humidities of outdoor air, the extracted air temperatures, and the heating and cooling loads are averaged per section.

The sections are classified in such a way that the control strategy in each section is the same. The more sections are used, the higher the accuracy will be. Van Mierlo (1986) demonstrated that a partition of the psychrometric chart as given in Figure 7.2 results in calculation results with differ less than 5.1%, as compared to those obtained with an hour-by-hour simulation approach. The accuracy is acceptable for practical applications and therefore, it is used for the present study.

For each section in the psychrometric chart, the average values of the heating load, the cooling load, the outdoor temperature and humidity are

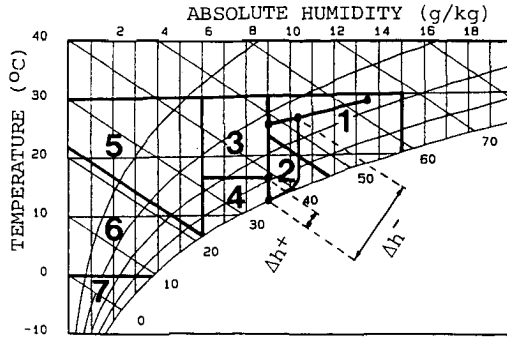


Figure 7.2 The section division of psychrometric chart for office hours and the example of air handling in Mollier diagram.

calculated. This results in a combination of Q , T and X for each section. Then the energy consumption is calculated for each section, which is required by the HVAC system to compensate the space load Q . This energy is expressed by the matrices $E_{gas}(T,X)$ and $E_{electricity}(T,X)$. For instance, for the air handling process shown in Figure 7.2, the amounts of energy for heating and for cooling and air transport can be calculated as:

$$E_{gas} = \Delta h^+ \dot{m} / \eta_b \quad (\text{kW}\cdot\text{h}) \quad (7.1)$$

$$E_{electricity} = \Delta h^- \dot{m} / \eta_{ch} + \Delta p_{fan} \dot{m} / (\eta_{fan} \rho) \quad (\text{kW}\cdot\text{h}) \quad (7.2)$$

where η_b , η_{ch} and η_{fan} are the efficiencies of boilers, chillers and fans respectively. They depend on various variables, such as load, and can be determined in many ways (Van Paassen 1986). The $\Delta h^- \dot{m}$ and $\Delta h^+ \dot{m}$ are the heat removed by cold water and the heat supplied by hot water respectively.

Multiplication of the elements of the energy matrix with corresponding elements of the probability matrix and with the total hours of the considered period gives the energy consumption of each possible combination of Q , T and X . Summing all the products is the total cost of energy consumption.

$$C_{gas} = \gamma_1 \cdot \sum_Q \sum_T \sum_X P(Q,T,X)^+ \cdot E_{gas} N \quad (\text{Dutch Guilders}) \quad (7.3)$$

$$C_{electricity} = \gamma_2 \cdot \sum_Q \sum_T \sum_X P(Q,T,X)^- \cdot E_{electricity} N \quad (\text{Dutch Guilders}) \quad (7.4)$$

where γ_1 and γ_2 are the price weighted factors for gas and electricity respectively and N is the number of office hours in the period or number of weekend and night hours in the period (calculation can be carried out for office and night hours separately).

By this method, only the non-identical situations are calculated in contrast to the hour-by-hour approach, where identical situations encountered at different moments of time, are recalculated all over again. A more detailed description of the program ENERK is given in literature (Van Paassen 1981, 1986).

7.2 Annual Energy Consumption of the Climate Room

The computer program ENERK is applied here to analyze the annual energy consumption of the room shown in Figure 3.1. In order to save computing time, the weather data of the Dutch short reference year are used for the predictions.

It is assumed that there are 55 office hours each week, i.e. from 7:00 to 18:00 from Monday through Friday. During these office hours, the air temperature in the middle point of the occupied zone is maintained to be $22.0^{\circ}\text{C} \pm 2.0 \text{ K}$ and the absolute humidity to be 6.0 g/kg to 9.0 g/kg . If the air temperature is in the range between 20.0 to 24.0°C , there is no heat extraction in the room. However, ventilation is always necessary for fresh air during office hours. It is supposed that there is always 300 W convective heat released into the room air in the office hours. This amount of heat is considered to be the convective heat from the occupants, the appliances, etc. in the room. For weekends and night hours, there is no internal heat gain in the room and the air conditioning system is switched off. Therefore, there is no energy consumption during weekends and night hours. From April to September, an external venetian blind is used to reduce heat gain through the window.

The efficiencies of the primary equipment are assumed to be constant. The pressure of the ventilator is 1400 Pa and its efficiency is 0.6 . The efficiency of the boiler is 0.75 and the COP value of the chiller is 3.5 .

The energy analysis is performed for two types of air conditioning systems, i.e., a "variable air volume" system and a "constant air volume" system. The variable air volume system and the constant air volume system here mean that the air handling processes are the same as those for normal variable air volume systems and constant air volume systems. However, the inlet and outlet locations of the room may be different and these will be discussed later. In each system, the annual air-conditioning load is calculated by ACCURACY under two kinds of air supply and air exhaust systems.

7.2.1 Variable air volume system

In the variable air volume system, two kinds of air supply and air exhaust systems are studied. They are the cooling system 1 and cooling system 4 as shown in Figure 3.3. These two air supply and air exhaust systems are used both for cooling and for heating. When the room needs heating, a radiator, which is placed under the window, is employed.

As indicated in chapter 4, there is a vertical air temperature difference in the room with the cooling system 1 during cooling period and no air temperature difference with the cooling system 4. According to Chen and Van der Kooi (1988c), there is hardly any vertical air temperature difference in the room for both the systems during heating period.

When the cooling system 1 is used, the supply air temperature must be higher than 16.0°C . Thus, the air temperature distribution in the occupied zone satisfies the comfort requirements. But, the supply air temperature for cooling system 4 can be lower, because the fresh air is supplied outside of the occupied zone. In order to compare the energy consumption with the two air supply and air exhaust systems, the computations are performed in two groups:

- (1) with the same supply air temperature,
- (2) with different supply air temperatures.

7.2.1.1 With the same supply air temperature

In this subsection, we will discuss the results for cooling system 1 and cooling system 4 with the same supply air temperature (16.0°C).

It is very possible that the room sometimes needs heating and sometimes requires cooling, although the outdoor climate may be in the same section of the psychrometric chart. Because the control strategies for cooling and heating are different, they must be described separately in each section. The control strategies of the variable air volume system for cooling and heating with cooling system 1 are presented in a psychrometric chart as shown in Figure 7.3 and 7.4.

Although the heat extraction in sections 2 and 3 for heating is zero, ventilation is still required for office hours (i.e. P^+ is not equal to zero). Therefore, the control strategies for these two sections are also presented. However, according to the results computed by ACCURACY, there is no heating in section 1 and no cooling in section 7 (i.e. P^+ in section 1 and P^- in section 7 are zero). Thus, the control strategies for these two sections are unnecessary. The control strategies for cooling system 4 are the same as those for cooling system 1.

Table 7.1 presents the heat extraction of the room, the heat removed by cold water and the heat supplied by hot water (via the heater and the radiator) in different sections of the psychrometric chart for cooling system 1 (with a vertical air temperature difference for cooling). Table 7.2 shows the results for cooling system 4 (without a vertical air temperature difference for cooling). Although the computations are performed with the weather data of the short reference year, the results have been extended for a normal reference year by multiplying by a factor 2868/440, where 2868 and 440 are the numbers of office hours for the normal reference year and for the short reference year respectively.

From these two tables, we can see that the relationship between the heat

TABLE 7.1

The heat extraction, the heat removed by cold water and the heat supplied by hot water in the variable air volume system with cooling system 1 (kW·h)

Sections in psychro. chart	1	2	3	4	5	6	7	Total
Heat extraction (cooling)	114.3	121.7	239.2	17.9	69.8	2.8	-	565.7
Heat removed by cold water	154.0	104.7					-	258.7
Heat supplied by hot water	37.2	41.6				5.9	-	84.7
Heat supply (heating)	-	0.0	0.0	26.6	25.3	199.0	177.1	428.0
Heat removed by cold water	-	1.8						1.8
Heat supplied by hot water	-	5.0	6.2	51.6	51.8	347.2	244.5	706.3

TABLE 7.2

The heat extraction, the heat removed by cold water and the heat supplied by hot water in the variable air volume system with cooling system 4 (kW·h)

Sections in psychro. chart	1	2	3	4	5	6	7	Total
Heat extraction (cooling)	124.6	132.4	254.2	18.4	76.6	2.9	-	609.1
Heat removed by cold water	182.7	139.3					-	322.0
Heat supplied by hot water	51.6	54.9				5.9	-	112.4
Heat supply (heating)	-	0.0	0.0	26.6	25.3	200.1	177.0	429.0
Heat removed by cold water	-	1.8						1.8
Heat supplied by hot water	-	5.6	9.4	51.6	51.8	347.2	244.5	710.1

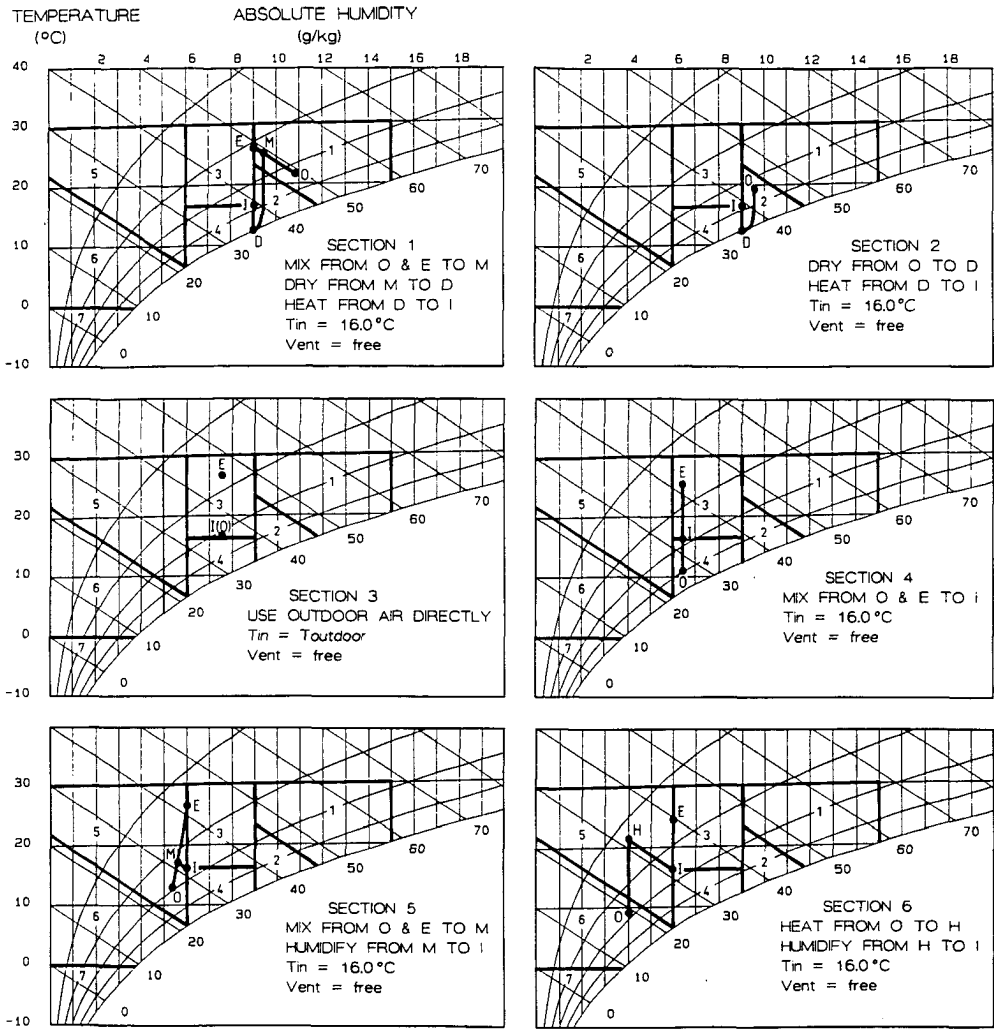


Figure 7.3 The control strategies for cooling in each section of the psychrometric chart for the variable air volume system with cooling system 1 (O - outdoor air, E - air extracted, D - dew point, I - air supplied by inlet, M - mixing point, H - heating point).

extraction and the heat removed by cold water and supplied by hot water is very complicated. In section 1 as shown in Figure 7.3, for example, the enthalpy difference between the outdoor air and the dew point is higher than that between the extracted air and the air supplied. Therefore, the heat removed by cold water is higher than the heat extraction. However, in section 3, free cooling can be used so that heat removed by cold water is zero.

In cooling system 1 (with a vertical air temperature difference for cooling), the average room air temperature is higher than that at the controlled point. This is because the controlled point is in the middle of the occupied zone, which is in the lower part of the room. This means that

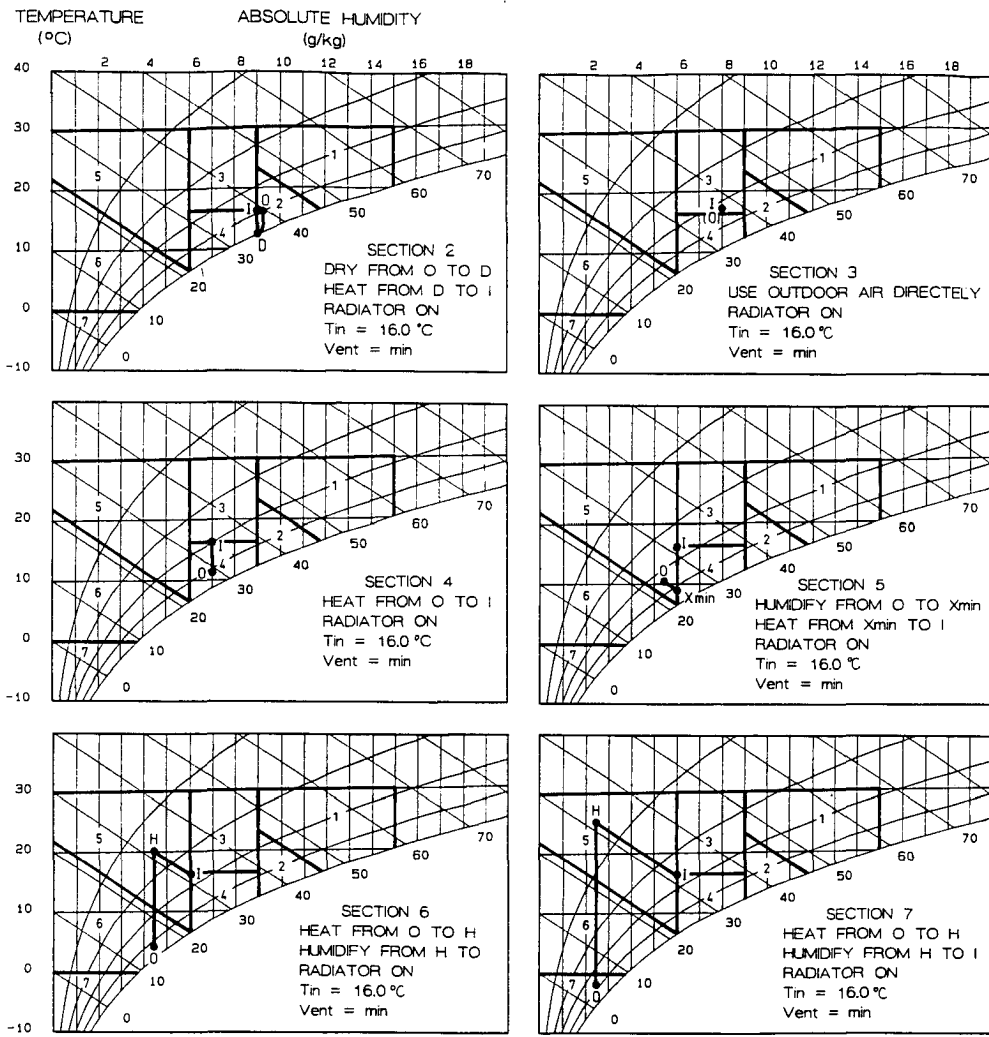


Figure 7.4 The control strategies for heating in each section of the psychrometric chart for the variable air volume system with cooling system 1 (O - outdoor air, E - air extracted, D - dew point, I - air supplied by inlet, M - mixing point, H - heating point).

the average room air temperature of cooling system 1 is higher than that of cooling system 4, since the average room air temperature in the latter case is the same as that at the controlled point. As a result, the heat extraction of cooling system 1 in cooling period is lower as indicated in Table 7.1. However, the difference of the heat removed by cold water between the two cases is larger than that of the heat extraction. The reason is that the temperatures of the air extracted are also higher in cooling system 1 and the corresponding supplied airflow is, therefore, much smaller.

Table 7.3 presents the computational results of the energy consumption during cooling period for cooling system 1 (with a vertical air temperature

TABLE 7.3

The energy consumption in the variable air volume system
with cooling system 1 during cooling period*

Sections in psychro. chart	1	2	3	4	5	6	7	Total
Chiller (kW·h)	44.0	29.9					-	73.9
Ventilator (kW·h)	21.0	23.5	52.7	3.8	13.5	0.8	-	115.3
Boiler (kW·h)	49.6	55.4				7.8	-	112.8
Humidified water (kg)					10.9	3.1	-	14.0
De-humidified water (kg)	11.5	24.0					-	35.5

* The supply air temperature is 16.0°C.

TABLE 7.4

The energy consumption in the variable air volume system
with cooling system 1 during heating period*

Sections in psychro. chart	1	2	3	4	5	6	7	Total
Chiller (kW·h)	-	0.5						0.5
Ventilator (kW·h)	-	0.9	1.3	4.8	4.1	13.5	4.1	28.7
Boiler (kW·h)	-	6.6	8.3	68.8	69.1	462.9	326.0	941.7
Humidified water (kg)	-				3.4	44.2	27.9	75.5
De-humidified water (kg)	-	0.1						0.1

* The supply air temperature is 16.0°C.

TABLE 7.5

The energy consumption in the variable air volume system
with cooling system 4 during cooling period*

Sections in psychro. chart	1	2	3	4	5	6	7	Total
Chiller (kW·h)	52.2	39.8					-	92.0
Ventilator (kW·h)	29.2	31.0	70.6	4.3	17.9	0.8	-	153.8
Boiler (kW·h)	68.8	73.2				7.2	-	149.2
Humidified water (kg)					13.4	3.1	-	16.5
De-humidified water (kg)	11.3	31.5					-	42.8

* The supply air temperature is 16.0°C.

TABLE 7.6

The energy consumption in the variable air volume system
with cooling system 4 during heating period*

Sections in psychro. chart	1	2	3	4	5	6	7	Total
Chiller (kW·h)	-	0.5						0.5
Ventilator (kW·h)	-	1.0	2.0	4.8	4.1	13.5	4.1	29.5
Boiler (kW·h)	-	7.5	12.5	68.6	60.1	462.9	326.0	946.6
Humidified water (kg)	-				3.4	44.2	27.9	65.5
De-humidified water (kg)	-	0.2						0.2

* The supply air temperature is 16.0°C.

difference for cooling) and Table 7.4 shows the results during heating period. Table 7.5 and 7.6 give the results for cooling system 4 (without a vertical air temperature difference for cooling). The comparison of the energy consumption between the two cases is illustrated in Figure 7.5. The annual energy consumption of the chiller and the ventilator for cooling system 1 is 26% smaller than that for cooling system 4 and that of the boiler it is 3% smaller.

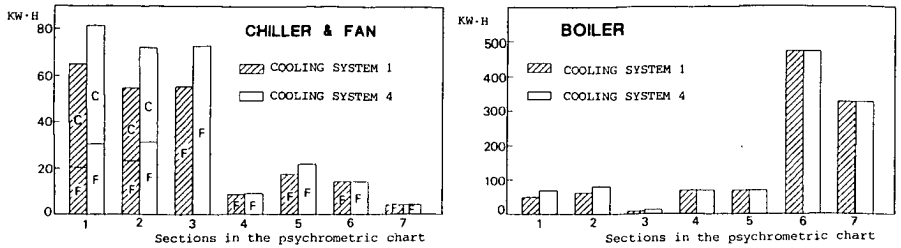


Figure 7.5 The annual energy consumption of the variable air volume system between the two kinds of air supply and air exhaust systems (C - Chiller, F - Fan).

According to the results computed by ACCURACY as shown in Table 7.1, the heat extraction for cooling is higher than the heat supply for heating. But the total energy consumption by the boiler seems to be ten times higher than that by the chiller and the ventilator as expressed in Tables 7.3 to 7.6. This is because the efficiency of the boiler is low (0.75) and the COP value of the chiller is high (3.5) and a part of the energy is required for re-heating during the cooling period. However, the prices for gas, which is used by the boiler, and for electricity, which is used by the chiller and the ventilator, are different. According to the Municipal Electricity Company in Amsterdam, one kW·h electricity costs Dfl. 0.2724 (Dutch Guilders) and one cubic meter gas Dfl. 0.0447. Because one cubic meter gas delivers 9.72 kW·h heat, one kW·h gas energy costs Dfl. 0.046. With such a price, the costs of annual energy consumption are shown in Table 7.7. It is clear that the cost for the chiller and the ventilator is higher than that for the boiler. The total cost of the energy consumption for cooling system 1 (with a vertical air temperature difference for cooling) is about $(125.6-108.0)/108.0 \times 100\% = 16\%$ less than that for cooling system 4 (without a vertical air temperature difference for cooling).

7.2.1.2 With different supply air temperatures

This subsection will demonstrate the results of cooling system 1 and cooling system 4 with different supply air temperatures. The supply air temperature for cooling system 1 is 16.0°C and for cooling system 4 is 12.5°C. Because the supply air temperature for cooling system 4 is lower, the air mass flow supplied can be smaller in sections 1, 2, 4, 5 and 6 for cooling as shown in Figure 7.3. On the other hand, re-heating becomes unnecessary in sections 1 and 2 during cooling period.

When the supply air temperature for cooling system 4 is 12.5°C, there is still no vertical air temperature difference in the room. Thus, the heat extraction for cooling and the heat supply for heating is the same as those in the case with the supply air temperature 16.0°C as shown in Table 7.2.

Since re-heating is unnecessary for cooling system 4 (supply air temperature 12.5°C) and the supply mass flow is smaller in some sections during cooling period, the energy consumption is smaller in these sections. The computed results are presented in Table 7.8. But, the energy consumption for cooling system 4 during heating period is the same as those given in Table 7.6. Compared with the results of cooling system 1 (supply air temperature 16.0°C) shown in Tables 7.3 and 7.4, the annual energy consumption of the chiller and the ventilator of cooling system 4 (supply air temperature 12.5°C) is the same and of the boiler is 10% smaller. The cost of

TABLE 7.7

The annual cost of the room energy consumption (Dutch Guilders)

Air handling sys.	Air supply sys	Inlet temp	Chiller	Ventilator	Boiler	Total
Variable air volume	cooling sys. 1	16.0	20.27	39.22	48.51	108.0
	cooling sys. 4	16.0	25.20	49.93	50.44	125.6
	cooling sys. 4	12.5	17.57	42.52	43.67	103.8
Constant air volume	cooling sys. 1	free	34.32	136.96	69.80	241.1
	cooling sys. 4	free	31.41	132.05	58.94	222.4

TABLE 7.8

The energy consumption in the variable air volume system
with cooling system 4 during cooling period*

Sections in psychro. chart	1	2	3	4	5	6	7	Total
Chiller (kW·h)	36.3	27.7					-	64.0
Ventilator (kW·h)	20.3	21.6	70.6	1.6	12.0	0.5	-	126.6
Boiler (kW·h)						2.8	-	2.8
Humidified water (kg)					13.4	3.0	-	16.4
De-humidified water (kg)	7.7	22.3					-	30.0

* The supply air temperature is 12.5°C.

the annual energy consumption in cooling system 4 with supply air temperature 12.5°C is given in Table 7.7. This is 4% less than or nearly the same as that in cooling system 1 with supply air temperature 16.0°C.

Of course, the cost of the annual energy consumption is not the only standard for evaluating a system. It should be based on the same comfort standard and the same cost of the air-conditioning equipment, etc.. Indoor air velocity, air temperature and contaminant distributions are very different between cooling system 1 and cooling system 4. Some people may prefer cooling system 1 for better air quality and some may need cooling system 4 for a uniform indoor air temperature distribution. The indoor environment of each system has been discussed in chapter 4.

7.2.2 Constant air volume system

In the constant air volume system, the supplied mass flow is maintained to be 0.09 kg/s (a ventilation rate of five times per hour) for all office hours. The energy consumption is also calculated for cooling system 1 and cooling system 4. Cooling system 1 and cooling system 4 are employed both for cooling and for heating. Because no radiator is used for heating in cooling system 1, there is always a vertical temperature difference in the room air both for cooling and heating. Since the room air is mixed very well in cooling system 4 both for heating and for cooling, no vertical temperature exists.

The control strategies for heating and cooling in cooling system 1 are illustrated in a psychrometric chart as shown in Figures 7.6 and 7.7 respectively. In cooling system 4, the averaged enthalpy of the room air extracted in section 1 for cooling is lower. Thus, it is more economical to mix the air extracted with the outdoor air and then to dry it to the dew point D. This is the only difference in the control strategies between the two air supply and air exhaust systems.

The computational results of the energy consumption for the two cases are presented in Tables 7.9 to 7.12. The comparison of the energy consumption between the two cases is illustrated in Figure 7.8. The annual energy

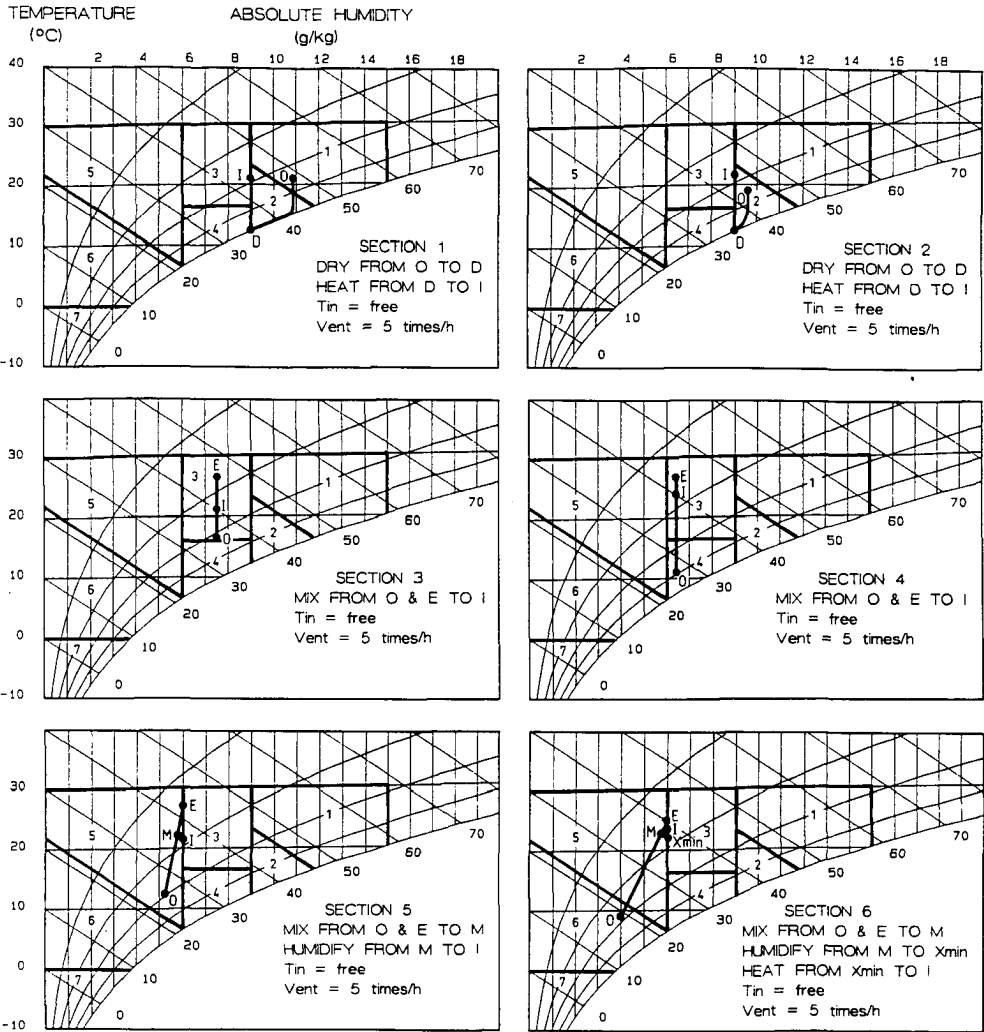


Figure 7.6 The control strategies for cooling in each section of the psychrometric chart for the constant air volume system with cooling system 1 (O - outdoor air, E - air extracted, D - dew point, I - air supplied by inlet, M - mixing point, H - heating point).

consumption of the chiller and the ventilator of cooling system 1 (with a vertical air temperature difference) is 2% larger than that of cooling system 4 (without a vertical air temperature difference) and that of the boiler is 16% bigger.

The cost of the energy consumption for the constant air volume systems is also shown in Table 7.7. The total cost for cooling system 1 is $(241.1 - 222.4) / 222.4 \times 100\% = 8\%$ higher than that for cooling system 4.

As mentioned above, there is always a vertical temperature difference of room air in cooling system 1. Because the mass flow supplied is fixed and the

TEMPERATURE
(°C)

ABSOLUTE HUMIDITY
(g/kg)

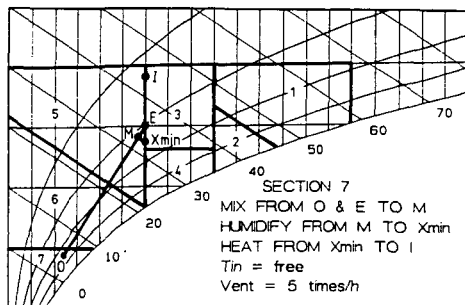
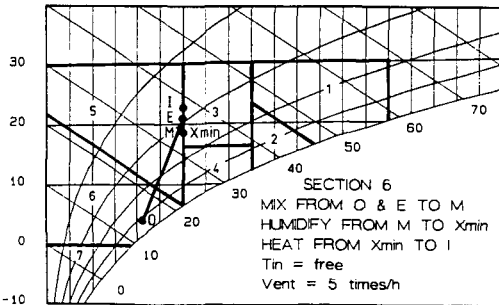
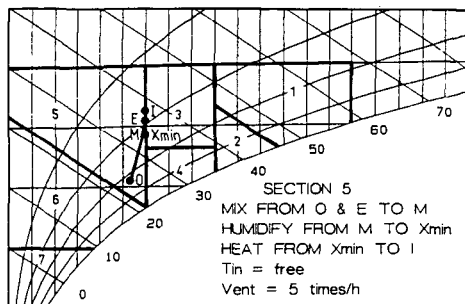
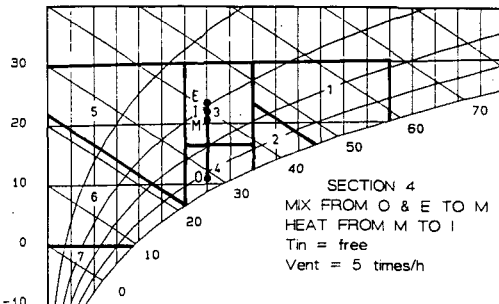
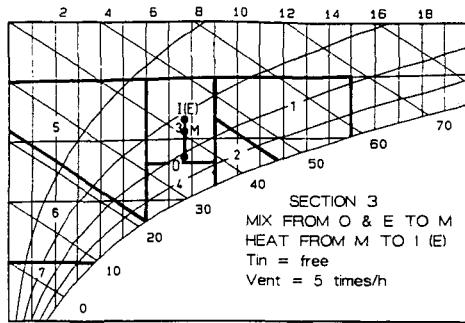
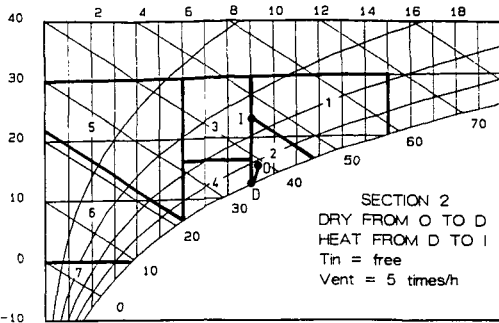


Figure 7.7 The control strategies for heating in each section of the psychrometric chart for the constant air volume system with cooling system 1 (O - outdoor air, E - air extracted, D - dew point, I - air supplied by inlet, M - mixing point, H - heating point).

air temperature extracted from the room is higher, the supply air temperature of the room must be higher too. This will use more energy to re-heat the air from the dew point to the supply point.

From the results of the variable volume system and the constant volume system, the energy consumption of the variable air volume system is much smaller than that of the constant air volume system. However, this much depends on the supplied airflow rate in the constant air volume system.

TABLE 7.9
The energy consumption in the constant air volume system
with cooling system 1 during cooling period

Sections in psychro. chart	1	2	3	4	5	6	7	Total
Chiller (kW·h)	65.9	55.4					-	121.3
Ventilator (kW·h)	30.9	43.4	92.6	13.7	26.3	9.2	-	216.1
Boiler (kW·h)	169.1	273.0				9.7	-	451.8
Humidified water (kg)					10.1	3.5	-	13.6
De-humidified water (kg)	112.4	44.3					-	156.7

TABLE 7.10
The energy consumption in the constant air volume system
with cooling system 1 during heating period

Sections in psychro. chart	1	2	3	4	5	6	7	Total
Chiller (kW·h)	-	4.7						4.7
Ventilator (kW·h)	-	9.1	12.6	48.0	41.1	134.8	41.1	286.7
Boiler (kW·h)	-	67.5	7.8	74.4	73.4	479.3	363.2	1066.
Humidified water (kg)	-				3.4	44.1	29.0	76.5
De-humidified water (kg)	-	1.5						1.5

TABLE 7.11
The energy consumption in the constant air volume system
with cooling system 4 during cooling period

Sections in psychro. chart	1	2	3	4	5	6	7	Total
Chiller (kW·h)	55.1	54.3					-	109.4
Ventilator (kW·h)	30.9	42.3	84.6	13.7	26.3	8.0	-	205.8
Boiler (kW·h)	82.7	165.3				7.3	-	255.3
Humidified water (kg)					13.4	3.2	-	16.6
De-humidified water (kg)	11.2	43.0					-	54.2

TABLE 7.12
The energy consumption in the constant air volume system
with cooling system 4 during heating period

Sections in psychro. chart	1	2	3	4	5	6	7	Total
Chiller (kW·h)	-	5.9						5.9
Ventilator (kW·h)	-	10.2	20.6	48.0	41.1	136.0	41.1	279.0
Boiler (kW·h)	-	75.9	12.7	69.4	69.7	469.2	329.2	1026.
Humidified water (kg)	-				3.4	44.5	28.0	75.9
De-humidified water (kg)	-	2.9						2.9

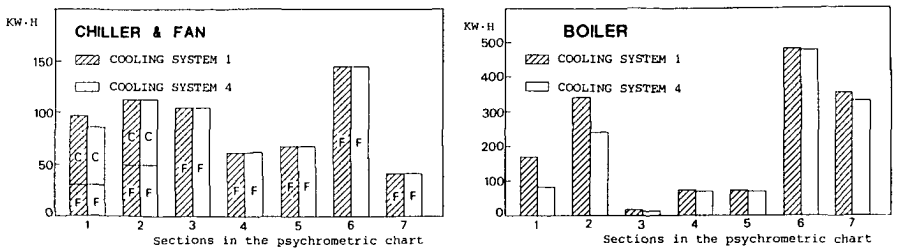


Figure 7.8 The annual energy consumption of the constant air volume system between the two kinds of air supply and air exhaust systems (C - Chiller, F - Fan).

7.3 Conclusions

The following paragraphs may provide the main points from the current chapter:

(1) The air supply and air exhaust systems of a room have a very significant influence on building energy consumption. They must be considered in air-conditioning load calculations and building energy analysis.

(2) In the variable air volume system and with same supply air temperature (16.0°C), cooling system 1 (with a vertical air temperature difference for cooling) will save 26% energy on the chiller and the ventilator and 3% on the boiler, compared with cooling system 4 (without a vertical air temperature difference for cooling). This is because the mass flow supplied for cooling system 1 is lower all the time. The cost of the annual energy consumption for cooling system 1 is 16% smaller than that for cooling system 4.

(3) However, if the supply air temperature for cooling system 1 (with a vertical air temperature difference for cooling) is remained as 16.0°C and that for cooling system 4 (without a vertical air temperature difference for cooling) is controlled at 12.5°C, the cost of the annual energy consumption is nearly the same.

(4) In the constant air volume system, cooling system 1 (with a vertical temperature difference both for cooling and heating) requires 2% more energy for the chiller and ventilator and 16% more for the boiler, compared with cooling system 4 (without a vertical air temperature difference both for cooling and heating).

SUMMARY

A research was carried out in order to study the influence of different kinds of air supply systems in an air-conditioned room on the comfort and energy consumption. The research was performed by numerical simulation as well as experiments. Until some years ago, it was not possible to compute the airflow and temperature distribution in a room. Therefore, the comfort in the room in relation to the air supply systems could not be calculated and uniform temperature distributions were assumed in air-conditioning load calculations. Due to the development in computational studies of fluid flow, now it is possible to deal with these problems by using a suitable airflow program and combining it with an air-conditioning load program. However, experiments are required to validate the calculated results.

The experiments were carried out in a full-scale climate room with different air supply systems, heat gains from heated venetian blinds and ventilation rates. The measurements concerned room airflow patterns, air temperature-, air velocity- and contamination concentration-fields, air-conditioning load, enclosure surface temperatures, and convective heat transfer on walls.

With respect to the influence of different kinds of air supply systems on comfort, the airflow computer programs, CHAMPION SGE and PHOENICS, have been used for the numerical simulation of airflows in the room. The computational method involves the solution, in finite-domain form, of two-dimensional (CHAMPION SGE) and three-dimensional (PHOENICS) equations for the conservation of mass, momentum, energy, concentration, turbulence energy and the dissipation rate of turbulence energy, with wall function expressions for solid boundary conditions. The ventilation efficiency and temperature efficiency, which are used for the evaluation of indoor air quality and energy consumption, are also calculated.

The airflow programs calculate the airflow distributions in the room under heating and cooling conditions with the following two types of systems:

- (1) systems with a vertical stratification of air temperature within the room, where air inlets are located near the floor and air outlets near the ceiling;
- (2) well-mixed systems without a vertical stratification of air temperature with the room where the inlets and outlets are situated near the ceiling and floor of the room respectively.

A few approximations are used to predict three-dimensional airflows by the two-dimensional program CHAMPION SGE. These approximations are: (1) treating the heat transfer through the walls in the third dimension as thermal sources or sinks, (2) concentrating the heat transfer in a two-dimensional domain, and (3) using adjusted inlet temperatures.

It has been found that the agreement between the three-dimensional computations and the measurements is acceptable for practical applications, but the computation is rather expensive. The CPU time on an IBM 3083 JX1 computer is about 80 minutes if the calculation using PHOENICS is started with uniform initial field values and with a total grid number of $18 \times 18 \times 23$. A two-dimensional computation using CHAMPION SGE costs 2 minutes CPU time for a grid number of 18×27 . The two-dimensional computations are much cheaper and the results, although not very precise, can be used for many practical purposes. The temperature efficiency and ventilation efficiency of the first type of air supply system are much higher than those of the second type.

For studying the influence of air supply systems and consequently the air temperature distributions on air-conditioning load, a new, user-friendly, personal computer program, ACCURACY, has been constructed. The program is a coupling of a cooling load program and an airflow program. It is based on the room energy balance method and uses Z-transfer functions for the calculation of heat flow through walls and energy balance equations for windows. The computer program solves three-dimensional, transient equations for the conservation of energy and contamination concentration using airflow patterns. These are precalculated from dedicated computer programs such as PHOENICS and CHAMPION SGE. The influence of room air supply systems on the temperature distribution and indoor air quality, and subsequently on the heat extraction of the room, can be calculated using ACCURACY. The program also determines the ventilation efficiency and temperature efficiency.

Indoor temperature distributions can be considered in ACCURACY by the following methods:

- (1) using uniform temperature distribution of room air,
- (2) applying fixed temperature differences of room air,
- (3) assuming temperature differences of room air proportional to air-conditioning load,
- (4) calculating temperature differences of room air as a function of air-conditioning load and ventilation rate,
- (5) using airflow currents, which are pre-calculated by an airflow program, to determine temperature differences of room air.

It can be concluded that method (1) only gives good results for the computation of air-conditioning load with uniform temperature distribution of room air. Methods (2) and (3) can be used for a room with non-uniform air temperature distribution, but the calculated air-conditioning load deviates with the measurements. However, method (3) gives better results than method (2). The computing time for method (2) is the same as for method (1), but for method (3), it is about 2.5 times higher. The best way is to use methods (4) and (5) by which the calculated results are in very good agreement with the measurements. Method (4) is suitable for the annual hour-by-hour computation of air-conditioning load. It uses the same computing time as method (3). In methods (2), (3) and (4), the temperature differences of room air are determined by computation or measurements. Calculation by means of an airflow program is rather expensive, as mentioned above. Because method (5) is also used for calculating air temperature and contaminant concentration distributions in the room, this method is much more expensive (10 to 100 times higher) than the first one, but it gives more detailed information. The cost depends on the grid number used.

The energy analysis program, ENERK, has been used for the calculation of the annual energy consumption of the room with different kinds of air supply systems. The energy consumption has been studied for a variable air volume system and a constant air volume system under the two types of air supply systems as mentioned above. The results showed that the air temperature distribution in a room is very important in the predictions of building energy consumption. For the variable air volume system, the energy required by the chiller and the ventilator with the first type of air supply systems (with a vertical temperature stratification) is 26% smaller than that with the second type of air supply systems (without a vertical temperature stratification), when the supplied air temperature for both the systems is the same.

Samenvatting

Om de invloed van diverse luchttoevoersystemen in een geklimatiseerde ruimte te bestuderen op het comfort en het energiegebruik is een onderzoek uitgevoerd. Dit onderzoek werd uitgevoerd door middel van een numerieke simulatie en door experimenten. Tot voor enkele jaren was het niet mogelijk om de luchtstroming en de temperatuurverdeling in een vertrek te berekenen. Daarom kon ook de mate van behaaglijkheid in het vertrek niet worden berekend en werd bij de berekening van de koel- of warmtelast een uniforme temperatuurverdeling in het vertrek aangenomen. Ten gevolge van nieuwe ontwikkelingen op het gebied van stromingsberekeningen is het thans mogelijk deze probleem op te lossen door het toepassen van een daarvoor geschikt luchtstromingsprogramma en door dit te koppelen met een koellastprogramma. Voor het valideren van deze berekende resultaten zijn echter experimenten noodzakelijk.

De experimenten werden uitgevoerd in een klimaatkamer op ware grootte met verschillende luchttoevoersystemen, warmtevoer via de verwarmde jalouzieën en mate van ventilatie. De metingen betroffen verdelingen van de luchttemperatuur, snelheid, en verontreinigings concentratie, koel- en warmtelasten, oppervlaktetemperaturen van de binnenbegrenzings en convectieve warmteoverdracht bij wanden.

Met betrekking tot de invloed van verschillende luchttoevoersystemen op de behaaglijkheid zijn de luchtstromingsprogramma's CHAMPION SGE en PHOENICS gebruikt voor de numerieke simulatie van de luchtstroming in de kamer. De berekeningsmethode is gebaseerd op de oplossing van twee-dimensionale (CHAMPION SGE) en drie-dimensionale (PHOENICS) balansvergelijkingen voor massa, impulsmoment, concentratie van verontreinigingen, turbulente energie en viskeuze dissipatie, met wandfuncties voor vaste wand begrenzingen. De ventilatie-effectiviteit en temperatuur-effectiviteit, die zijn gebruikt voor het evalueren van de binnenlucht kwaliteit en het energiegebruik zijn ook berekend.

Met de luchtstromingsprogramma's zijn de luchtsnelheidsverdelingen in de kamer berekend voor koel- en verwarmingssituaties met de volgende typen luchttoevoer systeem:

- (1) systemen met verticale temperatuurstratificatie, waarbij de inlaatopeningen geplaatst zijn bij de vloer en de uitlaatopeningen bij het plafond,
- (2) goed gemengde systemen zonder verticale temperatuurstratificatie, bij de inlaatopeningen geplaatst zijn bij het plafond en de uitlaatopeningen bij de vloer.

Enkele benaderingen zijn gebruikt om drie-dimensionale luchtstroming te voorspellen met het twee-dimensionale programma CHAMPION SGE. Deze benaderingen zijn: (1) behandeling van de warmtestroom door de wanden in de derde dimensie als positieve of negatieve warmtebronnen, (2) het concentreren van de warmteoverdracht in een twee-dimensionaal vlak, en (3) het gebruik van aangepaste luchttoevoertemperaturen.

Gebleden is dat de overeenkomst tussen drie-dimensionale berekeningen en de metingen acceptabel is voor praktische toepassingen, maar de berekeningen zijn vrij kostbaar. De CPU tijd op een IBM 3083 JX1 computer bedraagt ongeveer 80 minuten voor het geval dat de berekening met PHOENICS gestart wordt een uniform veld en met een totaal aantal roosterpunten $18 \times 18 \times 23$. Een twee-dimensionale berekening met CHAMPION SGE kost 2 minuten CPU tijd met een aantal roosterpunten 18×27 . De twee-dimensionale berekeningen zijn veel goedkoper en de resultaten kunnen, hoewel niet erg nauwkeurig, gebruikt worden voor veel

practische toepassingen. De temperatuur-effectiviteit en de ventilatie-effectiviteit van het eerste type luchttoevoersysteem zijn veel beter dan die van het tweede type.

Om de invloed van het luchttoevoersysteem en diens gevolg de luchttemperatuurverdeling op de koellast na te gaan, is een nieuw gebruikersvriendelijk computerprogramma, ACCURACY, samengesteld voor de berekening van de koellast en verdeling van luchttemperatuur en concentratie van verontreinigde lucht. Het programma is in wezen een koppeling van een koellastprogramma en een luchtstromingsprogramma. Het is gebaseerd op de energiebalans methode en gebruikt Z-transformatiefuncties voor de berekening van de warmtestroom door de wanden en energiebalans vergelijkingen voor de ramen. Het computerprogramma lost de instationaire vergelijkingen op voor de energiebalans en verontreinigingsconcentratie, gebruik makend van luchtstromingspatronen, die van te voren zijn berekend met hiervoor geëigende programma's zoals PHOENICS en CHAMPION SGE. De invloed van luchttoevoersystemen op de temperatuurverdeling en kwaliteit van de binnenlucht en daarna op de warmteonttrekking uit het vertrek, kan worden berekend met ACCURACY. Het programma bepaalt ook de ventilatie-effectiviteit en temperatuur-effectiviteit.

Temperatuurverdelingen van de binnenlucht kunnen in ACCURACY in rekening worden gebracht op de volgende manieren:

- (1) door een uniforme temperatuurverdeling voor de vertreklucht aan te nemen,
- (2) door vaste temperatuurverschillen voor de vertreklucht toe te passen,
- (3) door de luchttemperatuurverschillen evenredig met de koellast te veronderstellen,
- (4) door de temperatuurverschillen te berekenen als een functie van koellast en ventilatievoud,
- (5) door luchtstromingspatronen, die van te voren berekend zijn met een luchtstromingsprogramma te gebruiken om de temperatuurverschillen te bepalen.

Geconcludeerd kan worden dat methode (1) alleen goede resultaten oplevert voor koellastberekeningen van een vertrek met een uniforme temperatuurverdeling. Methoden (2) en (3) kunnen worden toegepast voor een vertrek met niet-uniforme temperatuurverdeling, maar de berekende resultaten wijken af van de metingen. Methode (3) levert echter betere resultaten op dan methode (2). De rekentijd van methode (2) is gelijk aan die van methode (1), maar voor methode (3) is deze 2,5 maal groter. De beste manier is om methoden (4) en (5) te gebruiken, waarvan de berekende resultaten zeer goed overeenstemmen met de metingen. Methode (4) is geschikt voor de berekening van de uurlijkse koellast gedurende een jaar. Deze methode gebruikt dezelfde rekentijd als methode (3). Bij de methoden (2), (3) en (4) moeten de luchttemperatuurverschillen bepaald worden berekening of door metingen. Wanneer zij worden berekend met een luchtstromingsprogramma is dit vrij kostbaar, zoals hierboven vermeld. Omdat methode (5) ook uurlijks de verdeling van luchttemperatuur en verontreinigingsconcentratie in het vertrek berekent, is deze methode veel duurder (10 tot 100 maal) dan methode (1). De kosten hangen sterk af van het gebruikte aantal roosterpunten. Deze methode geeft echter zeer gedetailleerde informatie.

Het energiegebruikprogramma ENERK is gebruikt voor de berekening van het jaarlijkse energiegebruik voor het vertrek met verschillende typen luchttoevoersysteem. De resultaten toonden aan dat de temperatuur stratificatie in het vertrek van grote invloed is bij de berekening van het energiegebruik. De energie benodigd voor de koelmachine en de ventilator voor het eerste luchttoevoersysteem (met verticale temperatuur stratificatie) is 26% lager dan voor het tweede luchttoevoersysteem (zonder verticale temperatuur stratificatie), wanneer de toevoerluchttemperatuur voor beide systemen dezelfde is.

室内空气流动、空气质量与建筑物能耗

陈 清 焰

为了探讨空调房间不同送回风系统对舒适和能耗的影响,本文采用数值模拟和实验的方法进行研究。几年前,由于不能计算室内空气流动和温度分布,所以不同送回风系统对舒适的影响就无法计算,并且在空调负荷计算中假设房间温度均匀分布。由于几年来计算流体力学的发展,现在是可能通过应用合适的流体计算程序并将其与空调负荷程序相结合来解决这问题的。然而,计算结果仍需实验验证。

实验是在一具有不同送回风系统,不同窗户得热和不同送回风量的原型房间内进行的。测量参数为气流形状、空气温度场、空气速度场、有害物质浓度场、空调负荷、围护结构表面温度和对流换热量。

关于不同送回风系统对舒适的影响,我们采用CHAMPION SGE和PHOENICS这两个流体计算程序作房间室内气流数值模拟计算,其计算方法涉及解有限元体形式的二维(CHAMPION SGE)和三维(PHOENICS)质量、动量、能量、浓度、紊流能量和紊流能量耗散率的守恒方程,并采用壁函数表示固体边界条件。同时也计算用于评价室内空气质量的通风效率和评价房间能耗的温度效率。

流体计算程序计算在供热和制冷条件下采用下列两类不同送回风系统的室内空气流动分布:

①送风口在靠近地面处,回风口在靠近天花板处,这种系统的房间空气存在垂直温度分层;

②送风口在靠近天花板处,回风口在靠近地面处,这种完全混合系统的房间空气不存在垂直温度分层。

二维程序 CHAMPION SGE 采用一些近似方法计算三维气流,这些近似方法是:①把第三维的传热处理成热源;②把传热集中在二维区域;③使用等效进口温度。

我们发现三维计算结果与测量数据的吻合程度在实际应用中是可以接受的,但比较费时。如采用均匀初时值和 $18 \times 18 \times 23$ 个网格点在IBM3083 JX1计算机上、PHOENICS需要80分钟CPU时间,用CHAMPION SGE作 18×27 个网格点的二维计算只需要2分钟CPU时间。相对地说,二维计算比较便宜,尽管其结果不是很精确,但可在许多工程实际中应用。第一类

送回风系统的通风效率和温度效率均比第二类的高。

为了探讨空调房间送回风系统,即空气温度分布对能耗的影响,作者新编制一个程序- ACCURACY。该程序实际上是流体计算程序和空调负荷程序的结合。它基于房间热平衡方法,利用z传递函数计算围护结构的传热和能量平衡方程计算窗户的传热。该程序利用流场解有限元体形式的,不定常三维能量和浓度方程。这些流场是预先由 PHOENICS 或 CHAMPION SGE 计算好的。ACCURACY 能计算房间送回风系统对温度分布和空气质量以及对房间除热量的影响,也可确定通风效率和温度效率。

在 ACCURACY 中,室内温度分布以下列方法加以考虑:

- ①采用均匀房间空气温度;
- ②采用固定的房间空气温差;
- ③假设房间空气温差与空调负荷成正比;
- ④把房间空气温差作为空调负荷和通风量的函数;
- ⑤应用预先由流体程序计算好的流场计算房间空气温差。

结论是只有在具有均匀空气温度的房间里,第一种方法才能给出正确的空调负荷计算结果。尽管第二种和第三种方法可以用于非均匀房间空气温度分布的场合,但是其计算结果与实验比较有偏差,然而,第三种方法比第二种好。第二种方法的计算时间与第一种方法相同,但第三种方法要贵2.5倍。最好是使用第四种和第五种方法,因为其计算结果与实验非常吻合。第四种方法适合于作全年逐时负荷计算,它所用计算时间与第三种方法相同。在第二、三、四种方法中,房间空气温差可由计算或实验来确定。如上所述,通过流体计算程序计算比较贵。由于第五种方法也用于计算房间空气温度分布和有害物浓度分布,因而比第一种方法贵很多(10-100倍),但是它给出详细的信息,其费用取决于所用的网格点。

为了研究不同送回风系统的房间全年能耗,我们用能量分析程序 ENERK 计算变风量系统和定风量系统在上所述两类送回风系统下的能耗。结果表明室内空气温度分布在作建筑物能耗预测中非常重要。对变风量系统当第一类和第二类送回风系统的送风温度相同时,第一类送回风系统(存在垂直温度分层)的制冷机和风机能耗比第二类送回风系统(不存在垂直温度分层)的少26%。

REFERENCES

- Adams, J.C.Jr. and Hodge, B.K. 1977. "The calculation of compressible, transitional, turbulent, and relaminarizational boundary layers over smooth and rough surfaces using an extended mixing length hypothesis", AIAA paper 77-682, Albuquerque, New Mexico.
- Afonso, C.F.A.; Maldonado, E.A.B. and Skarek, E. 1986. "A single tracer-gas method to characterize multi-room air exchanges", Energy and Buildings, vol.9.
- Alamdari, F.G. and Hammond, G.P. 1983. "Improved data correlations for buoyancy-driven convection in rooms", Building Services Engineering Research & Technology, vol.4, no.3, pp.106-112.
- Alexander, D.K. and Etheridge, D.W. 1980. "The British gas multicell model for calculating ventilation", ASHRAE Transactions, vol.86, part 2.
- Anderson, D.A.; Tannehill, J.C. and Pletcher, R.H. 1984. Computational Fluid Mechanics and Heat Transfer, Hemisphere Publishing Cop.
- ASHRAE 1972. ASHRAE Handbook -1972 Fundamentals, American Society of Heating, Refrigerating, and Air-Conditioning Engineer, Atlanta.
- ASHRAE 1975. Procedure for Determining Heating and Cooling Loads for Computerizing Energy Calculations, Energy calculation 1, ASHRAE task group on energy requirements.
- ASHRAE 1979. Cooling and Heating Load Calculation Manual, ASHRAE GRP 158, American Society of Heating, Refrigerating, and Air-Conditioning Engineers, New York.
- ASHRAE 1980. Bibliography on Available Computer Programs in the General Area of Heating, Refrigerating, Air Conditioning and Ventilating. 2nd Edition.
- ASHRAE 1981. ASHRAE Handbook -1981 Fundamentals, American Society of Heating, Refrigerating, and Air-Conditioning Engineers, Atlanta.
- ASHRAE 1985. ASHRAE Handbook -1985 Fundamentals, American Society of Heating, Refrigerating, and Air-Conditioning Engineers, Atlanta.
- ASHRAE 1987. Indoor Air Quality, ASHRAE J., July, pp.18-38.
- Bahnfleth, D.K.; Moseley, T.D. and Harris, W.S. 1957. "Measurement of infiltration in two residences, part 1: Technique and measured infiltration", ASHRAE Transactions, vol.63, pp.439-452.
- Ball, H.D. 1983. "The impact of lighting fixtures on heating and cooling loads - application to design", ASHRAE Transactions, vol.89, part 2A.
- Ball, H.D. and Green, D. 1983. "The impact of lighting fixtures on heating and cooling loads - mathematical model", ASHRAE Transactions, vol.89, part 2A.
- Bauman, F.; Gadgil, A.; Kammerud, R.; Altmayer, E. and Nansteel, M. 1983. "Convective heat transfer in buildings: recent research results", ASHRAE Trans., vol.89, Pt.1A.
- BLAST 1979. The Building loads Analysis and System Thermodynamics Program-Users Manual - vol.1 (U.S. Army Construction Engineering Research Laboratory Report E-153).
- Boussinesq, J. 1877. "Essai sur la théorie des eaux courantes", Mem. Présentés Acad. Sci., vol.23, p.46, Paris.

- Bradshaw, P., Ferriss D.H. and Atwell N.P. 1967. "Calculation of boundary-layer development using the turbulent energy equation", J. of Fluid Mech., vol.28, part 3, pp.593-616.
- Broyd, T.W.; Dean, R.B.; Oldfield, S.G. and Moulton, A. 1983. "The use of a computational method to assess the safety and quality of ventilation in industrial buildings", Conference on Heat and Fluid Flow in Nuclear and Process Plant Safety, London, pp.65-74.
- Burch, D.M.; Peavy, B.A. and Powell, F.J. 1974. "Experimental validation of the NBS load and indoor temperature prediction model", ASHRAE Transactions, vol.80, part 2.
- Bushnell, D.M.; Cary, A.M.Jr. and Holley, B.B. 1975. "Mixing length in low Reynolds number compressible turbulent boundary layers", AIAA J., vol.13, pp.1119-1121.
- Castro, I.P. 1984. "Effects of free stream turbulence on low Reynolds number boundary layers", J. of Fluids Eng., ASME Trans., vol.106.
- Cebeci, T. and Smith, A.M.O. 1974. Analysis of Turbulent Boundary Layers, Academic Press, New York.
- Chambers, T.L. and Wilcox, D.C. 1976. A Critical Examination of Two-Equation Turbulence Closure Models, AIAA Paper 76-352, San Diego, California.
- Chen, Qingyan 1983. Frequency Response of the Thermal State of a Room, HVAC & R Student-83 reports (part 1), (in Chinese), Qinghua University, Beijing.
- Chen, Qingyan 1985a. Modelling Three Dimensional Air Flows and Heat Transfer in an Air-Conditioned Room with PHOENICS, Report no.346A, TNO Applied Physics Institute, Delft.
- Chen, Qingyan 1985b. Modelling Two Dimensional Air Flows and Heat Transfer in an Air-Conditioned Room with CHAMPION SGE, Report no.ST-234, Lab. of Refrigeration and Indoor Climate, Delft University of Technology, Delft.
- Chen, Qingyan 1986a. A few Approximated Methods for Predicting 3D Air Flow and Heat Transfer in Rooms via 2D Computer Code CHAMPION SGE, Report no.K-115, Lab. of Refrigeration and Indoor Climate, Delft University of Technology, Delft, 1986.
- Chen, Qingyan 1986b. Air Flows and Heat Transfer in a Room: Further Measurements and Computations by the Computer Code PHOENICS, Report no.K-117, Lab. of Refrigeration and Indoor Climate Technology, Delft University of Technology, Delft.
- Chen, Qingyan 1987a. The Mathematical Foundation of the CHAMPION SGE Computer Code (revision), Report no.K-118, Lab. of Refrigeration and Indoor Climate Technology, Delft University of Technology, Delft.
- Chen, Qingyan 1987b. CHAMPION SGE and GROCS: An Instruction Manual, Version 2.1, Report no.K-119, Lab. of Refrigeration and Indoor Climate Technology, Delft University of Technology, Delft.
- Chen, Qingyan 1987c. The Listing of CHAMPION SGE and GROCS, Version 2.1, Report no.K-120, Lab. of Refrigeration and Indoor Climate Technology, Delft University of Technology, Delft.
- Chen, Qingyan 1987d. The Fundamentals of the Computer Code ACCURACY. Report no.K-126. Laboratory of Refrigeration and Indoor Climate Technology, Delft University of Technology. Delft.
- Chen, Qingyan 1987e. The Instruction Manual of the Computer Code ACCURACY. Report no.K-134. Laboratory of Refrigeration and Indoor Climate Technology, Delft University of Technology. Delft.
- Chen, Qingyan 1987f. Methodology for Air Movement and Air-Conditioning Load Modelling and Initial Computations by the Computer Code ACCURACY', Report no.K-128, Lab. of Refrigeration and Indoor Climate, Delft University of Technology, Delft.

- Chen, Qingyan 1988. The Listing of the Computer Code ACCURACY, Report no.K-142. Laboratory of Refrigeration and Indoor Climate Technology, Delft University of Technology, Delft.
- Chen, Qingyan and Kooi, J. van der 1987a. "Experiments and 2D approximated computations of 3D air movement, heat and concentration transfer in a room", Proceedings of the International Conference on Air Distribution in Ventilated Spaces, vol.4a, ROOMVENT-87, Stockholm.
- Chen, Qingyan and Kooi, J. van der 1987b. "Measurements and computations on air movement and temperature distribution in a climate room", Proceedings of XVIIth International Congress of Refrigeration, vol.E, Vienna.
- Chen, Qingyan and Kooi, J. van der 1988a. "ACCURACY - a computer program for combined problems of energy analysis, indoor airflow and air quality", ASHRAE Transactions, vol.94, part 2.
- Chen, Qingyan and Kooi, J. van der 1988b. "Indoor airflow, air quality and energy consumption of buildings: new starting points, new opportunities", to appear in Journal of Refrigeration. (in Chinese).
- Chen, Qingyan and Kooi, J. van der 1988c. "Buoyancy-affected flow and its influence in cooling load determination of a ventilated room: comparison between computations and experiments", unpublished paper.
- Chen, Qingyan; Kooi, J. van der and Meyers, A. 1988. "Measurements and computations of ventilation efficiency and temperature efficiency in a ventilated room", Energy and Buildings, vol.12, no.2.
- Chou, P.Y., 1945. "On the velocity corrections and the solution of the equations of turbulent fluctuation", Quart. Appl. Math., vol.3, pp.38-54.
- Coblentz, C.W and Achenbach, P.R. 1963. "Fixed measurements of air infiltration in ten electrically heated houses", ASHRAE J., July, pp.69-74.
- Daly, B.J. and Harlow, F.H. 1970. "Transport equations in turbulence", Phys. Fluids, vol.13, pp.2634-2649.
- Deardorff, J.W. 1970. "A numerical study of three-dimensional turbulent channel flow at large Reynolds numbers", J. Fluid Mech. vol.42, pp.453-480.
- DOE-2 1981. Reference Manual Version 2.1A, Los Alamos Scientific Laboratory: Report LA-7689-M, Version 2.1A (Report LBL-8706 Rev. 2, Lawrence Berkeley Laboratory).
- Donaldson, C.duP. 1972. "Calculation of turbulent shear flows for atmospheric and vortex motions", AIAA J. vol.10, pp.4-12.
- Driest, E.R. van 1956. "On turbulent flow near a wall", J. Aeronaut. Sci. vol.23, p.1007.
- ESP-I 1978. Energy Simulation Program Engineering Manual (Automated Procedures for Engineering Consultants, Dayton, OH).
- Fairey, P.W. and Kerestecioglu, A.A. 1985. "Dynamic modeling of combined thermal and moisture transport in buildings, effects on cooling loads and space conditions", ASHRAE Transactions, vol.91, part 2A.
- Feustel, H.E. and Kendon, V.M. 1985. "Infiltration models for multicellular structures - a literature review", Energy and Buildings, vol.8, pp.123-136.
- Förch, E.J.L. 1983. Handleiding KOELA and KOELB, Report no.ST-220, Lab. for Refrigeration and Indoor Climate Technology, Delft University of Technology.
- Frost, W. and Bitte, J. 1977. "Statistical concepts in turbulence", Handbook of Turbulence, vol.1, pp.53. Plenum Press, New York.

- Gadgil, A.; Goldstein, D.; Kammarud, R. and Moss, J. 1979. "Residential building simulation model comparison using several building energy analysis programs", Proceedings of the 4th National Passive Solar Conference, USA.
- Gosman, A.D.; Nielson, P.V.; Restivo, A. and Whitelaw, J.H. 1980. "The flow properties of rooms with small ventilation openings", J. of Fluids Eng. ASME Trans., vol.102, pp.316-323.
- Granville, P.S. 1976. "A modified law of the wake for turbulent shear flows", J. of Fluid Eng., ASME Trans., vol.98, pp.578-580.
- Gunton, M.C.; Rosten, H.I.; Spalding, D.B. and Tatchell, D.B. 1983. PHOENICS: An Instruction Manual, TR/75/, CHAM Ltd., London.
- Hammond, G.P. 1982a. "Complete velocity profile and "optimum" skin friction formulas for the plane wall-jet", J. of Fluids Eng., ASME Trans., vol.104.
- Hammond, G.P. 1982b. "Profile analysis of heat/mass transfer across the plane wall-jet", Proc. of 7th Int. Heat Transfer Conf., Munich, vol.3.
- Hancock, P.E. and Bradshaw, P. 1983. "The effect of free-stream turbulence on turbulent boundary layers", J. of Fluids Eng., ASME Trans., vol.105.
- Hanjalić, K. and Launder, B.E. 1972. "A Reynolds stress model of turbulence and its application to asymmetric shear flows", J. Fluid Mech., vol.52, pp.609-638.
- Harlow, F.H. and Nakayama, P.I. 1968. Transport of Turbulence Energy Decay Rate, LA Report no.3854, Los Alamos Sci. Lab., University of California.
- Hittle, D.C. 1979. The Building Loads Analysis and System Thermodynamics (BLAST) Program, Version 2.0: Users Manual, Volume 1. U.S Army Construction Engineering Research Laboratory Technical Report E-153.
- Hjertager, B.H. and Magnussen, B.F. 1977. "Numerical prediction of three dimensional turbulent flow in a ventilated room", Heat transfer and turbulent buoyant convection, Washington, Hemisphere Publ. Cop.
- Holmes, M.J. 1982. The Application of Fluid Mechanics Simulation Program PHOENICS to a Few Typical HVAC Problems, Ove Arup & Partens, London.
- Hoorstra, T.G. 1986. Capaciteitsberekening voor Stralingsverwarming, Report no.ST-256, Lab. of Refrigeration and Indoor Climate Technology, Delft University of Technology, Delft.
- Horrige, P.; Woodson, E.; Khan, S. and Tock, R.W. 1983. "Thermal optical comparisons of accepted interior window treatments", ASHRAE J., Feb.
- Huffman, G.D. and Bradshaw, P. 1972. "A note on von Karman's constant in low Reynolds number turbulent flows", J. of Fluid Mechanics, vol.53, p.45.
- Ito, N.; Kimura, K. and Oka, J. 1972. "A field experiment study on the convective heat transfer coefficient on exterior surface of a building", ASHRAE transactions, vol.78, part 1.
- Jiang, Yi 1982. "State-space method for the calculation of air conditioning loads and the simulation of thermal behavior of the room", ASHRAE Transactions, vol.82, part 2, pp.121-141.
- Jury, E.I. 1964. Theory and application of the Z-transform method. Wiley and Sons, New York.
- Kimura, K. 1977. Scientific Basis of Air Conditioning, Applied Science Pub. Ltd., London.
- Kimura, K. and Stephenson, D.G. 1969. "Solar radiation on cloudy days", ASHRAE Transactions, vol.75, part 1.
- Kolmogorov, A.N. 1942. "Equations of turbulent motion of an incompressible fluid", Izv. Akad. Nauk SSSR Ser. Phys. vol.6, no.1/2, pp.56-58.
- Kooi, J. van der and Bedeke, K. 1983. "Improvement of cooling load programs by measurements in a climate room with mass." Proceedings of the XVth International Congress of Refrigeration. vol.E, pp.54-60, Paris.

- Kooi, J. van der and Förch, E. 1985. "Calculation of the cooling load by means of a more-air-points-model." Proceedings of CLIMA 2000 World Congress. vol.4, pp.395-401, Copenhagen.
- Kooi, J. van der and Chen, Qingyan 1986. "Numerical simulation of air movement and temperature field in a room with cold and hot window surface", EUROMECH-207 Colloquium on Natural Convection. Delft.
- Kooi, J. van der and Chen, Qingyan 1987. "Improvement of cooling load programs by combination with an air flow program." Proceedings of the XVIIth International Congress of Refrigeration. vol.E. Vienna.
- Kovaszny, L.S.G. 1970. "Turbulent shear flows", Convegno sulla teoria della turbolenza, Rome.
- Kraichnan, R.H. 1959. "The structure of isotropic turbulence at very high Reynolds number", J. Fluid Mechanics. vol.5, p.497.
- Kumar, S. 1983. "Mathematical modelling of natural convection in fire - a state of the art review of the field modelling of variable density turbulent flow", Fire and Materials, vol.7, no.1, pp.1-24.
- Kusuda, T. 1969. "Thermal response factor for multilayer structure of various heat conduction systems", ASHRAE Transactions, vol.75, part 1.
- Kusuda, T. 1976. NBSLD - Computer Program for Heating and Cooling Loads in Buildings, NBS BSS 69, U.S. Dept. of Commerce.
- Kusuda, T. 1985. "Summary of recent activities on building energy simulation analysis in north America", Building Energy Simulation Conference, Seattle, WA, USA.
- Kusuda, T. and Bean, J.W. 1981. "Comparison of calculated hourly cooling load and indoor temperature with measured data for a high mass building tested in an environmental chamber", ASHRAE Transactions, vol.87, Pt.1.
- Kusuda, T.; Pierce, E.T and Bean, J.W. 1981. "Comparison of calculated hourly cooling load and attic temperature with measured data for a Houston test house", ASHRAE Transactions, vol.87, part 1.
- Lafeber, M. 1987. Numerical and Physical Aspects of Large Eddy Simulation of Turbulent Flows, Ph.D. Thesis, Delft University of Technology, Delft.
- Lauder, B.E. 1979. "Stress-transport closures: into the third generation", Proceedings of the First Symposium on Turbulent Shear Flows, Springer-Verlag, New York.
- Lauder, B.E. and Spalding, D.B. 1972. Mathematical Models of Turbulence, Academic Press, London and New York.
- Lauder, B.E. and Spalding, D.B. 1974. "The numerical computation of turbulent flows", Computer Methods in Applied Mechanics and Energy. vol.3. pp.269-289.
- Leslie, D.C. 1973. "Developments in the theory of turbulence", Clarendon Press, Oxford.
- Leur, P.H.E. van de 1983. Numerieke Berekeningen van de Turbulente Gestratificeerde Luchtstroming in een Gang, Afstudeerverslag, Delft University of Technology, Delft.
- Liddament, M.W. 1986. "Air infiltration calculation techniques - an applications guide", Air Infiltration and Ventilation Center, U.K.
- Liem, S.H and Paassen, A.H.C. van 1982. Establishment of Short Reference Years for Calculation of Annual Solar Heat Gain or Energy Consumption in Residential and Commercial Buildings (Part 1), Final report contract no. ESF-010-80 N(B), Delft University of Technology, Delft.
- Mackey, C.O. and Wright, L.T. 1944 "Periodic heat flow - homogeneous walls and roof", ASHVE Transactions, vol.50, p.293.
- Mast, W.D. 1972. "Comparison between measured and calculated hourly heating and cooling loads for an instrumented building", ASHRAE Symposium Bulletin no. 72-2.

- McBride, M.F.; Jones, G.D.; Mast, W.D. and Sepsey, C.F. 1975. "Field validation test of the hourly load program developed from the ASHRAE algorithms", ASHRAE Transactions, vol.81, part 1.
- McDonald, H. and Fish, R.W. 1973. "Practical calculations of transitional boundary layers", Int. J. Heat Mass Transfer, vol.16, pp.1729-1744.
- McQuiston, F.C. 1984. "A study and review of existing data to develop a standard methodology for residential heat and cooling load calculations", ASHRAE Transactions, vol.90, part 2A.
- Mierlo, W.J.M. van 1986. Onderzoek naar de Nauwkeurigheid van het Programma "ENERK", Report no.ST-255, Lab. of Refrigeration and Indoor Climate Technology, Delft University of Technology, Delft.
- Mitalas, G.P. 1968. "Calculation of transient heat flow through walls and roofs", ASHRAE Transactions, vol.74, part 2.
- Mitalas, G.P. 1982. Basement Heat Loss Studies at DBR/NRC, National Research Council of Canada, Division of Building Research, Ottawa.
- Mitalas, G.P. and Arseneault, J.G. 1970. "FORTRAN IV program to calculate Z-transfer functions for the calculation of transient heat transfer through walls and roofs", Proceedings of the Conference on Use of Computers for Environmental Engineering Related to Buildings, Gaithersburg, Maryland.
- Mitalas, G.P. and Stephenson, D.G. 1967. "Room thermal response factors", ASHRAE Transactions, vol.73, part 2.
- Muncey, R.W. 1981. Heat Transfer Calculation for Buildings, Applied Science Publication, London.
- NECAP. 1975. NASA Energy/Cost Analysis Program: vol.1, User's Manual and vol.11, Engineering Manual (NASA Report CR-2590).
- Ng, K.H. and Spalding, D.B. 1972. "Turbulence model for boundary layers near walls", Phys. Fluids, vol.15, pp.20-30.
- Nielson, P.V. 1974. Flow in Air Conditioned Rooms, Ph.D. Thesis, Technical University of Denmark, Copenhagen.
- Nielsen, P.V. 1982. "A room air temperature model for HVAC simulation." Proceedings of the First International Conference on System Simulation in Buildings, Liège, Belgium.
- Nielson, P.V.; Restivo, A. and Whitelaw, J.H. 1979. "Buoyancy-affected flows in ventilated rooms", Numerical Heat Transfer, vol.2, pp.115-127.
- Nieuwstadt, F.T.M. and Brost, R.A. 1986. "The decay of convective turbulence", J. Atm. Sci. vol.43.6, pp.532-546
- Orszag, S.A. 1977a. "Lectures on the statistical theory of turbulence", Fluid Dynamics, New York.
- Orszag, S.A. 1977b. "Numerical simulation of turbulent flows", Handbook of Turbulence, vol.1. pp.281. Plenum Press, New York.
- Oegema, S.W.T.M. 1970. "De berekening van het binnenklimaat in gebouwen met behulp van een digitale rekenautomaat", Applied Physics Dept., Delft University of Technology, Delft.
- Paassen, A.H.C. van 1981. Indoor Climate, Outdoor Climate and Energy Consumption, Ph.D. Thesis, Delft University of Technology, Delft.
- Paassen, A.H.C. van 1986. "Design of low energy HVAC-systems with a computerized psychrometric chart", The 2nd International Conference on System Simulation in Buildings, Liège, Belgium.
- Pan, W.Q. 1980. The Basis of Fluid Mechanics, Mechanical Industry Press, Beijing.
- Parker, G.B. 1986. "Measured air exchange rates and indoor air quality in multifamily residences", Energy and Buildings, vol.9.

- Parmelee, G.V. and Aubele, W.W. 1952. "The shading of sunlit glass - an analysis of the effect of uniformly spaced flat opaque slats", ASHVE Transactions, vol.58.
- Parmelee, G.V. and Vild, D.J. 1953. "Design data for slat type sun shade for use in load estimating", ASHVE Transactions, vol.59.
- Patankar, S.V. 1980. Numerical Heat Transfer and Fluid Flow, Hemisphere Publishing Corporation.
- Patankar, S.V. and Spalding, D.B. 1970. Heat and Mass Transfer in Boundary Layers, Intertext Books, London.
- Peavy, B.A.; Burch, D.M.; Powell, F.J. and Hunt, C.M. 1975. "Comparison of measured and computer-predicted thermal performance of a four-bedroom wood-frame townhouse", NBS Building Science Series 57.
- Piece, F.J.; McAllister, J.E. and Tennant, M.H. 1982. "Near-wall similarity in three-dimensional turbulent boundary layers - Part I model review". Three Dimensional Turbulent Shear Flows, ASME, New York.
- Pletcher, R.H. 1978. "Prediction of turbulent boundary layers at low Reynolds numbers", AIAA J., vol.14, pp.696-698.
- Prandtl, L. 1926. "Ueber die ausgebildete Turbulenz", Proceedings of the Second International Congress for Applied Mechanics, Zürich, pp.62-74.
- Prandtl, L. 1945. "Uber ein neues Formelsystem für die ausgebildete Turbulenz, Nachr Akad. der Wissenschaft in Göttingen", van den Loock und Ruprecht, pp.6-19.
- Pun, W.M. and Spalding, D.B. 1976. A General Computer Program for Two-Dimensional Elliptic Flows, HTS/76/2, Imperial College, London.
- Putell, L.P. 1978. The Turbulent Boundary Layer at Low Reynolds Number, Ph.D. Thesis, University of Maryland.
- Reinartz, A. and Renz, U. 1984. "Calculation of the temperature and flow field in a room ventilated by a radial air distributor", Int. J. of Refrigeration, vol.7, no.5, pp.308-312.
- Rodi, W. 1976. "A new algebraic relation for calculating the Reynolds stress", Z. Angew. Math., vol.56, 219.
- ROOMVENT-87, 1987. Proceedings of International Conference on Air Distribution in Ventilated Spaces, vol.3. Stockholm.
- Ross, H.; Goodman, M. and Birdsall, B. 1982. "The impact of ventilation rates on the design of office buildings", ASHRAE Transactions, vol.88, part 1.
- Rosten, H.I. and Spalding, D.B. 1981. The Mathematical Basis of the PHOENICS EARTH Computer Code, CHAM TR/58b/, London.
- Rotta, J. 1951. "Statistische Theorie nichthomogener Turbulenz", Z. Phys., vol.129, pp.547-572.
- Rubesin, M.W. 1976. "Numerical turbulence modelling", AGARD Lecture Series no.86 on Compressible Turbulent Boundary Layers, vol.2, Rhode Saint Genese, Belgium.
- Sakamoto, Y. and Matsuo, Y. 1980. "Numerical predictions of three-dimensional flow in a ventilated room using turbulence models", App. Math. Modeling, vol.4, no.1.
- Sato, A.; Ito, N.; Kimura, K. and Oka, J. 1972. "Research on the wind variation in the urban area and its effects in environmental engineering no.7 and no.8 - study on the convective heat transfer on exterior surface of buildings", Transactions of Architectural Institute of Japan, no.191.
- Schumann, V. 1973. "Results of a numerical simulation of turbulent channel flows", Reactor Heat Transfer, Gesellschaft für Kernforschung, Karlsruhe, pp.230-251.

- Shan, J.P. 1985. "The development of researches on air conditioning load calculation method of buildings in China", CLIMA 2000, vol.2, pp.377-382, Copenhagen.
- Simpson, R.L. 1970. "Characteristics of turbulent boundary layers at low Reynolds numbers with and without transpiration", J. of Fluid Mechanics, vol.42, pp.769-802.
- Spalding, D.B. 1969. "The calculation of the length scale of turbulence in some shear flows remote from walls", Progress in Heat and Mass Transfer, vol.2, pp.255-266. Oxford, Pergamon Press.
- Spalding, D.B. 1981. "Turbulence modelling: solved and unsolved problems", The Appendix of CHAM report TR/58b/, London.
- Stephenson, D.G. and Mitalas, G.P. 1967. "Cooling load calculation by thermal response factor method", ASHRAE Transactions, vol.73, part 2.
- Stephenson, D.G. and Mitalas, G.P. 1971. "Calculation of heat conduction transfer functions for multilayer slabs", ASHRAE Transactions, vol.77, part 2, pp.117-126.
- Sun, Tseng-yao 1968. "Shadow area equations for window overhangs and side fins and their application in computer calculation", ASHRAE Semiannual meeting, Ohio, Paper no. 2059.
- Tennekes, H. and Lumley, J.L. 1972. A first Course in Turbulence, MIT Press, London.
- Tennekes, H. and Lumley, J.L. 1977. "A first course in turbulent shear flows", Studies in Convection, vol.2, p.1. Academic Press, London.
- Todorović, B. 1984. "Distribution of solar energy following its transmittal through window panes", ASHRAE Transactions, vol.90, part 1B.
- Todorović, B. 1985. "Calculative determination of distribution of solar radiation transmitted through windows", CLIMA 2000, vol.2, pp.383-389.
- Weele, A.M. van 1983. Handleiding bij het Program RESP1, Handleiding bij het Program RESP2, Report no.K-102, Lab. for Refrigeration and Indoor Climate Technology, Delft University of Technology, Delft.
- White, B.R. 1981. "low-Reynolds-number turbulent boundary layers", J. of Fluids Eng., ASME Trans., vol.103.
- Wilcox, D.C. and Traci, R.M. 1976. "A complete model of turbulence", AIAA Paper 76-351, San Diego, California.
- Woodson, E.; Horridge, P.; Khan, S. and Tock, R.W. 1983. "Solar optical properties of accepted interior window treatments", ASHRAE J., Aug.
- Yamazaki, K.; Komatsu, M. and Otsubo, M. 1987. "Application of numerical simulation for residential room air conditioning", ASHRAE Transactions, vol.93, part 1.
- Yoshino, H. 1986. "Airtightness and ventilation strategy in Japanese residences", Energy and Buildings, vol.9.
- Zanden, J. van der. 1986. HYDRO - A set of Program for Fluid Flow and Heat Transfer, User's Manual, Delft University of Technology, Delft.

NOMENCLATURE

A	apparent solar constant	(W/m ²)
A	grid surface area	(m ²)
A	van Driest's constant (A=26.0)	(-)
A,B,C,D	elements of the s-transmission matrix	(-)
A(i)	absorptivity for direct solar radiation	(-)
a	absorptivity for diffuse solar radiation	(-)
a	coefficient of the finite-domain equation	(-)
a	thermal diffusivity of materials	(m ² /s)
B	atmospheric solar constant	(-)
BG	ground reflected radiation for a cloudless condition	(W/m ²)
BS	diffuse sky radiation for a cloudless sky condition	(W/m ²)
C	additive constant in the inner layer logarithmic velocity profile	(-)
C	coefficient of source	(-)
C	concentration	(m ³ /m ³ ·air)
C	convection	(-)
C	convective coefficient in the finite-domain equations	(-)
C _f	friction coefficient	(-)
C _p	constant-pressure specific heat	(J/kg·K)
C ₁ , C ₂ , C ₃ , C _D , C ₁ , C _v	coefficients in k-ε turbulent model	(-)
C _μ	constant in wall function formula (C _μ =0.09)	(-)
CC	cloud cover	(-)
CCF	cloud cover factor	(-)
CN	clearness number	(-)
D	diffusion coefficient in the finite domain equations	(-)
D	diffusion coefficient of concentration	(m ² /s)
D(z)	z-transfer function	(-)
d	coefficient in pressure correction equation	(m ² ·s/kg)
E	energy consumption	(kW·h)
E	function of wall roughness (E=9.0)	(-)
E _b	emissive power of black body	(W/m ²)
E(z)	z-transfer function	(-)
F	view factor matrix	(-)
F _{1,2}	view factor from plane 1 to 2	(-)
g	gravity	(m/s ²)
H	height of the room	(m)
H	specific enthalpy	(J/kg)
H	transmission matrix of a wall	(-)
h	enthalpy	(J)
h	hour angle	(degrees)
h _{in}	height of air inlet	(m)

I	unit matrix	(-)
I_D, I_{Dc}	direct radiation on a tilted surface under a cloudless sky and a cloudy sky respectively	(W/m ²)
I_{dcs}, I_{dcf}	diffuse and reflect radiation on a vertical surface under a cloudy sky	(W/m ²)
I_{DH}, I_{dH}	direct and diffuse radiation on a horizontal surface under a cloudless sky	(W/m ²)
I_{DHc}, I_{dHc}	direct and diffuse radiation on a horizontal surface under a cloudy sky respectively	(W/m ²)
I_{DN}	direct normal solar radiation	(W/m ²)
I_{ds}, I_{df}	diffuse and reflect radiation on a vertical surface under a cloudless sky	(W/m ²)
I_{TH}, I_{THC}	total solar radiation on a horizontal surface under a cloudless sky and a cloudy sky respectively	(W/m ²)
K(z)	z-transfer function of a multilayer wall	(-)
k	kinetic energy of turbulence	(J/kg)
L	characteristic length scale of the room	(m)
L	Laplace transformer	(-)
l	characteristic length scale in flow boundary	(m)
M	layer number of a multilayer wall	(-)
M	matrix	(-)
m	mass exchange rate	(kg/s)
m	mass flow rate	(kg/m ² ·s)
N	total surface number of the room	(-)
N	office hour number or night and weekend hour number	(-)
O(z)	output of z-transfer function	(-)
P	probability	(-)
P, Q, R	coefficients for calculating CCF	(-)
p	pressure	(Pa)
Q	cooling load	(W)
Q	total heat exchange	(W)
q	heat flux	(W/m ²)
q	excitation matrix	(-)
R	radiation	(W/m ²)
R(i)	reflectivity for direct solar radiation	(-)
R_m	local Reynolds number ($=u_m y_m / \nu$)	(-)
R_θ	Reynolds number based on momentum-deficit thickness, ($=u_\infty \theta / \nu$)	(-)
r	reflectance	(-)
r	reflectivity for diffuse solar radiation	(-)
S	shade ratio	(-)
S	source term of general fluid property	(-)
SALT	solar altitude	(degrees)
SAZM	solar azimuth angle	(degrees)
T	temperature	(K, °C)
T	temperature matrix	(-)
T(i)	transmissivity for direct solar radiation	(-)
t	general time	(s)
t	transmissivity for diffuse solar radiation	(-)
U	wind velocity above buildings	(m/s)

u	air flow velocity near outside surfaces	(m/s)
u	velocity component in X-direction	(m/s)
u_m	jet velocity maxima (peak) at given x-position	(m/s)
V	cell volume	(m ³)
V	flow velocity	(m/s)
V	source value	(-)
v	velocity component in Y-direction	(m/s)
W	width of the room	(m)
WA	azimuth angle of a surface	(radians)
WT	tilted angle of a surface	(radians)
w	velocity component in Z-direction	(m/s)
w_{in}	width of air inlet	(m)
X	absolute humidity of outdoor air	(g/kg·air)
X, Y, Z	three directions of cartesian coordinate	(m)
x	general coordinate	(m)
x, y, z	three directions of cartesian coordinate	(m)
y_m	cross-stream distance from the wall to the point $u=u_m$	(m)
y_p	distance to walls	(m)
ZA_j, ZB_j, ZD_j, Zl_j	z-transfer factors	(-)

Greek Symbols

α	matrix vector of α_{ic}	(-)
α_{ic}	convective heat exchange coefficient on inside surface (W/m ² ·K)	
α_{oc}	convective heat exchange coefficient on outside surface (W/m ² ·K)	
α_r	radiative heat exchange coefficient	(W/m ² ·K)
β	gas expansion coefficient	(1/K)
β_n	roots of transfer function element B	(-)
Γ	diffusion coefficient	(N·s/m ²)
γ	weighting factor for heating and cooling	(-)
Δ	difference	(-)
Δ	sampling interval	(s)
ΔT	vector of temperature difference	(K)
δ	a small positive value	(-)
δ	declination angle	(degrees)
δ_{ij}	Kronecker delta function	(-)
ϵ	dissipation rate of turbulence energy	(J/kg·s)
ϵ	wall emissivity	(-)
η	incident angle of solar radiation on a surface	(degrees)
η_T, η_V	temperature efficiency and ventilation efficiency	(-)
θ	Laplace transform of wall temperature	(-)
θ	momentum thickness, $\int_0^\infty u(1-u/u_\infty)/u_\infty dy$	(m)
κ	von Karman's constant ($\kappa=0.435$)	(-)
λ	heat conductivity	(W/m·K)
μ	fluid viscosity	(N·s/m ²)
ν	fluid kinetic viscosity	(m ² /s)
ρ	fluid density	(kg/m ³)

ρ_g	ground reflectivity	(-)
σ	Schmidt or Prandtl number	(-)
σ_0	Stefan-Bolzman constant ($\sigma_0=5.67 \times 10^{-8}$)	($W/m^2 \cdot K^4$)
τ	Reynold's stress	(Pa)
ϕ	general fluid property	(-)
ϕ	Laplace transform of q	(-)
ψ	impulse response of heat flux	(-)
ψ	radiative heat exchange factor	(-)

Subscripts

A	appliances
a	ambient
B	buoyancy
b	black body
C	cavity
c	cloudy
c	convection
ch	chiller
D	diffusion
D	direct
d	adjust value
d	diffuse
eff	effective coefficient
ex	extra
ex	extraction
F	next cell face
f	solar radiation reflection from ground
g	glass
H	horizontal
H	specific enthalpy
I	infiltration
I	subscripts denoting grid point (main cell)
i	inside
i	subscripts denoting grid point (velocity cell)
i,j,l	subscripts denoting coordinate directions
in	inlet
k	kinetic turbulence energy
L	lights
l	laminar
m	middle layer of a window
mass	mass flow
n	current time
o	outlet
o	outside
o	reference point
occu	occupied zone
P	occupant
P,N,S,E,W,H,L,T	subscripts denoting directions (main cell)
p,n,s,e,w,h,l,t	subscripts denoting directions (velocity cell)
R,r	radiation
R,r	room
s	sky (diffuse solar radiation from sky)

s	wall surface
t	total
t	transmission of radiation
t	turbulent
v	venetian blinds
ϵ	dissipation rate of turbulence energy
λ	conduction
ϕ	general fluid property
-	previous time step

Superscripts

o	overall
+	dimensionless variable
\rightarrow	vector
-	average component of turbulence parameters
'	fluctuating component of the parameters of turbulence
'	correction values
*	guessed values

CURRICULUM VITAE

The author was born on September 1, 1958 in Fujian Province, China. He graduated at Bangtou Middle School, Fujian, China in 1974. After spent four years in his birthplace as a farmer and a builder, he began his studies in the Department of Thermal Energy Engineering of Qinghua University, Beijing, China. The degree of Bachelor in Engineering was granted in July, 1983.

Subsequently he had an intensive English program in Shanghai Foreign Language Institute, China. In December, 1984, he continued his studies in the Faculty of Mechanical Engineering of Delft University of Technology. Graduate work in the field of indoor climate technology was performed under the guidance of Prof.Ir. R.W.J. Kouffeld and Dr.Ir. J. van der Kooi, leading to the title of "werktuigkundig ingenieur" (mechanical engineer) on December 10, 1985.

Since January 1, 1986, the author has been a research assistant in the Laboratory for Refrigeration and Indoor Climate Technology and has worked on the study presented in this thesis under the guidance of Prof.Ir. R.W.J. Kouffeld, Prof.Dr.Ir. F.T.M. Nieuwstadt and Dr.Ir. J. van der Kooi.

ACKNOWLEDGEMENTS

I am grateful to Prof.Ir. R.W.J Kouffeld, Prof.Dr.Ir. F.T.M. Nieuwstadt and Dr.Ir. J. van der Kooi for creating this research program, guiding the research and offering supports in any case.

Particular thanks are given to Mr. Jaap Keuvelaar for having drawn a part of the illustrations and to the graduate students and technical staff members of the Laboratory for Refrigeration and Indoor Climate Technology for their assistance in this work. I want to express my sincere gratitude to all those who contributed to the achievement of this dissertation.

Finally I express my appreciation to all staff members of the laboratory for their nice reception and friendly atmosphere I found during my stay in Delft.

o